Neoepitope recognition in cancer mice models

Suarez Hernandez, Sara

Publication date:
2022

Document Version
Publisher's PDF, also known as Version of record

Neoepitope recognition in cancer mice models

PhD Thesis

Sara Suárez Hernández

June 2022

Neoepitope recognition in cancer mice models

Department of Health Technology
Technical University of Denmark

Kemitorvet
Building 202
2800 Kgs. Lyngby

Preface

The following PhD thesis has been submitted to the Technical University of Denmark, Department of Health Technology, as part of requirement for obtaining a PhD degree. The project was supervised by Sine Reker Hadrup (Professor, Section for Experimental and Translational Immunology, Department of Health Technology, Technical University of Denmark) and Dennis Christensen (Statens Serum Institute). The research was founded by The Danish Innovation Fund (project NeoPepVac).

The thesis is comprised of a common introduction followed by two relevant manuscripts, an additional chapter stating results from a pilot study, and finally an epilogue discussing the major findings of this work.

Copenhagen, June 2022

Summary

The discovery of immune recognition of cancer implied the existence of a natural *defence* against malignant cells. This way, aiming to boost the body's own immune cells to eliminate cancer – so called immunotherapy – is changing the paradigm of cancer treatment. Neoepitopes comprise tumor antigens arising from mutated gene products originated during tumor development. By being uniquely presented by cancer cells in the context of major histocompatibility complex (MHC) molecules, they allow T cells to distinguish between cancer and healthy cells. In addition, owing to their random mutation nature, neoepitopes are highly individual and are paving the way towards the development of fully tumor-specific and personalized immunotherapies. However, they require the use of computational tools to predict them from the tumor's genomic data. While current algorithms can successfully identify naturally occurring neoepitopes, far from all are recognized by T cells, thus limiting the efficacy of neoepitope-based therapies. This way, prioritization of therapeutically relevant candidates presents a challenge, as the rules governing neoepitopes' immunogenicity remain to be understood.

The work presented in this thesis explores $CD8^+$ T cell neoepitope recognition in preclinical murine models, aiming to gain knowledge on the characteristics driving neoepitope immunogenicity.

In the first study, we characterized neoepitope-specific $CD8^+$ T cells across the preclinical syngeneic tumor models EMT6, 4T1 and CT26. We employed a high-throughput DNA barcode labeled pH-2 multimer screening in spleens and/or tumors, resulting in experimental detection of 25, 15 and 18 neoepitopes respectively. These syngeneic tumor models are widely used for preclinical evaluation of immunotherapies. In addition, given that they are highly homogeneous in comparison to human tumors, mapping the neoepitope recognition landscape of such models may contribute to defining the determinants of neoepitope immunogenicity.

In the second study, we experimentally examined the influence of key parameters previously hypothesized to influence neoepitope immunogenicity. We immunized Balb/c naïve mice with short CT26 neoepitopes formulated in CAF09b adjuvant. The limited fraction of immunogenic peptides evidenced the need to evaluate larger peptide pools to confirm the observed differences across neoepitopes with distinct MHC-I binding capacity and self-similarity scores. This way, the substantial amount of "real life" data arising from on-going clinical trials of neoepitope-based immunotherapies may prove to be a better source compared to preclinical models, despite the great heterogeneity among cancer patients

Finally, on the last Chapter I evaluated the antitumor reactivity of adoptively transferred SIINFEKL-specific $CD8^+$ T cells in a B16BL6-OVA tumor model. This study served as a pilot study to evaluate the superior capacity of antigen (Ag)-scaffolds to expand murine OVA-specific $CD8^+$ T cells. By mimicking the immunological synapse between T cells and Ag presenting cells, expansion with Ag-scaffolds rendered higher yields of SIINFEKL-specific $CD8^+$ T cells with superior tumor control capacity. This framework is intended to be used to expand the neoepitope-specific $CD8^+$ T cells detected in the first study and evaluate their tumor killing capacity in the relevant syngeneic tumor model.

Altogether, the research presented in this thesis contributes to the understanding of neoepitope immunogenicity in preclinical syngeneic models, which if translatable, will ultimately support the development of neoepitope-based immunotherapies in the clinic.

Dansk resumé

Opdagelsen af immungenkendelse af kræft antydede eksistensen af et naturligt *forsvar* mod ondartede celler. Målet om at booste kroppens egne immunceller for at eliminere kræft - såkaldt immunterapi – har på denne måde ændret paradigmet for kræftbehandling. Neoepitoper omfatter tumorantigener udspringet af muterede genprodukter, der stammer fra tumorudvikling. De giver T-celler mulighed for at skelne mellem kræft og raske celler ved at være unikt præsenteret af kræftceller i konteksten af MHC-molekyler. Neoepitoper er desuden meget individuelle på grund af en enorme mutationsdiversitet i kræft og direkte målretning mod disse kræver fuldt personaliserede immunterapier. I det seneste år er der opstået udvikling af beregningsværktøjer til at forudsige neoepitoper fra tumorens genomiske data.
Mens nuværende algoritmer kan identificere MHC-præsenterede neoepitoper, genkendes langt fra alle af T-celler, hvilket begrænser effektiviteten af neoepitop-baserede terapier. Denne måde udgør prioritering af terapeutisk relevante kandidater en udfordring, da reglerne for neoepitopers immunogenicitet skal stadig blive forstået.

Arbejet der præsenteres i denne afhandling, undersøger CD8+ T-celle neoepitop genkendelse, med formålet at opnå viden om egenskaberne der driver neoepitop immunogenicitet.

I den første studie karakteriserede vi neoepitop-specifikke $CD8^+$ T celler på tværs af de prækliniske syngeniske tumormodeller EMT6, 4T1 og CT26. Vi brugte en høj-througput DNA strægkode mærkeret pH-2 multimer screening i milte og/eller tumorer, hvilket resulterer i eksperimentel påvisning af henholdsvis 25, 15 og 18 neoepitoper.

Disse syngeniske tumormodeller er meget brugt til præklinisk evaluering af immunterapier. Derudover, kan kortlægning af neoepitop-genkendelseslandskabet for prækliniske syngeniske modeller bidrage til at definere determinanterne for neoepitop-immunogenicitet fordi at de er meget homogene i sammenligning med humane tumorer.

I den anden studie, undersøger vi indflydelsen af nøgleparametre, der tidligere er antaget at påvirke neoepitopimmunogenicitet.

Vi immuniserede Balb/c naive mus med korte CT26 neoepitoper formuleret i CAF09b adjuvans.
Den begrænsede andel af immunogene peptider, der kunne anvendes i disse undersøgelser, viste ikke en signifikant forskel relateret til MHC-I-bindingskapacitet og selvlighedsscore, men beviste behovet for at evaluere større peptidpuljer for at bekræfte sådanne forskelle. Alternativt tyder dette på, at den betydelige mængde af "virkelige" data, der stammer fra igangværende

kliniske forsøger med neoepitop-baserede immunterapier, kan vise sig at være en bedre kilde sammenlignet med prækliniske modeller på trods af den store heterogenitet blandt cancerpatienter.

Til sidst, i den sidste afnsit har jeg evalueret antitumorreaktiviteten af adoptivt overførte SIINFEKL-specifikke CD8+ T-celler i en B16BL6-OVA tumormodel. Denne studie tjente som en pilotundersøgelse til at evaluere den bedre antigen-stilladsers kapacitet til at udvide murine OVA-specifikke CD8+ T-celler. Ved at efterligne den immunologiske synapse mellem T-celler og antigenpræsenterende celler, gav ekspansion med antigen-stilladser højere udbytter af SIINFEKL-specifikke CD8+ T-celler med overlegen tumorkontrolkapacitet. Denne ramme er påtænkt til at blive brugt til at udvide de neoepitop-specifikke CD8+ T-celler som var opdaget i den første undersøgelse og evaluere deres antitumor i den relevante syngene tumormodel.

Samlet, bidrager forskningen som er præsenteret i denne afhandling til forståelsen af neoepitopimmunogenicitet i prækliniske syngene modeller, som, hvis de kan oversættes, i sidste ende vil understøtte udviklingen af neoepitop-baserede immunterapier i klinikken.

Acknowledgements

First, I wish to thank my supervisor Sine for taking me on as a master student and guiding me all the way to finalizing this PhD thesis. Thank you for always being positive, optimistic, and critical, but also allowing me to slow down the pace and readjust when I needed it.

I am also grateful to the mouse handling team of the group, for giving me the toolbox to continue this project on my own. Huge thanks to Nadia, for the random troubleshooting emails and shared frustrations and successes, even when she wasn't at DTU. Mo, Signe, Amalie, Line, Annie and Siri for opening my eyes to realize when I needed help and giving it even when I did not ask. Sådan! Tusind tak til Anni og Bente, mine bedste dansk lærere og lab wizzards. One is very lucky to find Danes like you with the patience to understand whatever sounds I was making. For being there to give a hand, help with Fortessa or Aria at whatever time and having all the patience in the world when I came with a suddenly urgent order. Huge thanks also to all the amazing people at Sine's group. The good energy keeps on increasing with every new addition. For making long lab days very fun and scientific discussions always productive and inspiring. Special thanks to my neighbours in the office, Mohsen and Tao, for making our island area an international snack restaurant and always a fun space.

I would also like to thank the groups of Katharina Lahl, William Agace, and Vasileios Bekiaris for providing mouse models to this project and truly inspiring immunology discussions. To Allan Mowat, for all the tutorials that are so helpful to understand the puzzle of immunology. I am very grateful to Rasmus, Elisa and Sarunas that have taught me more than what I helped them with.

A big thank you to my super-women in science, Agnès and Isabel. I am forever grateful to have shared this journey with you two. Agnès, for your understanding and encouragement to always act. Isabel, for being the best desk-mate and traveller of the up and downs throughout the three years. Thank you for helping me so many times with the mice, reagents, and emotions. For critically revising drafts of this thesis and for all the random and inspiring discussions we always have.

Thank you to Noelia, for giving me tools to navigate this process.

I would like to express my deepest gratitude to my most beloved ones. To Ásdís, for your last-minute help with this thesis and practical, fun and sweet mindset. To Shahana, Berni and Ariadni, my padak lovers, for being the best people one could have to de-stress over lunch breaks (and over basket practice, drinks, walks, or delicious daahl at home). To Alvaro, for your constant

check-ups even when Switzerland took you away from us. To Omar, Jose, Juani, and Coti, for making every shared apartment a party and a home, even when the PhD was taking too much energy from me. To Giulia and Tommi, for always being there with your fun, kind and amazing energy. To my Pandas: Anna-Maria, my Sofakis and Balbi, Monday and Thursday practices with you got me through the weeks in the toughest months. To Andrea and Diana, my “motiveret” ladies, learning Danish was never so relaxing and fun.

Many thanks to Laura, Esther, Martina, Marian, Luis, las Pepas, Isaac and Guille for the company and all the love when I came back home to recharge.

To my family, for always supporting me and making home a safe space where I can always come back to. To my grandma, for sending me magic energy boosts. To Pedro, for pushing me to complete this PhD.

Lastly, I would like to thank my love Javi for always being my home. Thank you for being the illustrator guru of this thesis and for taking care of everything so I could focus on writing. For being the happiest and the best person I could have by my side.

For all the love and support, I am extremely grateful!

Sara

List of abbreviations

ACT	Adoptive cell transfer
Ag	Antigen
APCs	Antigen-presenting cells
BTLA	B- and T-lymphocyte attenuator
CAF09b	Cationic adjuvant formulation 09b
CAR	Chimeric antigen receptor
cDC	Conventional dendritic cell
cDNA	Complementary DNA
CPI	checkpoint inhibitor therapy
CTLA-4	Cytotoxic T-lymphocyte-associated protein 4
DAMPs	Damage-associated molecular patterns
DCs	Dendritic cells
DNA	Deoxyribonucleic Acid
EL	Eluted ligand
GEMMs	Genetically modified mouse models
GM-CSF	Granulocyte-macrophage colony-stimulating factor
HPV	Human papillomavirus
HSCs	Hematopoietic stem cells
IL	Interleukin
ILCs	Innate-like lymphocytes
INF	Interferon
LN	Lymph node
MAIT	Mucosal-associated invariant T cells
MDSCs	Myeloid-derived suppressor cells
MHC	Major histocompatibility complex
mRNA	Messenger RNA
NARTs	Neoepitope-specific CD8+ T cells
NGS	Next generation sequencing
NK	Natural Killer
NLRs	NOD-like receptors
NSG	NOD SCID gamma mouse strain
PAMPs	Pathogen-associated molecular patterns
PD-1	Programmed death 1
PDX	Patient-derived xenografts
pMHC	Peptide-major histocompatibility complex
poly-IC	Polynosinic:polycytidylic acid
PRR	Pattern recognition receptors
RNA	Ribonucleic acid
RNAseq	RNA sequencing
SCID	Severe combined immunodeficiency

SNVs	Single-nucleotide variants
SVs	Structural variants
TAAs	Tumor associated antigens
Tc	Cytotoxic T cell
TCF-1	T cell factor 1
TCR	T cell receptor
Teff	Effector T cell
Tex	Exhausted T cell
TGF-β	Transforming growth factor beta
Th	Helper T cell
TILs	Tumor-infiltrating lymphocytes
TIM-3	T cell immunoglobulin domain and mucin domain 3
TLRs	Toll-like receptors
TMBs	Tumor mutational burden
TME	Tumor microenvironment
TNFa	Tumor necrosis factor
TPM	Transcripts per million
Tpmem	Precursor of memory T cell
Tregs	T regulatory cell
TSAs	Tumor specific antigens
UV	Ultraviolet
VEGF	Vascular endothelial growth factor

Content

Chapter 1: The immune system

The immune system refers to the body's own *defense* mechanisms against disease. Its function is to protect organisms from infectious pathogens, such as parasites, bacteria, or viruses, while it also eliminates cancer cells. This is made possible by specialized immune cells, namely white blood cells or leukocytes, holding a variety of receptors that can distinguish pathogenic patterns and/or abnormal self [1]. Most leukocytes generate in the bone marrow from hematopoietic stem cells during embryonic development and are replenished throughout life. Some differentiate and seed tissues during embryonic development before birth, allowing an "early life education" of the immune system. Recent studies suggest that prenatal exposure to microbial compounds from the mother's microbiota or to non-pathogenic microorganisms during the first two years of life, *educate* leukocytes to tolerate otherwise harmful agents [2]. However, aberrant immune responses may lead to autoimmune disorders, in which immune cells react against the body's own constituents such as the pancreas' insulin-producing islets of Langerhans in diabetes mellitus type. In addition, sensitivity to certain typically harmless agents such as pollen may trigger activation of the immune response and derive in allergies. To prevent entry of external pathogens into the organism, physical barriers such as skin, and mucous membranes, such as oral, respiratory, and gut, provide the first barrier of protection from pathogens present in the environment or food we eat. Here, chemical compounds produced at mucosal surfaces act as natural antimicrobial substances. If microbes overcome this first layer of protection, innate immune cells – specialized in sensing conserved microbial structures – will initiate an immune response. While some pathogens will be cleared by the innate immune cells, others may require elimination by the highly specific B and T cell receptors from the adaptive immune system.

From innate to adaptive immunity

The innate immune system allows rapid sensing of pathogens or transformed cancerous cells through invariant receptors named pattern recognition receptors (PRRs). PRRs recognize pathogen-associated molecular (PAMPs) structures conserved in evolution e.g., peptidoglycans from the bacterial cell wall; and damage-associated molecular patterns (DAMPs) released from stressed or dying cells, such as DNA or RNA [3]. PRRs have different locations within the cell, thus detecting both extracellular and intracellular dangers. They comprise transmembrane and cytoplasmic proteins, so-called toll-like receptors (TLRs) and NOD-like receptors (NLRs) respectively, mainly expressed by myeloid immune cells such as macrophages, neutrophils, or dendritic cells (DCs). Additionally, a more recently discovered subset of innate cells, called innate-like lymphocytes (ILCs), modulate immune responses by rapidly secreting cytokines in response to tissue-environmental factors. Therefore, they play a key role in tissue homeostasis [4].

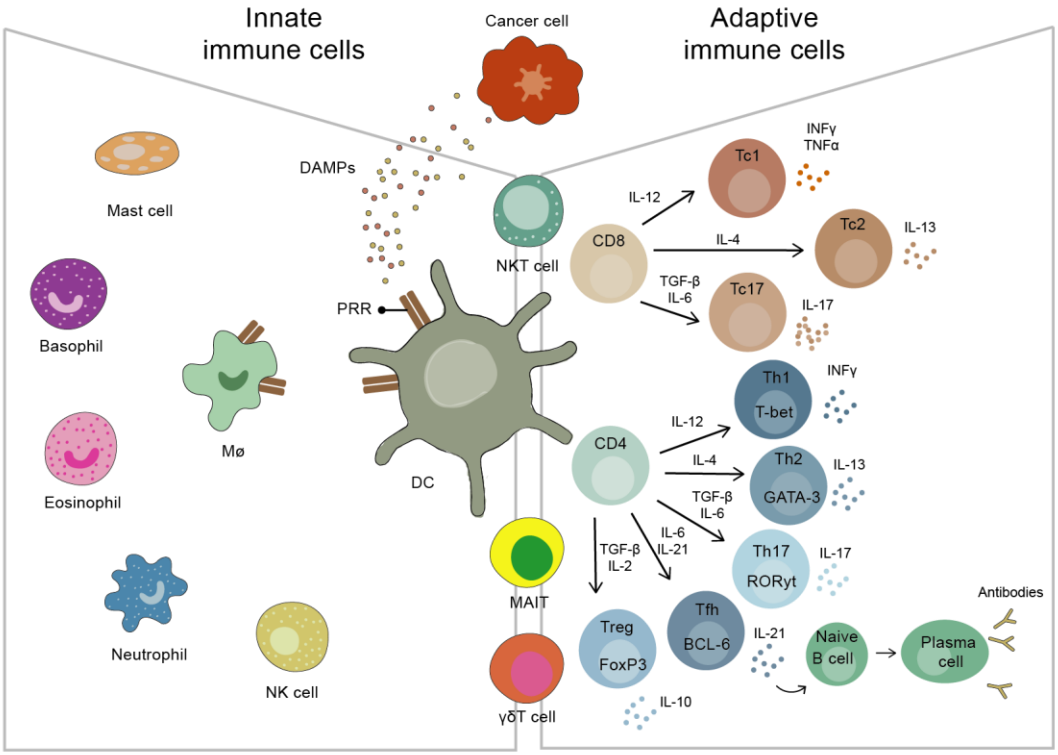

Figure 1: The innate and the adaptive immune system.
The innate immune system provides the first line of defense, being able to sense danger signals from e.g., dying cancer cells through pattern recognition receptors (PRR). Innate cells are: neutrophils, mast cells, basophils, eosinophils, natural killers (NK), macrophages (MΦ) and dendritic cells (DC). The adaptive immune system provides a later and highly specific response thanks to Ag-specific receptors on T and B cells. DCs bridge the innate and the adaptive immune response, as they sense danger through PRRs and activate CD4 and CD8 T cells. Depending on the cytokine environment imprinted by the innate response, CD4 helper (Th) and CD8 cytotoxic (Tc) cells will differentiate into various subsets discerning in transcription factors (T-bet, GATA-3, BCL-6, RORγt, FoxP3) and produced cytokines. Mucosal associated invariant cells (MAIT), NK T cells and γδ-T cells are innate-like adaptive cells, hence their placement at the interface.

Macrophages locate in tissues and comprise the first line of the cellular innate immune response [5]. They engulf and kill invading microorganisms upon PRR activation, followed by the release of chemokines and cytokines to further attract innate cells from the blood and initiate an immune response rapidly. On the other hand, while DCs also phagocytize and degrade pathogens, their main function is to activate T cells and consequently, the adaptive immune response [6]. To do so, they migrate through the lymphatics to the draining lymph nodes, where they present the degraded pathogens, so-called Ags (Ag), to naïve T cells on the major histocompatibility complex (MHC) [7]. T cells are characterized by highly specific T cell receptors (TCRs), holding random sequences genetically rearranged during T cell development and are capable of recognizing a plethora of peptide-MHC complexes (pMHC). Upon pMHC recognition, DCs assist T cells to

differentiate and specialize depending on the cytokine environment imprinted by the initial innate response [8]. However, activation of multiple T cell subsets permits a multi-faceted range of responses, from direct killing of infected or cancerous cells by $CD8^+$ T cells, to antibody generation as the result of naïve B cell activation by follicular helper $CD4^+$ T cells [9]. In addition, upon a first Ag encounter, the adaptive immune system generates immunological memory shaped by memory T and B cells. These subsets will quickly mount strong and specific immune responses upon re-exposure to the same Ag. This way, memory, as well as the specificity of the response, characterize the adaptive immune system. To shape it, it requires longer times (days-weeks) compared to the innate response (immediate). Furthermore, non-conventional lymphocytes namely, γδ-T cells, NK T cells and mucosal associated invariant T cells (MAIT) hold a limited TCR repertoire that can rapidly respond to environmental factors in an MHC-independent manner, thus being on the verge of innate and adaptive immunity as illustrated in Figure 1 [10].

However, for the scope of this thesis, I will further use the term T cell when referring to conventional $CD4^+$ and $CD8^+$ T cells.

Conventional T cells

T cells generate in the bone marrow from hematopoietic stem cells, which can give rise to both myeloid and lymphoid cells. T, B, and Natural Killer (NK) cells share a common lymphoid progenitor (CLP). CLPs leave the bone marrow to colonize the thymus, where they differentiate into T cells through a series of maturation steps (refer to T cell recognition of the peptide:MHC complex) [11]. $CD4^+$ and $CD8^+$ T cells comprise the first identified T cell subsets holding the capacity for immunological memory [12]. They are characterized by expressing a diverse repertoire of TCRs, composed of an invariant CD3 co-receptor and an $\alpha\beta$ chain heterodimer, to recognize a wide range of antigenic peptides processed by professional Ag-presenting cells (APCs) [13]. As mentioned, the high TCRs' diversity results from a random genetic re-arrangement process, which comprises multiple V, D and J gene segments in the β chain (and V and J segments in the α chain). This process results in novel aminoacid sequence combinations of the Ag-binding region of the TCRs that allow recognition of Ag from nearly all pathogens or self-cancerous cells. In addition, the two different subsets of conventional T cells are named based on the expression of the CD4 or CD8 co-receptors, conferring them the capacity to distinctly bind MHC class II (MHC-II) or MHC class I (MHC-I) molecules respectively [14] (Figure 2A). These co-receptors orchestrate the phosphorylation signalling cascade downstream of the TCR, which confers the first signal needed for the activation of naïve T cells (Figure 2B). The second signal is given by binding of the APC ligands CD80/86 to the CD28 receptor on T cells, and lastly, cytokines will provide the third signal driving the differentiation of naïve T cells into effector cells depending on the cytokine environment [9] (refer to Figure 1 for details). For the scope of this thesis, I will only focus on type 1 helper $CD4^+$ T cells (T_h1) and type 1 cytotoxic $CD8^+$

T cells (T_c1), which are both polarized by IL-12. $CD4^+$ T_h1 cells support $CD8^+$ T_c1 cells to fight intracellular threats such as viral infections by secreting INFγ and IL-2. In addition, their essential role in licensing DCs via CD40L for successful activation of tumor-killing cytotoxic $CD8^+$ T cells has been recently described [15]. In turn, cytotoxic $CD8^+$ T cells mediate the killing of infected or cancerous cells via secretion of cytolytic molecules or cell-surface interaction through Fas/Fas ligand binding [16].

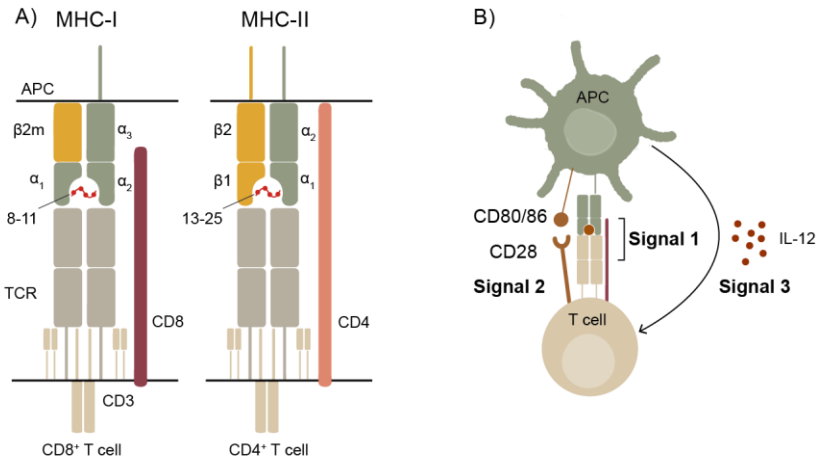

Figure 2: Immunological synapse between Ag presenting cells and T cells.
A) Peptide-loaded Ag presenting cells (APCs) and T cells interact via major histocompatibility complex (MHC) molecules and the T cell receptor (TCR). The CD8 or CD4 co-receptor permits the different interaction of CD8 and CD4 T cells with MHC-I or MHC-II molecules and the intracellular signalling cascade downstream of the TCR together with the CD3 co-receptor. **B)** Activation signals required for T cell priming. B_2m: beta-2-microglobulin; α and β subunits; CD: cluster of differentiation; IL: interleukin.

T cell recognition of the peptide:MHC complex

The MHC complex, also called human leukocyte Ag (HLA), comprises the most polymorphic locus of the human genome [17], with over 10000 different HLA molecules described in 2018 [18]. This polymorphism facilitates the display of a highly diverse repertoire of pathogen and host-derived peptide-ligands, allowing the exposure of extracellular and intracellular pathogens on MHC-II and MHC-I molecules respectively. Furthermore, a subset of DCs termed cDC1s, is highly specialized in cross-presentation, which comprises the loading of exogenous phagocytized peptides onto MHC-I molecules. This process is crucial for priming antitumor immunity and will be further discussed later (refer to “T cell recognition of cancer”). In addition, presentation of self-derived peptides to T cell precursors during thymic development has been proven as a required step for T cell maturation [19]. Briefly, epithelial cells in the thymus present self-derived peptides with two objectives: 1) select the TCR:pMHC pairs capable of forming stable complexes (positive

selection) [20]; and 2) de-select or eliminate those re-arranged TCRs strongly recognizing self-derived peptides (negative selection) [21]. Therefore, positive selection accounts for the MHC restriction of a given TCR, which is only capable of interacting with certain MHC/HLA haplotypes complexes depending on the residue's interactions between the amino acid sequences on both sides. On the other hand, negative selection reduces the risk of autoimmunity by eliminating those self-reactive T cells that, upon high-affinity binding, are more prone to react against *"self"*. This way, those surviving negative selection hold TCRs with low affinity for self-peptides, which renders them tolerogenic [22]. However, not all the self-Ags are expressed in the thymus, implying a risk of autoreactive T cells in the periphery when mature T cells leave the thymus. But owing to the absence of inflammation, and of co-stimulatory signals by APCs, such interactions appear to induce tolerance [23]. In addition, regulatory T cells (Tregs), which comprise a different subset of $CD4^+$ T cells expressing the transcription factor Foxp3 and TCRs highly specific for self-Ags, function to maintain self-tolerance [24]. Overall, tolerance is a highly regulated process in the thymus (central tolerance) and in tissues and lymph nodes (peripheral tolerance), by which T cells are capable of distinguishing self from pathogenic non-self.

Ag-processing and presentation leads to generation of different peptides, some of which are destined to form pMHC complexes recognized by non-self-reactive, hence non-tolerized, high-affinity TCRs. When presented by professional APCs and upon providing all the necessary T cell activation signals (illustrated in Figure 2), T cells will, in turn, mount highly specific and strong immune responses against pathogenic threats. Transformed cancer cells as such, have proven to be *different enough* from self to allow the modulation of immune responses against cancer.

Chapter 2: Cancer and the immune system

Cancer is a set of diseases covering uncontrolled cell proliferation with the potential to invade the bloodstream and spread to other parts of the body. During cell division, the DNA replication machinery may introduce mutations in a cell's DNA, that accumulate over time resulting in indefinite proliferation and tissue outgrowth. Cancer is therefore defined as a genetically driven disease with a multifactorial causation ranging from environmental factors such as sunlight's UV radiation to inherited genetic defects or viral infection. In addition, owing to the heterogeneity within and between tumors, the complexitiy to understand the molecular mechanisms leading to cancer keeps on growing. This way, the recurrent review "The Hallmarks of Cancer" periodically revises the literature intending to map common trades across different cancer types (latest version [25]). Within the last two decades, the five initial characteristics related to sustained proliferation and invasiveness became ten, extending the list to e.g. avoiding immune destruction. In addition, the list further includes enabling characteristics, or in other words, the mechanisms by which pre-cancerous cells acquire the beforementioned hallmarks and progress into malignant tumors. However, defining cancer enablers is somewhat controversial, as many of the mechanisms are dual players in preventing or breaking the speed of cancer progression and promoting tumor growth, as e.g., inflammation.

This way, the immune system was first described to have a tumor-suppressor role, by which innate and adaptive immune cells could distinguish healthy from aberrant tumor cells and specifically kill the latter, in a process termed immunosurveillance. However, as stated above, the inflammatory response also promotes cancer. Therefore, the shift from the inflammatory response having a host-protective role, towards promoting a selective pressure resulting in the escape of immune recognition and cancer outgrowth, comprises the current understanding of immune regulation of cancer [26].

Cancer immunoediting

The early findings that tumors grown in mice lacking an immune system were rejected when transplanted into immunocompetent hosts demonstrated the protective role of the immune system against cancer. However, when tumors were grown in immunocompetent animals, they would progressively develop when transplanted into naïve immunocompetent recipients, suggesting that the immune system could no longer *see* and kill cancer cells [27]. This way, it was defined that the immune system shapes or *edits* the way a tumor is visible to immune cells in a multi-step process termed cancer immunoediting (illustrated in Figure 3) [26]. Immunosurveillance is the first phase of this process, in which a coordinated response between the innate and the adaptive immune system may result in detection and elimination of cancer cells before the tumor is

clinically apparent. At this point, the tumor is characterized by an immunogenic status, meaning that it is detectable by T cells capable of mounting efficient tumor-killing responses (Figure 3A). However, less immunogenic cancer cell variants may not be eliminated during this process, thus entering an equilibrium phase in which the tumor does not grow due to a balance between killing of immunogenic cells and growth of the resistant variants. Lastly, in an attempt by cancer cells to evade immune recognition, they may induce: i) Changes in the cancer cell to prevent tumor recognition (e.g. downregulation of surface expression of MHC-I molecules); or ii) Inhibition of $CD8^+$ T cell effector functions (e.g. through expression of checkpoint-inhibitor ligands, such as PD-L1), hence preventing $CD8^+$ T cell recognition and resulting in immune escape and tumor establishment.

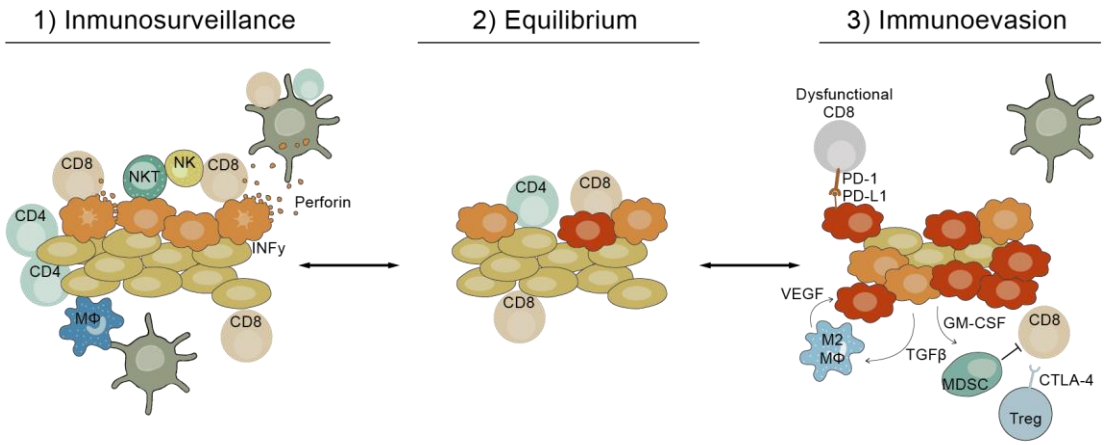

Figure 3: Immunoediting.
A) Immunosurveillance (elimination phase): cancer cells present Ags on the surface and are recognized and attacked by T cells. **B)** Equilibrium phase: owing to the immune pressure by T cell killing of tumor cells, cancer cell variants (red) may evolve to avoid immune recognition. **C)** Immune evasion phase: poorly immunogenic cancer cell variants outgrowth the ones targeted by the immune system, also secreting e.g., TGFβ propitiating the establishment of an immunosuppressive tumor microenvironment. Figure inspired by [115].

The tumor microenvironment

Nevertheless, cancer and immune cells are not the unique players of tumorigenesis. Solid tumors further include multiple recruited stromal cell types such as endothelial cells or the organ's extracellular matrix composing the tumor microenvironment (TME) [28]. The constant interaction between them modulates tumor progression by e.g. promoting blood irrigation through angiogenesis; or tumor rejection via recruitment and infiltration of activated cytotoxic T cells (Figure 3B). This way, the TME is crucial in shaping the crosstalk between cancer and immune cells. This crosstalk is orchestrated by cytokines and chemokines produced by the cancer, stromal and immune cells in the TME. While cytokines regulate growth, apoptosis, activation, and

differentiation of target cells [29], chemokines promote trafficking of immune cells into the tumor [30]. For example, many tumors produce vascular endothelial growth factor (VEGF) [31], which is required for angiogenesis, one of the hallmarks of cancer. Furthermore, tumors escaping immune control are also characterized by secreting immunosuppressive cytokines such as TGF-β [32] or granulocyte-macrophage colony-stimulating factor (GM-CSF), which are respectively involved in macrophage differentiation towards the suppressive M2 subtype and recruitment of myeloid-derived suppressor cells (MDSCs) [33]. In turn, cytokines produced by these immunosuppressive myeloid cells further promote differentiation of $CD4^+$ T cells towards Tregs [34] or direct inhibition of activated $CD8^+$ T cells. This way, tumor cells can modulate the immune content of the TME and avoid $CD8^+$ T cell tumor killing (Figure 3C).

Tumors have been classified as “hot” or “cold” when are highly or poorly infiltrated by lymphocytes respectively. However, in some cases the infiltrate might not be able to penetrate the tumor core from stromal areas thus restricting T cells to the periphery. These tumors are referred to as “immune excluded”, which are generally caused by a tumor vasculature with aberrant permeability [35].

Overall, the TME shapes the responsiveness or resistance of a given tumor to the action of the immune system and comprises the target of several therapies such as anti-VEGF antibodies [31].

T cell recognition of cancer

The TCR specificity enables T cells to distinguish between healthy and transformed cells and thereby places T cells, particularly cytotoxic $CD8^+$ T cells, at the core of anti-cancer immunity. As cancer makes itself detectable to T cells by its mutational origin, which alters the surface Ag landscape of tumor cells differentiating itself from the healthy tissue. However, the crosstalk between the two is a complex multistep process – termed the Cancer-Immunity Cycle [36]– and occurs across different compartments in the body and is mediated by diverse factors, simplified in Figure 4.

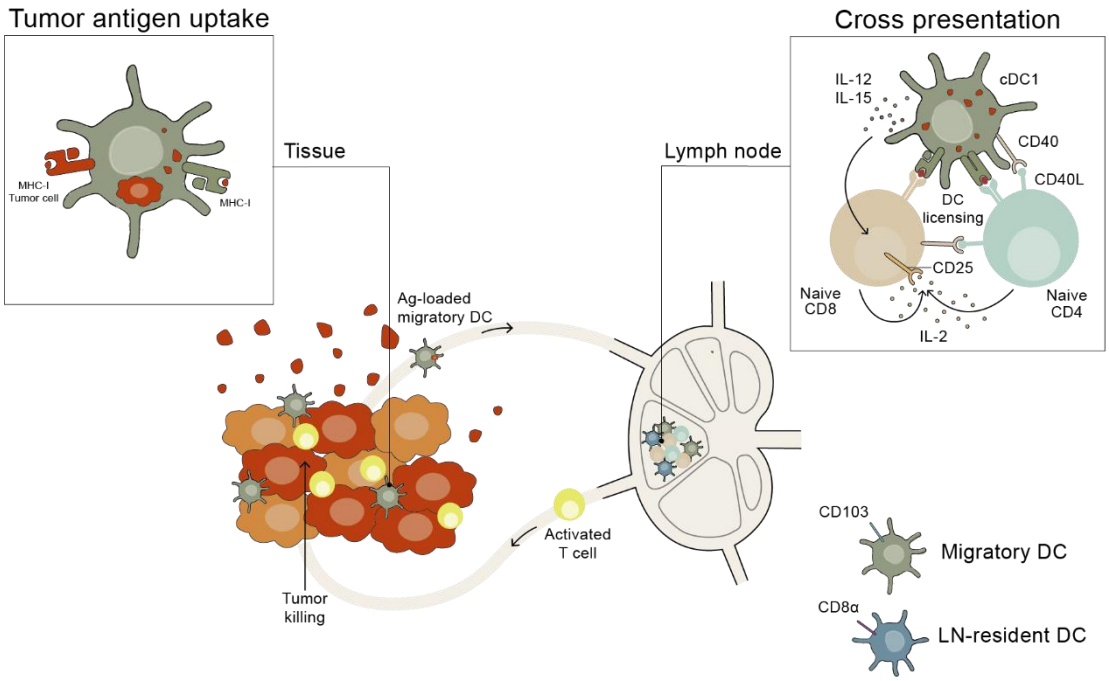

Figure 4: The crosstalk between tumors and the immune system.
Migratory DCs take up Ags released from dying cancer cells and travel to the lymph node (LN). Here, specialized migratory and lymph node (LN)-resident cross-presenting cDC1s prime naïve $CD8^+$ and $CD4^+$ T cells. Activated T cells travel back to the tumor, where upon Ag-recognition, will exert tumor-killing. Figure inspired by [57].

To date, a large body of literature demonstrates that conventional type 1 DCs (cDC1s) are the main facilitators of $CD8^+$ T cell recognition of cancer [37]. While cancer cells present Ags in MHC molecules, they fail to provide the required signals for efficient $CD8^+$ T cell activation (refer to Figure 2B). Until now, cross-presentation of exogenous tumor-derived Ags by cDC1 to naïve $CD8^+$ T cells is believed to be the exclusive mechanism of activating antitumor immunity [38], [39]. In addition, it was recently demonstrated that priming of $CD4^+$ T cells and CD40-CD40 ligand interaction was required for successful $CD8^+$ T cell priming, a process termed DC licensing [15]. However, novel findings in murine tumor models demonstrate that "MHC-I cross-dressing" – which involves the acquisition of intact pMHC-I complexes from neighbouring cells – is sufficient for successful $CD8^+$ T cell priming across various tumor models [40]. Based on their observations, antitumor immunity – at least in murine tumor models – is independent of cross-presentation and might solely require MHC-I presentation by tumor cells for successful priming of antitumor effector T cells. Regardless, the first required step is the acquisition of tumor-derived Ags by cDC1s in the tumor, which then migrate to the draining lymph node (LN) and prime naïve $CD8^+$ T cells (Figure 4). Here, both migratory $CD103^+$ cDC1s from the periphery as well as LN-resident $CD8\alpha^+$ cDC1s

prime naïve $CD8^+$ T cells. At this point, upregulation of CD80/CD86 on cDC1s is required for successful activation of naïve $CD8^+$ T cells. TLR stimulation has been described to promote upregulation of CD80/CD86, the reason for TLR-agonists being widely used as adjuvants in cancer vaccination strategies [41]. Upon priming, tumor-specific $CD8^+$ T cells will proliferate in a process termed clonal expansion and migrate back to the tumor via the lymphatics. Lastly, upon recognition of the cognate Ag in tumor cells, $CD8^+$ T cells will induce tumor killing.

Aside from $CD8^+$ T cells, T_h1-type $CD4^+$ T cells greatly contribute to developing and sustaining antitumor immunity. While being crucial for licensing DCs and secreting IL-2 for successful $CD8^+$ T cell activation, they also trigger direct tumor-killing upon MHC-II recognition or via INFγ and TNFα secretion in an MHC-II independent manner [42].

Nevertheless, T cell-induced tumor killing is far from being a straightforward process and can be hindered by tumor cells through e.g., little Ag exposure, poorly permeable tumor vasculature and/or inhibitory signals provided by the tumor cells or the TME. Recent evidence also now suggests that persistent Ag exposure during tumor development drives differentiation of antitumor T cells towards dysfunctional phenotypes, resembling the characteristics of T cells in chronic viral infections [43].

T cell differentiation

$CD8^+$ T cells are established as the main drivers of tumor-killing due to their superior cytotoxic functions. For this reason, and for the scope of this thesis, the following section briefly summarises the most common phenotypes of differentiated murine $CD8^+$ T cells in cancer.

As previously outlined, clonally expanded tumor-specific $CD8^+$ T cells will induce tumor-killing upon encountering their cognate Ag. This process is mediated by the secretion of INFγ, TNFα, and granzymes, which characterize optimal effector $CD8^+$ T response (T_E) [44]. However, in the context of cancer immunity, $CD8^+$ T cells often fail to mount strong antitumor responses due to diminished effector functions. This weakened effector status is termed exhaustion and was first described in the context of chronic viral infections as result to sustained tumor Ag exposure [45]. Due to the limited survival and re-expansion potential of exhausted $CD8^+$ T cells (T_{EX}), it was widely assumed that memory cells (with proliferation potential) were absent in chronic viral infections, an so it was believed for cancer [46]. The discovery of precursor-exhausted $CD8^+$ T cells (T_{PEX}) subset in mice, characterized by the transcription factor TCF-1 and surface expression of the checkpoint inhibitory receptors PD-1, provided the missing link to understanding the capacity of checkpoint inhibitor therapy (CPI) in restoring effector $CD8^+$ T cell functions. This way, self-renewing T_{pex} cells comprise a dysfunctional $CD8^+$ T cell subset driven by checkpoint inhibitory receptors, which in lack of CPI reinvigoration, will maintain the T_{ex} population. In

addition, a precursor of memory CD8⁺ T cells (T_{PMEM}) has also been described, characterized by the highest proliferation and expansion capacity among the memory subsets [47].

This way, some cells will acquire higher proliferation or differentiation capacities, both within the memory and effector cells. However, different models have been proposed to explain the kinetics of the differentiation process [46]. The phenotype and characteristics of the different subsets are schematically illustrated in Figure 5, which does not necessarily represent sequential differentiation steps.

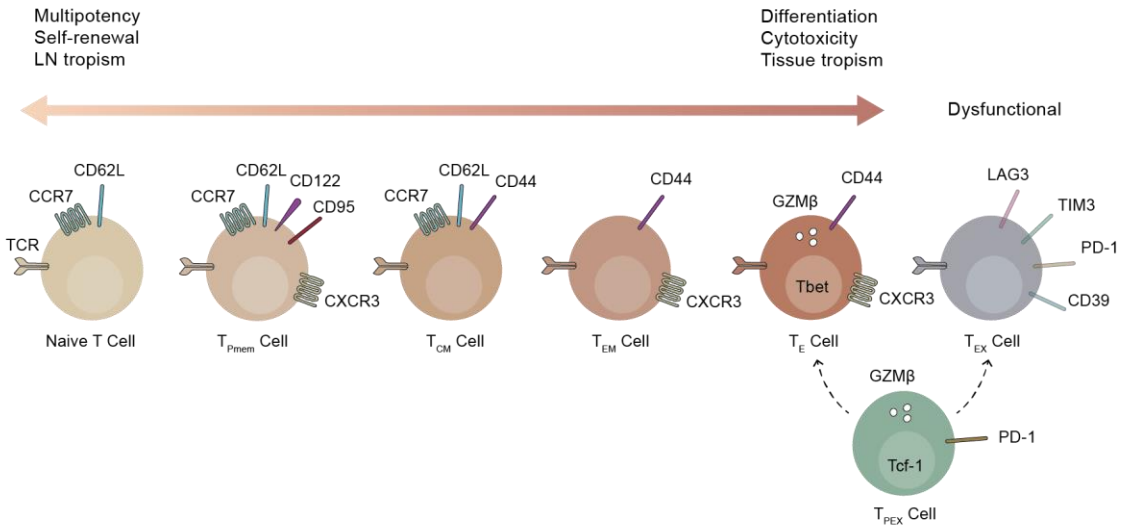

Figure 5: Mouse T cell differentiation subsets.

Upon T cell priming, naïve T cells differentiate into memory-like or effector-like subsets. They differ in their proliferation, cytotoxic capacity, and tissue location through the expression of different surface markers and/or transcription factors. Homing markers: CC-chemokine receptor 7 (CCR7), chemokine receptor 3 (CCR3). Differentiation marker: L-selectin (CD62L), glycoprotein CD44. IL-2 receptor β subunit (CD122). Fas receptor (CD95). Exhaustion markers: ectonucleotidase CD39, programmed cell death 1 (PD-1), lymphocyte activating gene 3 protein (LAG-3), T cell immunoglobulin and mucin domain-containing protein 3 (TIM-3). Pmem: precursor memory; CM: central memory; EM: effector memory; E: effector; EX: exhausted; PEX: precursor exhausted. Figure inspired by [116].

Cancer targets

The mutagenic nature of cancer drives aberrant protein expression, which serves as Ags for T cells to differentiate malignant from healthy cells (e.g., overexpression of certain Ags or expression of mutated gene products) [48]. The degree of dissimilarity between Ags present in cancer cells compared to healthy cells is, a determining factor in shaping the antitumor T cell response. Accordingly, tumor Ags have been classified as tumor-associated Ags (TAAs), which are expressed in both cancer and healthy cells; and tumor-specific Ags (TSAs), in which their expression is confined to the mutated cancer cells (represented in Figure 6). Within TSAs, neoantigens arise from the mutated gene products that originate alongside tumorigenesis. By

being absent in the healthy tissue, T cells that may recognize them are not subjected to central tolerance, thus being more prone to mounting effective antitumor responses than tolerized TAA-specific T cells. This way, neoantigens are believed to be the main drivers of the tumor's immunogenicity. Neoantigens can therefore be further classified depending on whether the mutation generates a novel MHC-I binder in the tumor cell absent in the healthy cell (Figure 6A); or if the mutated residue alters the TCR recognition domain of the presented epitopes (Figure 6B). This way, neoepitopes comprise a tumor-restricted target, paving the way towards development of tumor-specific immunotherapies with limited off-target risks. As neoepitopes comprise the core of the present thesis, their discovery and implications in immunotherapy are further discussed in the following section.

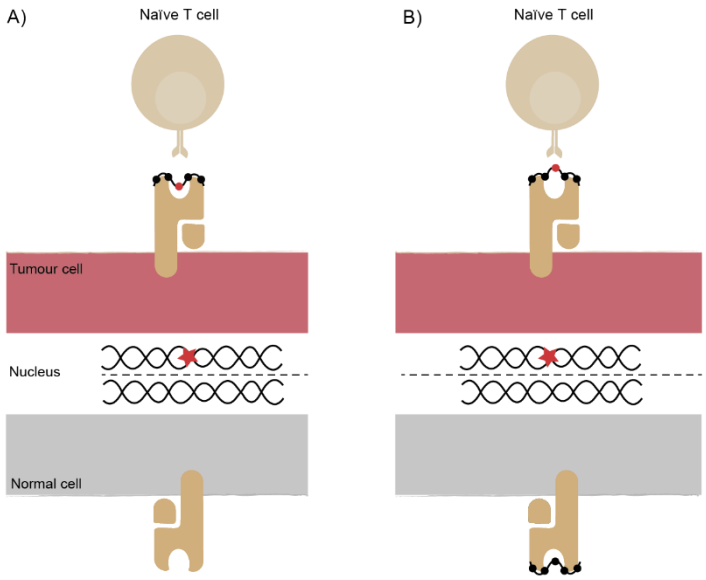

Figure 6: Neoepitope types.
A) The mutation in the tumor cell originates a new MHC-I binder absent in the normal cell. **B)** The mutation changes the TCR recognition domain.

Chapter 3: Immunotherapy

The discovery of immune recognition of cancer implied the existence of a natural *defense* against malignant cells. This way, aiming to boost the body's immune cells to eliminate cancer – so-called immunotherapy – changed the paradigm of cancer treatment [49]. To date, surgical removal of solid tumors remains the primary treatment line. Nevertheless, when not possible or to eliminate potential remains of malignant cells upon tumor resection, chemo- and radiotherapy comprise the second and third pillars of cancer treatment. These therapies however have the drawback of indistinctly targeting both healthy and cancerous cells, causing major adverse effects such as damage to healthy tissue.

Tumor-specificity immunotherapies hold, therefore, a major advantage, either when used alone or in combination with the aforementioned therapies. The development of tumor-targeted immunotherapies has been modulated through the past century, from the initial use of bacterial toxins for the treatment of sarcoma [50], to the approval of engineered chimeric Ag receptor (CAR) T cells for the treatment of multiple myeloma [51]. In addition, the development of blocking CPI antibodies such as anti-PD-1 or anti-CTLA-4, has allowed to shift the balance from growing tumors with immunosuppressed TMEs to tumor-rejection via reinvigorated functional tumor infiltrating lymphocytes (TILs) [52]. Their clinical efficacy in metastatic melanoma [53] and lung cancer [54] conferred the 2018 Nobel Prize in Physiology and Medicine to the discoverers of the first checkpoint inhibitors [55]. More recently, the improvement of neoepitope prediction tools and their identification across several cancer types is paving the way towards the development of fully personalized cancer immunotherapies, such as patient-specific therapeutic cancer vaccines [56], [57]. Findings linking the efficacy of CPI or adoptive cell transfer therapies with the presence of neoantigen-specific $CD8^+$ T cells (NARTs) within the TME or in the autologous T cell product respectively, have placed neoepitopes at the core of immunotherapy development [58], [59]. Therefore, modern immunotherapies such as CPI, cancer vaccines and adoptive cell therapy are further discussed in the context of neoepitope discovery.

Neoepitope discovery

Neoepitopes were first identified in the late 1980s, when mutagen treatment of a mouse model generated mutated tumor variants that were cytotoxically rejected by $CD8^+$ T cells [60]. They were termed "tum-" Ags, and upon screening the pool of responding T cells through cDNA screening, it was identified as the first tumor-rejection neoantigen. This finding marked the beginning of extensive clinical research, from which several neoantigens in melanoma and renal cell carcinoma patients were described [61] Since then, efforts in advancing the identification of neoepitopes in human cancers have been hampered by the cancer's random mutational nature,

as they are highly specific to a given tumor and rarely shared across patients [57]. However, advances in technologies such as next-generation sequencing (NGS) and high throughput screening of Ag-specific T cells have provided many available datasets [62]. These datasets, together with the fast-paced progress of immunopeptidomics and artificial intelligence are driving the development of a growing number of computational tools allowing the prediction of a patient's "neopeptidome" [63]. Current neoepitope prediction pipelines start by identifying the mutations of origin by comparing NGS data from a tumor biopsy and the healthy tissue counterpart. Yet, the complexity of neoepitope identification relies on integrating data for all the required steps involved in neoepitope generation, from transcription and translation of the mutation to Ag processing and MHC presentation [64]. As prediction tools rely on ligands eluted from MHC molecules, confirmation of the mutation expression in the tumor's RNA sequencing data and a predictive score of MHC binding is a common step across prediction tools [57]. However, several clinical and preclinical reports studying NARTs demonstrate that very few of the predicted candidates are recognized by T cells and capable of inducing strong T cell responses [65], [66]. This way, aiming to improve the prioritization of the immunogenic candidates, current prediction tools differ in the neoepitope characteristics they use to rank immunogenicity, e.g., neoantigen:MHC-I interaction [67].

Neoepitope characteristics

Neoepitopes have been categorized based on the type of somatic mutations giving rise to them. They can derive from a vast source of nonsynonymous mutations, by which the amino acid changes result in an altered protein sequence. These mutations include single-nucleotide variants (SNVs), insertions and deletions (indels), frameshift mutations, gene fusions and structural variants (SVs). In addition, open reading frames of viral genomes also comprise a neoepitope source in virus-associated tumors such as human papillomavirus (HPV)-induced cervical cancer. SNV burden has proven predictive of CPI efficacy in metastatic melanoma and non-small cell lung cancer [68], as SNV-neoepitope-based vaccines are showing encouraging results in vaccination trials for melanoma and glioblastoma [69], [70]. On the other hand, the potential of frameshift indels to generate altered sequence strains compared to the SNV's single-residue changes, may increase the likelihood of targeting non-tolerized T cells with higher-affinity TCRs when used as vaccination targets. This way, improved MHC binding affinity of the neoepitope compared to the unmutated sequence has shown correlation to T cell responses [71], while self-dissimilarity has proven predictive when the mutation does not improve MHC binding affinity [72]. Additionally, a later study found that frameshift mutations correlate better with clinical response to CPI than SNV alone [73], exemplifying the difficulty to link neoepitope characteristics with clinical benefit.

In view of this and the fact that some neoantigens induce functional T cell responses spontaneously while others need immunotherapeutic interventions e.g., CPI therapy, to do so, Luang et. al. recently proposed a “context-based” classification considering the clinical context for which a neoepitope gains therapeutic relevance [57]. This way, they outline the following categories: i) Guarding neoantigens capable of naturally inducing T cell responses; ii) Restrained neoantigens, which NARTs need immunotherapy to foster expansion and clinical benefit; or iii) Ignored neoantigens, for which a limited MHC presentation level requires vaccine-induced memory NARTs to induce antitumor responses.

Overall, successful prediction and prioritization of immunogenic neoepitopes call for an integration of multiple parameters within the prediction pipelines. The benefits of unifying the different characteristics considered by diverse prediction tools were shown by the TESLA consortium results, which highlighted four peptide-MHC features driving neoepitope’s immunogenicity: strong binding affinity, high tumor abundance, high binding stability and TCR peptide recognition [74]. Such multi-faceted tools together with the larger amounts of data from monitoring NARTs may pave the way towards a reality of a fully personalized and efficient cancer treatment approach.

Immune checkpoint blockade antibodies

Immune checkpoints are inhibitory receptors expressed by different immune cells to regulate their activation and proliferation. On $CD4^+$ and $CD8^+$ T cells, some are constitutively expressed on the cell surface (e.g., BTLA), while others are upregulated upon activation to prevent uncontrolled effector functions (e.g., CTLA-4, PD-1) and to maintain immune tolerance [75]. However, cancer cells express checkpoint inhibitor ligands to evade immunosurveillance by rendering the recognizing T cells dysfunctional. This way, CPI utilizes monoclonal antibodies to interrupt such co-inhibitory signals to restore $CD8^+$ T cell activation and thereby promote tumor regression [76].

The best characterized inhibitory receptors are CTLA-4 and PD-1, which led to the development of anti-CTLA-4 and anti-PD-1 monoclonal antibodies currently approved as a first-line treatment for various cancer types [77]. Both receptors allow T cell activation, survival, and production of INFγ, TNFα and IL-2. However, their mechanisms of action differ. CTLA-4 is the high-affinity homologous receptor of CD28 and thereby competes for binding to CD80/CD86 on the surface of APCs and prevents T cell activation when upregulated (refer to Figure 2). This way, anti-CTLA-4 antibodies promote T cell priming in the lymph nodes by allowing CD28-CD80/CD86 binding [78]. In addition, CTLA-4 is constitutively expressed on Tregs, and studies of anti-CTLA-4 mechanisms in mouse models show that its antitumor efficacy is driven by depletion of T cell-suppressive Tregs [79]. PD-1 on the other hand binds PD-L1, which is expressed in tissues and upregulated in healthy cells. Their interaction prevents the T cell activation signalling cascade downstream of the TCR. This way, tumor expression of PD-L1 is the most widely used biomarker

to predict a patient's benefit of anti-PD1 or anti-PD-L1 CPI blockade [80]. On the other hand, expression of the inhibitory receptors on the surface of $CD8^+$ T cells does not imply CPI benefit. As previously mentioned, phenotypic studies of $CD8^+$ T cells driving response to CPI treatment led to the discovery of the Tpex subset (refer to Figure 5 for details), which are believed to be necessary for the benefit of CPI therapy. This way, understanding the patient's immunological phenotypic characteristics is crucial in guiding the selection of those likely to benefit from CPI or other types of immunotherapies. Despite encouraging results of CPI therapy for the treatment of melanoma, responses to anti-CTLA-4, anti-PD-1, and anti-PD-L1 monotherapies are currently limited to 20-30% of the treated patients [81]. Even though greater survival rates are being achieved in clinical trials when different CPI are used in combination [81], far from all patients and cancer types benefit from this therapy. CPI treatment acts over an existent immune response, implying that immunogenic tumors with higher TMBs (e.g., melanoma) are more likely to benefit from this treatment. Recently, NARTs have been demonstrated to be the drivers of CPI responses in clinical and preclinical models, in line with TMB and neoepitope load being predictive of CPI benefit [82], [83]. However, tumors with low TMBs and neoepitope load might not benefit from this type of therapy [84], for which expansion of ignored NARTs through vaccination could provide an immunotherapeutic treatment option [57].

Cancer vaccines

Cancer vaccines aim to eradicate tumor cells, either by enhancing pre-existing antitumor immunity or through the generation of de novo responses by priming tumor-specific T cells [85]. However, owing to the persistent Ag exposure by tumor cells and generally immunosuppressive TMEs, the formulation of cancer vaccines requires a rational design to overcome central and peripheral tolerance while reinvigorating dysfunctional tumor-specific T cells. This way, essential considerations for the development of efficient cancer vaccines include the use of neoantigens as targets, the choice of the vaccine delivery format, and/or formulation with immunostimulatory adjuvants [86].

As outlined in previous sections, advances in neoepitope discovery outpaced the initial cancer vaccine approaches using full tumor lysate, irradiated tumor cells or TAAs. Nevertheless, targeting neoepitopes comes with potential challenges such as limited neoepitope presentation or tumor heterogeneity. Neoepitope-based vaccines, therefore, comprise multiple targets covering 2-30 different mutations per individual vaccine, while including both $CD4^+$ and $CD8^+$ T cell epitopes [57], [87]. This is crucial not only due to the indispensability of $CD4^+$ T cell help for effective $CD8^+$ T cell priming but also because $CD4^+$ T cells can drive cytotoxic responses against tumors expressing MHC-II [88] Regarding vaccine delivery formats, peptide, mRNA and DNA neoepitope-based vaccines are the most widely studied in the clinic and in preclinical models. While mRNA and DNA-encoded vaccines directly target the MHC-I presentation pathway by

expressing the neoepitopes intracellularly, exogenous peptide-based vaccines will be presented on MHC-II molecules to a greater extent. Therefore, adjuvants targeting cross-presenting DCs are crucial to foster $CD8^+$ T cell activation for peptide-based neoepitope vaccines [86]. This way, TLR agonists have been the most widely explored in the cancer vaccine context, as their stimulation on DCs induces maturation, and upregulation of CD80/86 and CD40 costimulatory molecules among other processes involved in promoting T cell activation and cross-presentation [89]. In this regard, double-stranded RNA TLR-3 agonist Poly-IC has shown improved efficacy of neoepitope-based vaccines in preclinical B16-F10 melanoma and MC38 colon carcinoma models[65], [90], and its safer version Poly-ICLC, is the most widely used adjuvant in on-going clinical trials [91]However, neoepitope-based vaccines have shown preferential induction of $CD4^+$ T cells over $CD8^+$ T cell responses. As $CD8^+$ T cells are the main drivers of tumor-killing, there is growing interest to foster $CD8^+$ T cell responses to neoepitope-based vaccines. This way, the novel CAF09b adjuvant has shown enhanced $CD8^+$ T cell activation compared to other Poly-IC-based formulations in murine models when administered intraperitoneally and is currently under clinical evaluation [92].

Neoepitope-based vaccines have to this day been proven as a feasible and safe cancer therapy with several vaccination strategies under clinical trials (revised in [86]). Its use in combination with CPI has shown improved antitumor responses compared to CPI alone in murine melanoma [93]. This way, vaccination might be required to boost NARTs' frequencies to render tumors with low TMBs responsive to CPI, as shown for glioblastoma [70]. Furthermore, CPI-driven reinvigoration of immunosuppressed TMEs might be crucial for the efficacy of cancer vaccines in certain tumors, thus motivating several clinical studies for combined therapies (revised in [86]). On the other hand, the individual feature of this therapy hinders the development of off-the-shelf neoepitope cancer vaccines. In this regard, the required manufacturing times might be critical for patients in advanced disease stages, which can be mitigated by choosing vaccination formats with shorter fabrication times.

Adoptive cell transfer

Adoptive cell transfer (ACT) therapies comprise the isolation of a patient's autologous T cells for *ex vivo* expansion before re-infusion for the elimination of cancer cells. This way, ACT allows *ex vivo* enrichment and/or selection of specific NARTs to create an individualized T cell product better fitted for killing of that particular tumor. In addition, isolated T cells have further been engineered in the form of chimeric Ag receptor (CAR)- and TCR-T cells. While CAR T cells are modified to express a surface antibody fragment instead of a TCR, engineered T cells comprise the desired TCR sequences. Only the latter is therefore capable of recognizing MHC-presented Ags. However, engineered T cells have not yet been applied in the context of neoepitope

recognition, although neoepitope-specific TCR-based chimeric receptors have been envisioned [94].

On the other hand, *ex vivo* expansion of TILs with high dose IL-2 is currently an established standard method, which allows the generation of up to $2x10^{11}$ TILs within five weeks [95]. This method offers a therapeutic option to metastatic melanoma patients irresponsive to standard therapies, being under phase III clinical trials [96]. In addition, *ex vivo* expansion permits screening of NARTs and their selection, and neoantigen-selected TIL products are currently under early clinical trials (NCT03997474, NCT04904185). This approach has shown a preliminary positive indication in preclinical patient-derived xenograft models [97]. *Ex vivo* expansion of NARTs offers a way to increase the numbers of therapeutically relevant T cell populations that might not be reached through e.g., vaccination, owing to an immunosuppressive TME hampering NARTs activation and proliferation.

Overall, the choice of immunotherapy depends on the disease scenario, while its use in combination (e.g. vaccination or ACT together with CPI blockade) might offer greater efficacy, thus motivating ongoing clinical trials. In addition, preclinical murine models provide a valuable tool to evaluate immunotherapy approaches and are further discussed in the following section.

Chapter 4: Mouse models in cancer

Mouse models have significantly contributed to the development of immunotherapies. The most relevant tumor models used for the study of cancer and immunotherapy are the following: genetically modified mouse models (GEMMs), carcinogen-induced, human and patient-derived xenografts (PDX), and syngeneic tumor models [98]. The main advantages of mice as preclinical animal models for the study of cancer comprise their accessibility, easy manipulation, and high tumor growth rates. In addition, GEMMs can be readily established, thus allowing the study of the mechanism of action of oncogenes or tumor suppressor genes in tumorigenesis. In addition, carcinogen-induced tumor models have also contributed to to better understanding the mechanisms behind carcinogen-induced cancer in humans e.g., tobacco-induced lung cancer [99]. On the other hand, human xenografts into immunocompromised murine strains such as nude or severe combined immunodeficiency (SCID) mice allow the establishment of human tumor cell lines within the mice. Due to dysfunction or lack of T and B cells, these mice are mainly used for the study of cytotoxic drugs. To study the crosstalk between cancer and immune cells, SCID mice were the first strain to get transplanted with human hematopoietic stem cells (HSCs). However, NK cell activity limited the establishment of primary tumor cells, which was overcome by the creation of the NOD SCID gamma (NSG) strain. By knocking-out *Rag1* and *Rag2*, this strain lacks mature T, B and NK cells. This allows for the establishment of human primary cancer cells and immune cells, thereby mimicking the patient's tumor and immunological microenvironments. of this thesis, their contributions, and limitations to the study of immunotherapy are further revised. PDX models are therefore widely used model to evaluate the treatment with anti-PD-1 and anti-CTLA-4 antibodies in preclinical settings, as they better mimic the chronic inflammatory response and TME of human tumors compared to syngeneic models, which were initially used to characterize the mechanism of action of CPI [100]. In addition, they might also contribute to evaluation of the efficacy of neoepitope-based immunotherapies as it allows the study of e.g., ACT of NARTs, serving as a validation of neoepitope's expression in the human tumor and the therapeutic potential of the selected specificities [97].

Lastly, and of relevance for the scope of this thesis, syngeneic tumor models comprise immunocompetent mice – generally from the C57BL/6 and Balb/c strains – into which histocompatible tumor cell lines can be transplanted. Their main advantage relies on the short time it takes to establish the tumor, as lagging times between tumor inoculation and tumor onset can be modulated by the number of inoculated cells. The fast kinetics of tumor growth, however, limit their therapeutic window. This is the main challenge when evaluating the effect of immunotherapies, as tumor growth outpaces the immunomodulatory effects of immunotherapy in some models thus limiting their translational potential [101]. For example, while melanoma shows

a great response to CPI in the clinic, preclinical melanoma models are refractory to this therapy [102]. This way, syngeneic models also fail to represent the human TME, especially when tumors are inoculated subcutaneously. Orthotopic inoculation of e.g., glioblastoma cell line intracranially, better models the natural TME although it complicates monitoring of tumor growth. In addition, the established immortal murine cell lines also fail to represent the heterogeneity of natural human tumors, thus presenting a potential challenge in evaluating immunogenicity of e.g., sub-clonal mutations present on immuno-edited cells.

Despite their translational limitations, syngeneic models have provided great contributions in the field of immunotherapy and neoepitope discovery. For example, the discovery that anti-CTLA-4 antibodies deplete Tregs in murine tumors in an Fc-dependent manner while it does not in humans [103], might contribute to the development of more efficient Tregs-depleting human anti-CTLA-4 antibodies [104]. In addition, syngeneic tumor models have contributed to the description of therapeutically relevant neoantigens across multiple tumor models (e.g., CT26 and B16F10) receiving CPI treatment and/or prophylactic or therapeutic vaccinations [105], [106].

Manuscript I

This study characterizes neoantigen-specific $CD8^+$ T cells across three commonly used syngeneic tumor models, namely the mammary (EMT6 and 4T1) and the colon (CT26) carcinoma models. We define $CD8^+$ T cell recognition towards 25, 15 and 18 neoepitopes respectively. Such mapping of spontaneously occurring NARTs towards tumor's neoepitopes can be used to study what factors drive neoepitope immunogenicity in preclinical tumor models.

Syngeneic tumor models have also greatly contributed to the understanding of the immunological mechanisms behind immunotherapy, providing significant discoveries such as the relevance of $CD4^+$ T cell responses in antitumor immunity and the need to include MHC-II binders in vaccination strategies [87]. In addition, various immunization studies across several syngeneic mouse models have contributed to defining characteristics driving neoepitope immunogenicity, although they remain to be better understood [71], [106].

Manuscript II

Understanding what characteristics make a neoepitope immunogenic in the clinic is hampered by the high heterogeneity of human tumors which difficults the task of “finding patterns”. Manuscript II explores previously hypothesized determinants of neoepitope immunogenicity through vaccination of naïve Balb/c mice. Neoepitopes were chosen in the basis of: 1) MHC-I binding capacity; 2) dis-similarity to self; 3) with a missense or frameshift mutation origin; and 4) in absence of a strong MHC-II binding motif within the long peptide sequence. The little number of responses found suggests that larger datasets may be required for defining such features.

On the other hand, neoepitope immunogenicity does not imply that boosting such NARTs results in a therapeutic benefit. Two studies in Lewis Lung carcinoma (LL2) [84] and CT26 models [107] showed that robust neoantigen immunogenic responses can be therapeutically irrelevant, placing syngeneic mouse models as a valuable tool to study resistance to immunotherapy. This way, evaluation of the therapeutic potential of immunogenic neoepitopes by means of e.g., tumor rejection, will further contribute to the understanding of why some NARTs fail to elicit potent antitumor responses.

Pilot study

Chapter 7 summarizes a pilot study conducted in an ovalbumin (OVA)-expressing melanoma B16BL6-OVA model, aiming to optimize a workflow to expand OVA-specific T cells in an Ag-specific manner, and evaluate their tumor-rejection capacity *in vivo* through ACT in combination with anti-PD-1 and anti-CTLA-4 therapy. The ultimate objective is to expand NARTs detected in Manuscript I and validate through ACT their tumor-killing capacity *in vivo* in the relevant syngeneic model.

To date, although syngeneic models fail to mimic the nature and heterogeneity of human cancers, they still provide essential knowledge that can be applied in clinical therapeutic settings.

Chapter 5: Manuscript 1

Assessment of neoantigen-specific $CD8^+$ T cells in murine CB6F1 tumor models

Murine syngeneic tumor models have been widely used in preclinical studies investigating immunogenicity of predicted neoantigens through e.g., immunization. Manuscript I provides a mapping of spontaneously-occurring neoantigen-reactive $CD8^+$ T cells across the commonly used breast cancer (EMT6 and 4T1) and colon carcinoma (CT26) models established in the CB6F1 murine hybrid strain. Owing to the homogeneity of syngeneic tumor models compared to the highly heterogenous human tumors, we believe this characterization provides valuable knowledge to study neoepitope immunogenicity.

The research presented here is an on-going study. We intend to extent the manuscript with further analysis validating the individual responses and their tumor-rejection therapeutic capacity.

Assessment of neoantigen-specific CD8$^+$ T cells in murine CB6F1 tumor models

Authors: Sara Suarez Hernandez[1], Nadia Viborg[$], Trine Sundebo Meldgaard[1#], Annie Borch[1], Tripti Tamhane[1], Amalie Kai Bentzen[1], Nana Overgaard Herschend[1¶], Anne-Mette Bjerregaard[1#], Sine Reker Hadrup[1]

Affiliations:

[1]Department of Health Technology, Technical University of Denmark, Lyngby, Denmark

$Current affiliation: Evaxion Biotech, Hørsholm, Denmark

#Current affiliation: Novo Nordisk, Bagsværd, Denmark

¶Current affiliation: Coloplast, Humlebæk, Denmark

Financial support: This research was funded in part by The Danish Innovation Fund (project NeoPepVac).

Corresponding author: Sine Reker Hadrup, Section for Experimental and Translational Immunology, Department of Health Technology, Technical University of Denmark, Kemitorvet Building 204, 2800 Kgs. Lyngby, Denmark. Phone: +45 35886290. E-mail: sirha@dtu.dk.

Abstract

Neoantigens arise from somatic mutations occurring during tumor development, entailing that neoantigen-recognizing T cells are not subjected to central tolerance. Therefore, neoantigens provide attractive targets for immunotherapies (e.g., cancer vaccines) owing to their potential to mount robust tumor-specific effector responses. However, far from all the predicted neoepitope candidates are presented in the surface of cancer cells and recognized by T cells. Understanding the determinants driving neoantigen-T cell recognition is therefore essential, especially in the context of neoantigen-based vaccines. Here, we characterize neoantigen-reactive $CD8^+$ T cells (NARTs) across EMT6, 4T1 and CT26 syngeneic tumor models established in the CB6F1 murine strain. Utilizing DNA-barcode peptide-MHC multimers, we show endogenous $CD8^+$ T cell recognition towards 25, 15 and 18 neoepitopes respectively. Surprisingly, even if CT26 displays the highest tumor mutational burden and number of expressed predicted H-2 binders; we detect a larger number of NARTs in the EMT6-tumor model. Interestingly, we observe NARTs restricted to $H\text{-}2^b$ molecules not expressed by the tumor cell line, indicating the uptake and cross-presentation by Ag presenting cells from the CB6F1 mice. Checkpoint inhibitor treatment (CPI) targeting PD-1 and CTLA-4 did not significantly alter the neoepitope-recognition landscape, although in certain models, it appears to increase the number of responses and the frequency of pre-existent NARTs. Such knowledge can be used to determine the factors contributing to neoepitopes' immunogenicity and to evaluate strategies that will boost neoepitope-specific $CD8^+$ T cell recognition.

Introduction

Expression of tumor-specific Ags that arise from non-synonymous mutations in tumor cells – so called neoantigens – permit T cells to distinguish malignant cells from the healthy tissue [1]. Furthermore, T cells recognizing them are not subjected to central tolerance, thus holding potential to mount potent antitumor T cell responses and representing attractive targets for immunotherapies. The advent of artificial intelligence and immunopeptidomics have allowed current state-of-the-art prediction tools to rapidly identify the mutational landscape of a particular tumor and its candidate neoantigens (extensively revised in [2]). However, preclinical, and early clinical data from neoantigen-based vaccination strategies suggest that a small fraction of predicted neoantigens are presented on the surface of cancer cells, from which only a minority is recognized by T cells [3], [4]. Therefore, there is a need for defining what characteristics make neoantigens immunogenic, and which of such neoepitopes provide antitumor activity, for which large datasets are required.

Immunocompetent syngeneic tumor mouse models, which harbour subcutaneously inoculated tumors from syngeneic or histocompatible cancer cell lines, are widely characterized and represent a valuable tool to understand NART reactivity (extensively revised in [5]). The whole genome and mutanome of murine tumor cell lines was first published in 2011 for leukemia APL [6], followed by the description of the melanoma B16F10 [7], the colon carcinoma CT26 [8], and the mammary carcinoma 4T1 cell line [9]. From this point, several studies established various syngeneic tumor models on the inbred strains C57BL/6 [3], [4], [7], [10]–[12] and Balb/c [8], [10], [13]–[16] to study neoepitopes involved in tumor-recognition. Most of these studies have been conducted in the context of prophylactic vaccination and prevention of tumor growth, or tumor-regression upon therapeutic vaccination. However, despite some of the beforementioned studies experimentally confirmed presentation of the neoepitope through immunopeptidomics, only a few of them were recognized by neoantigen-specific T cells (NARTs). As an example, Yadav et. al. identified 1290 neoepitopes from a colon carcinoma MC38 syngeneic murine model but only validated 7 pMHCs through mass spectrometry, from which 3 were immunogenic. This reflects the need to describe the neoepitope landscape of commonly used murine tumor cell lines and naturally occurring NARTs in syngeneic tumor models. This knowledge may provide a basis to understand neoepitopes' immunogenicity in preclinical models and ultimately, foster the development of efficient immunotherapies in the clinic.

In this work, we use DNA-barcode peptide-MHC (pMHC) multimers [17] to evaluate the $CD8^+$ T cell neoantigen-recognition landscape of commonly used syngeneic tumor models established in the CB6F1 hybrid strain. To facilitate the induction of T cell responses towards neoepitopes and to boost T cell-mediated tumor killing, tumor-bearing mice received immune checkpoint inhibitor (CPI) treatment comprising anti-PD1 and anti-CTLA-4 antibodies. In addition, we evaluate the

overlap when predicting neoepitopes from cell lines or tumor genetic material and the feasibility of establishing Balb/c and C57BL/6 syngeneic tumor cell lines in the CB6F1 strain. With detection of NARTs specific to 15-25 neoepitopes (representing 2-5% of the pMHC multimer library) in untreated and CPI-treated animals, we map immunogenic NARTs in preclinical models for breast cancer (EMT6 and 4T1) and colon carcinoma (CT26).

Results

Establishment of syngeneic tumor cell lines in the CB6F1 murine strain

By expressing all five histocompatibility-2 (H-2) alleles from its progenitors, the CB6F1 murine strain allows the engraftment of both Balb/c- and C57BL/6-syngeneic tumor cell lines (Figure 1A). Therefore, neoepitope-reactive CD8+ T cells (NARTs) restricted to all five H-2 alleles can be characterized for several syngeneic cell lines in a unifying mouse model. To evaluate whether tumor growth dynamics in CB6F1 mice are comparable to the syngeneic strain, we established CT26 and MC38 colon carcinoma tumor models in CB6F1 mice; and in Balb/c or C57BL/6 mice respectively (Supplementary Figure 1A, B). Anti-PD1 and anti-CTLA-4 CPI treatment was given to facilitate the induction of T cell responses towards neoepitopes and to boost T cell-mediated tumor killing (Supplementary Figure 1A). Isotype-matching control antibodies were given to control mice (see Methods for details). As deployed on Supplementary Figure 1B, both CT26 and MC38 cell lines successfully engrafted in the CB6F1 model, although CT26 tumors in CB6F1 mice receiving isotypes grew significantly slower compared to Balb/c. No differences were seen in between MC38-CB6F1 and MC38-C57BL/6. In addition, CPI responses from both CB6F1 models were comparable to the syngeneic strains.

Next, to evaluate potential differences in NARTs between steadily growing tumors and CPI-induced regressing tumors, we selected the three biggest or the three smallest tumors from the control or CPI-treated groups respectively (Figure 1C). Therefore, Figure 1D represents differences in tumor growth between samples included in our NART-screening analysis rather than sensitivity to CPI treatment. Splenocytes from the selected mice were also analysed.

To monitor the effect of CPI antibodies on T cell activation, splenocytes from CT26 and 4T1 tumor-bearing mice were stimulated with the respective tumor cell line and intracellularly stained for INFγ and TNFα. There was no clear effect on higher activation of $CD8^+$ T cells upon CPI treatment, as only one CT26 sample showed a convincing INFγ response (Supplementary Figure 1C). Furthermore, both splenocytes and tumors from the EMT6 model were characterized with a phenotype panel including various differentiation and activation surface markers (refer to Methods for details). Despite not significant, CPI treatment allowed greater infiltration of $CD8^+$ T cells over $CD4^+$ T cells into EMT6 tumors (Supplementary Figure 1D), which showed a functionally exhausted $PD1^+TIM\text{-}3^+$ phenotype (Supplementary Figure 1E). Such tendencies were not seen in the spleen (data not shown).

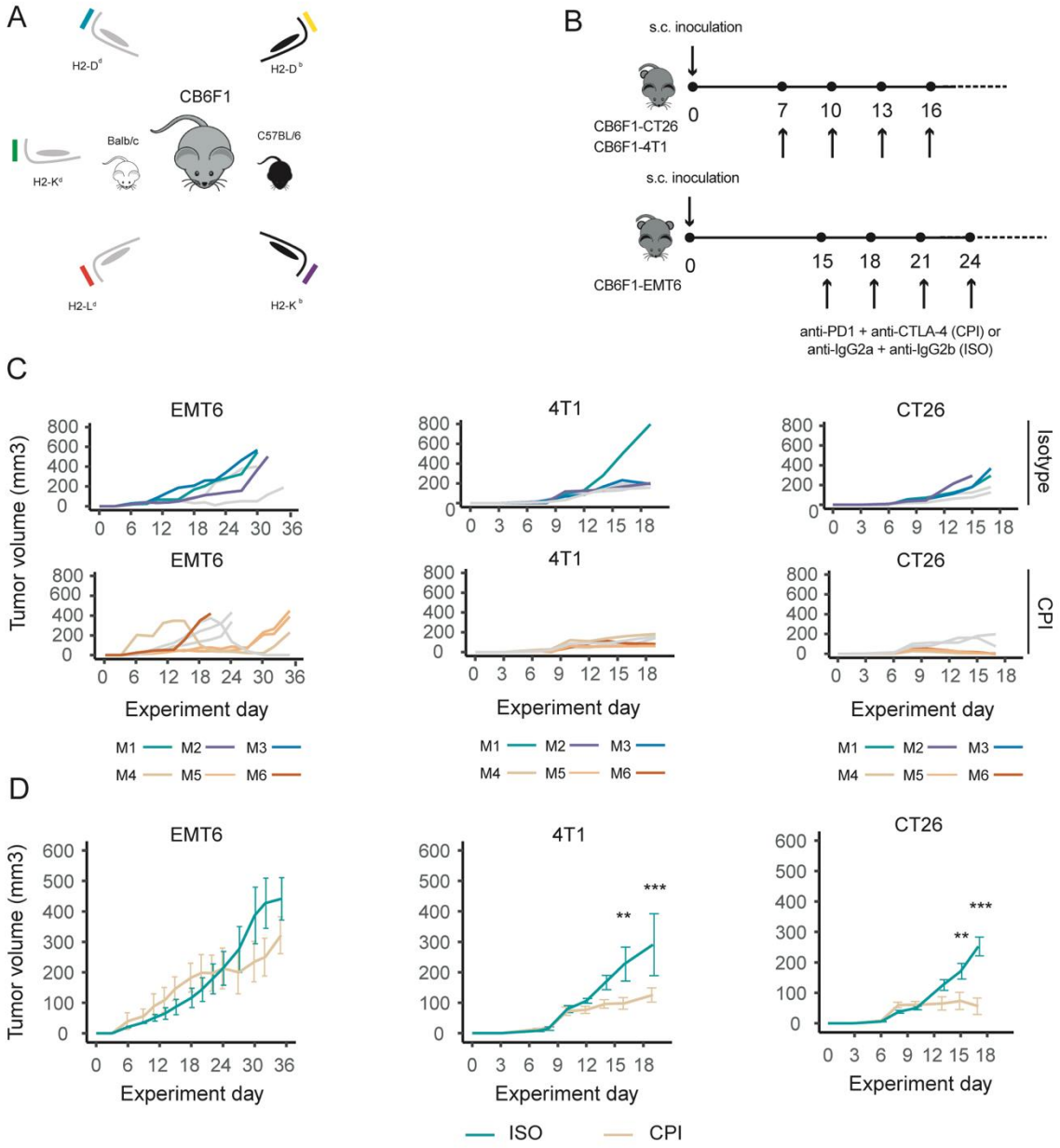

Figure 1: Establishment of syngeneic tumor cell lines in the CB6F1 murine strain.

A) Schematic overview of the H-2 alleles of the CB6F1 hybrid model. A mixed-effect linear model considering tumors a random effect and Bonferroni-corrected denotes p-values <0.05 and <0.01, as *, and ** respectively. **B)** Experimental *in vivo* design. **C)** Average growth of selected tumors throughout treatment with CPI or ISO (n=3; n=4 EMT6-CPI). **D)** Individual tumor growth plots. The three biggest tumors in the ISO-treated group and the three smallest in the CPI-treated group were selected for neoepitope screening (coloured).

Neoepitope prediction

Neoepitopes were predicted with MuPeXi software [18] using whole exome sequencing (WES) and RNAseq from the EMT6, 4T1 and CT26 tumor cell lines (Figure 2A, refer to Methods for details). DNA and RNA from CT26 tumors were also isolated to compare neoepitopes predicted from the cell line and tumors established in mice. CT26 displayed the highest tumor mutational burden (TMB) based on number of non-synonymous mutations, resulting in a greater number of expressed neoepitopes (>0.1 transcripts per million, TPM) predicted to bind all five H-2D^{b}, H-2K^{b}, H-2D^{d}, H-2K^{d} and H-2L^{d} alleles (Eluted Ligand (EL) %Rank score <2[19], Figure 2B). Expressed H-2 binders mainly derived from mis-sense mutation events, followed by frameshift mutations and insertions and deletions (indels) (Figure 2C). Next, neoepitopes were selected based on their respective H-2 binding affinity and expression level for inclusion in the pMHC multimer library (Figure 2D). Neoepitope libraries for the EMT6 and CT26 models comprised 100 candidates per H-2 allele with the lowest predicted EL %Rank score) and >0.1 TPM. Owing to the variable mutational burden, the EL %Rank of the included peptides varied accordingly, with 4T1-derived neoepitopes included despite a low EL %Rank to reach a total of 100 neoepitopes per H-2 allele (Figure 2E). As deployed on Figure 2F, the library was mostly comprised of mis-sense mutations (Figure 2F).

Furthermore, with the concern that the neoepitopes predicted from the cell line grown *in vitro* might not represent those expressed by the tumor *in vivo*, we investigated how conserved the CT26 neoepitope load was between the cell line and an excised tumor. Additionally, we included another CT26 cell line from a different provider. The overlap between the predicted neoepitopes is visualized in Figure 2G, showing that approximately 85% of the neoepitope candidates were shared across both cell lines and the tumor. This way, the chosen neoepitope candidates are representative of the tumors' neoepitope landscape. Investigating NARTs in the tumor-bearing mice will clarify whether they are presented in the context of H-2 molecules and recognized by CD8^{+} T cells *in vivo*.

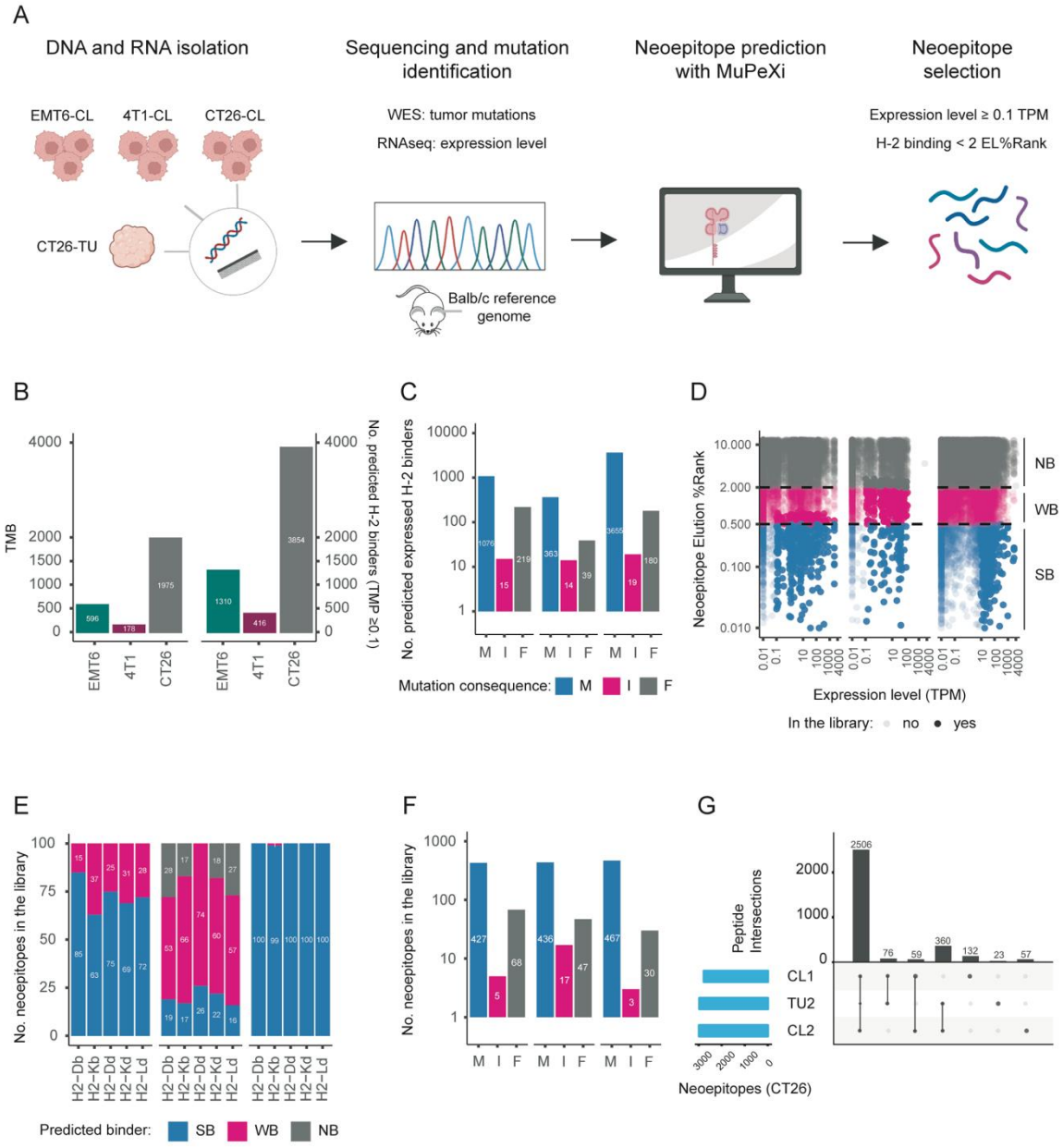

Figure 2: Neoepitope prediction and selection.

A) Overview of neoepitope prediction and library selection. **B)** TMB across cell lines and number of expressed predicted neoepitopes (TPM ≥0.1) with predicted H-2 binding capacity (EL %Rank <2). **C)** Distribution of predicted expressed H-2 binders across mutation type (M: Missense; I: Insertion; F: Frameshift). **D)** Unfiltered neoepitope prediction output coloured based on predicted H-2 strong binders (SB, EL%Rank <0.5); weak binders (WB, 0.5< EL%Rank <2); and non-binders (NB, EL%Rank >2), and whether selected for the library. **E)** Distribution of neoepitopes per H-2 allele included in the library coloured by predicted H-2 binding capacity. **F)** Distribution of library neoepitopes across mutation types. **G)** Overlap between neoepitopes predicted from two different CT26 tumor cell lines and one tumor counterpart. Figure A created with Biorender.com.

Identification of neoepitope-specific CD8$^+$ T cells

Based on the selected neoepitopes, we prepared DNA-barcode pMHC multimer libraries [17] to screen for a total of 500 pMHC complexes per tumor cell line (Supplementary Figure 2A). To ensure functionality of the assay, control epitopes for each H-2 allele were included on the panel and a spike-in sample comprising known proportions of specific CD8$^+$ T cells stained with the full panel as we describe in [20]. In addition, the CT26 panel included the dominant H2-L^d-restricted AH-1 epitope endogenously expressed by CT26 tumors as a functional control of the multimer panel [21]. It should be noted that both spleen and tumor samples from the EMT6 and 4T1 cell lines were analysed, while we only investigated CT26 splenocytes.

The DNA-barcode pMHC multimer technology allows detection of >1000 neoepitope-specific CD8$^+$ T cells in a single staining reaction by tagging each pMHC-multimer with a unique DNA barcode. In addition, pMHC multimers are comprised of a phycoerythrin (PE) fluorescent labeled dextran backbone, which allows fluorescence activated cell sorting (FACS) of CD8$^+$ T cells recognizing pMHC multimers. This way, neoepitopes being recognized by CD8$^+$ T cells can be indirectly recovered through sequencing the barcodes present in the sorted population. By keeping a sample of the DNA barcode pMHC multimer pool used for staining (referred to as baseline) the recognized neoepitopes can be inferred by comparing read-counts of a given barcode in the sorted cell sample to the distribution in the pMHC multimer mixture used for staining. This enrichment is shown as the logarithmic fold change (log_2FC) for the three studied models (Figure 3A-C), where significantly enriched barcodes are considered as the neoepitopes being recognized by the sorted CD8$^+$ T cells (referred to as responses, see Methods for details). The gating strategy and validation of the functionality of the panel by detection of the control epitopes in the spike-in sample is illustrated in Supplementary Figure 2B, C).

Figure 3: Identification of neoepitope-specific CD8$^+$ T cells.

Log_2 of sequenced pMHC associated barcodes enriched over the input library for each tumor model: **A)** EMT6; **B)** 4T1; and **C)** CT26 across ISO- and CPI-treated mice (rows) and spleens and tumors (columns). Coloured dots represent significantly enriched barcodes in the sorted population over the input library (log_2 >2, p-value <0.001and all input triplicate counts >20). Size represents the estimated frequency of the neoepitope-specific CD8$^+$ T cell population (except for the tumor in plot A). Labelled responses are the most dominant and/or conserved across all samples. **D)** 4T1_53 NARTs appear more frequent in tumors than in spleens. In between brackets, estimated frequency derived from multimer screening. **E)** Venn diagrams illustrating overlaps between detected NARTs in the individual mice. ISO: isotype; CPI: checkpoint inhibitor; M: mouse.

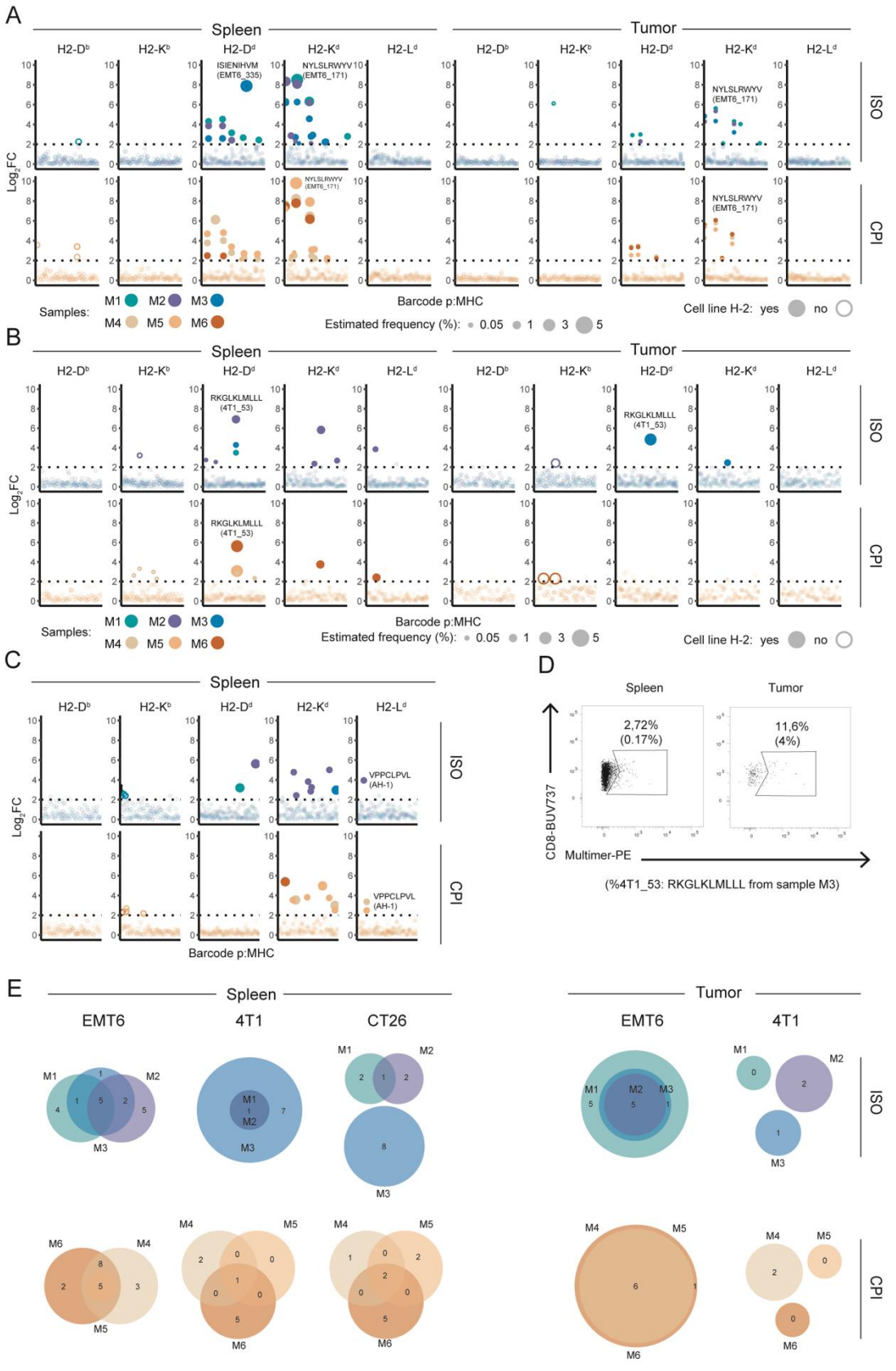
A
Spleen
Tumor
H2-Db
H2-Kb
H2-Dd
H2-Kd
H2-Ld
ISIENIHVM (EMT6_335)
NYLSLRWYV (EMT6_171)
ISO
CPI
Log2FC
Samples:
M1 M2 M3
M4 M5 M6
Barcode p:MHC
Estimated frequency (%): 0.05 1 3 5
Cell line H-2: yes no
B
RKGLKLMLLL (4T1_53)
C
VPPCLPVL (AH-1)
D
2,72% (0.17%)
11,6% (4%)
CD8-BUV737
Multimer-PE
(%4T1_53: RKGLKLMLLL from sample M3)
E
EMT6
4T1
CT26

From the 500 predicted neoepitopes included in the multimer library for each cell line, we detected NARTs specific for 25 EMT6-, 15 4T1- and 18 CT26-neoepitopes (outlined in Supplementary Table 1 and Figure 3A-C respectively). Most of the responses were restricted to H2-D^d and H2-K^d alleles across all cell lines, with only one response detected on H2-L^d for 4T1 and the previously described AH-1 CT26 epitope. Interestingly, all tumor models showed NARTs restricted to H-2^b alleles despite not being expressed by the tumor cell lines, indicating cross-presentation of neoantigens by Ag presenting cells. The estimated frequency of NARTs can be calculated from the barcode sequencing data by the following formula: $\%PE^+$ $CD8^+$ T cells x $\frac{\text{readcounts (barcode A)}}{\text{readcounts (barcode A+B+C)}}$; in which A, B and C are the detected responses in the respective sample. Owing to a technical issue, all $CD8^+$ T cells in EMT6 tumors were sorted, implying that the estimated frequency deployed on Figure 3A (Tumors) does not represent the NART proportion in tumors. NARTs were found in varying frequencies ranging from approximately 0.007%-5% of the total $CD8^+$ T cells. Interestingly, two neoepitopes (EMT6_335 and EMT6_171) dominated the NART response in the EMT6 model, accounting for approximately half of the NARTs in the respective samples (Figure 3A). Next, one NART response (4T1_53) was also shared across all splenocyte samples in the 4T1 model (Figure 3B). For CT26, while AH-1 was the unique response in H2-L^d, it did not dominate the Ag-specific response as other neoepitopes in the sample were found in similar frequencies (Figure 3C).

Even though we cannot compare NART frequencies across spleens and tumors of the EMT6 model, spleens appear to display a broader breadth of NARTs compared to tumors in both EMT6 and 4T1 models. On the 4T1 model, detection of 4T1_53 in both compartments of an individual mouse (M3, blue) suggests that NARTs locate in higher frequencies in the tumor (Figure 3D). As the proportion of multimer-specific CD8+ T cells can be misleading owing to the little number of CD8+ T cells in the sample, the frequency retrieved from the barcoding sequencing data is represented in brackets.

Interestingly, some NARTs were more shared across animals than others, indicating a certain level of inter-animal variation despite the homogeneity of inbreed strains and immortal cell lines (Figure 3E).

Lastly, one of the detected CT26 NARTs (CT26_175, refer to Supplementary Table 1 for details) was previously defined to be immunogenic and trigger $CD8^+$ T cell responses via INFγ ELISPOT [10]. In addition, we also found the *Nxf1* mutation to result in immunogenic neoepitopes in the 4T1 model, from which a different neoepitope has previously been defined to be immunogenic in the EMT6 model [15]. An overview of all mutations, including information on T cell recognition is provided in Supplementary Figure 3.

Effect of CPI therapy on detection of neoepitope-specific CD8⁺ T cells

We next evaluated whether anti-PD1 and anti-CTLA-4 therapy had an impact on the endogenous NART landscape. Despite no significant differences, CPI appeared to increase the breadth of NARTs in EMT6 spleens and tumors (Figure 4A), while it boosted their frequency in 4T1 spleens (Figure 4B). Due to difficulties in estimating frequency in 4T1 tumors, and in absence of NARTs restricted to the same neoepitope in tumors from ISO- and CPI-treated mice, the same comparison cannot be drawn. Interestingly, no differences were observed in the CT26 model despite showing the greatest difference in tumor growth between the ISO- and CPI-treatment groups *in vivo* (refer to Figure 1D).

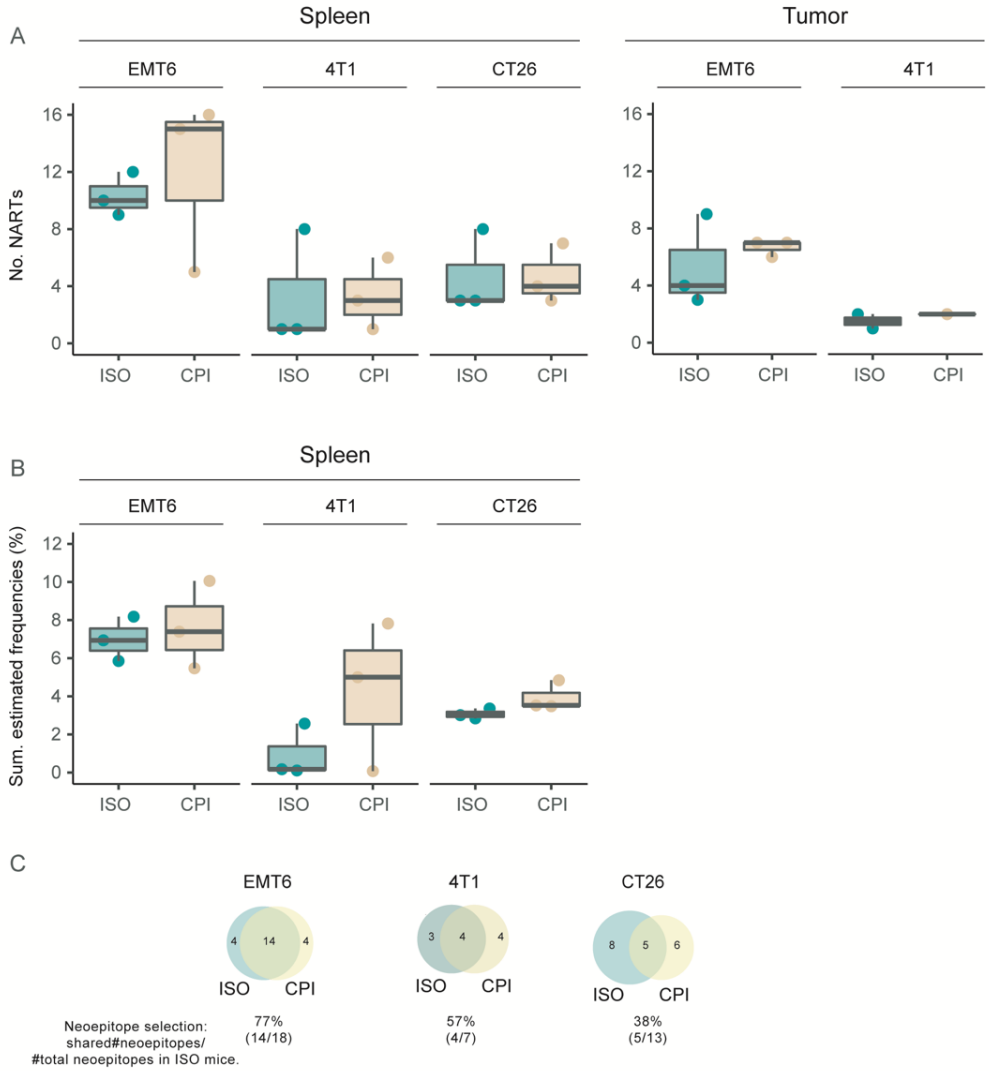

Figure 4: Effect of CPI therapy on detection of neoepitope-specific CD8⁺ T cells.

A) No. NARTs detected in ISO- and CPI- treated animals across all models (EMT6, 4T1, and CT26) in spleens and/or tumors. **B)** Sum of the frequencies of all NARTs detected in mice receiving ISO- or CPI. **C)** Venn diagrams illustrating overlaps between detected NARTs across treatments on each of the models. Neoepitope selection represents the proportion of NARTs detected in the ISO-treated mice that is conserved in the CPI-treated animals. Non-parametric Kruskal-Wallis t-test. No significant differences.

Additionally, we investigated the proportion of NART responses found in ISO-treated animals that were also detected in CPI-treated animals (referred to as “Neoepitope selection” in Figure 4C), as potential changes might be indicative of the modulation of NART responses by CPI treatment (e.g., immunoediting). Interestingly, 77%, 57% and 39% of NARTs detected in control spleens from the EMT6-, 4T1- and CT26-models respectively were also found in spleens from CPI-treated mice, indicating a greater shift in NART populations on the CT26 tumor model (Figure 4C). We could not describe whether the same occurs in tumors owing to the previously mentioned limited data.

T cell recognized neoepitopes do not show distinct patterns explaining their immunogenicity

Lastly, we evaluated whether T cell recognized neoepitopes shared common characteristics that would recapitulate previously described patterns of $CD8^+$ T cell recognition. However, no differences in eluted ligand or binding affinity rank scores, nor in self-similarity scores were observed [22], [23] (Figure 5A-C). In addition, most of the neoepitopes screened showed similar elution rank scores to the unmutated self-epitope, meaning that the studied mutations were predicted MHC-I conserved binders based on the prediction scores [23] (Figure 5D). Next, we wondered whether responses would cluster among neoepitopes with stronger MHC-I predicted binding capacity and high expression levels, as it was previously shown in patients from metastatic urothelial cancer [24], although detected and undetected responses were similarly scattered in the plot (Figure 5E). Lastly, the distribution of the responses across the mutation types matched the proportions from the selected neoepitopes in the library, with most NARTs recognising neoepitopes arising from mis-sense point-mutations.

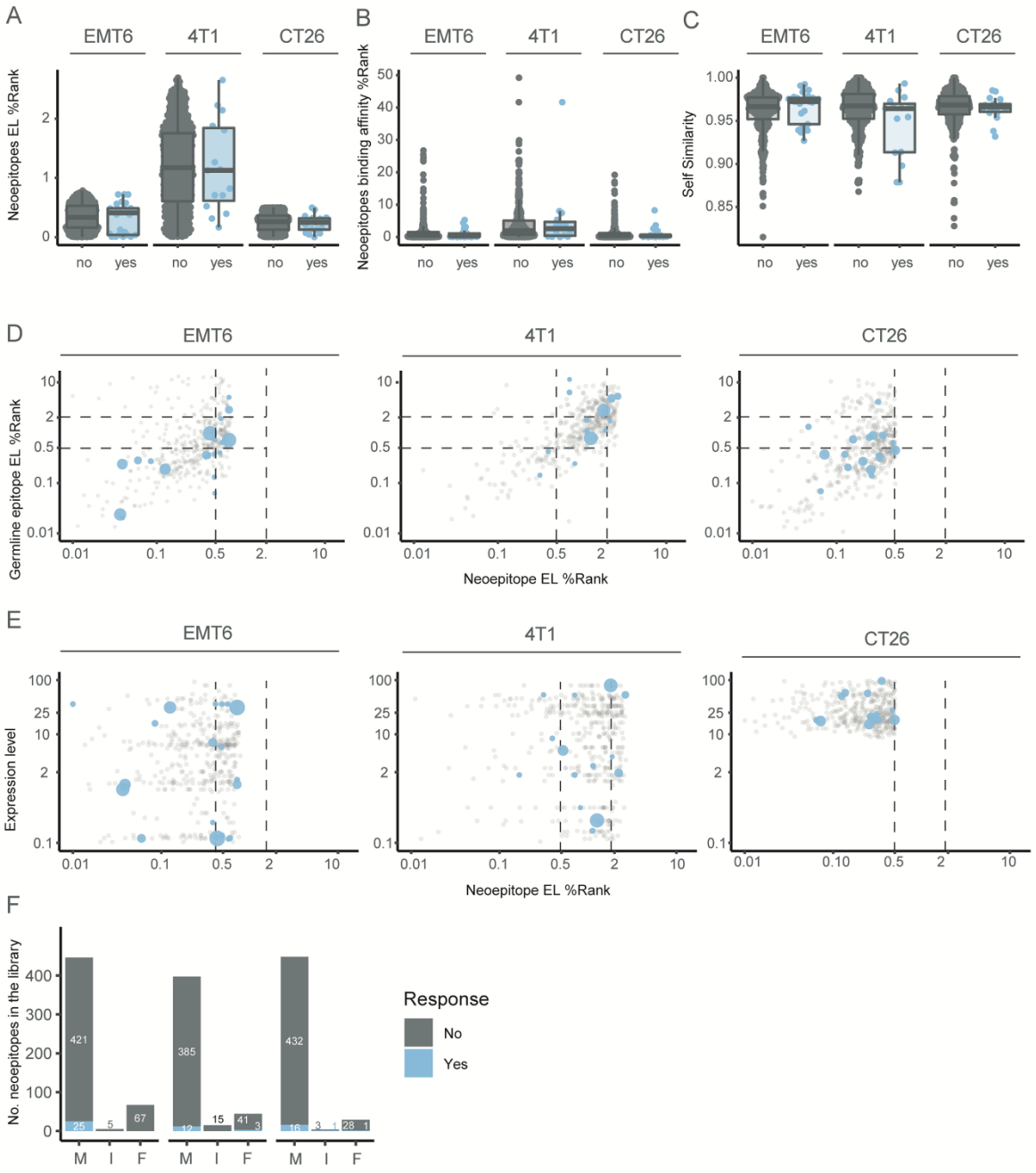

Figure 5: T cell recognized neoepitopes do not show distinct patterns explaining their immunogenicity. **A)** EL %Rank score; **B)** BA %Rank score; and **C)** Self Similarity score grouped according to T cell recognition. **D)** EL %Rank score for neoepitope and normal germline epitope colored by T cell recognition. **E)** EL %Rank score and expression level (TPM) of the neoepitopes colored according to T cell recognition. **F)** Distribution of predicted neoepitopes and T cell recognition across mutation types (M: Missense; I: Insertion; F: Frameshift).

Discussion

Here we performed a high-throughput analysis of NART recognition towards 500 neoepitope candidates predicted from the commonly used EMT6, 4T1, and CT26 syngeneic tumor cell lines. Firstly, we observed that neoepitopes predicted from *in vitro* grown tumor cell lines greatly overlap with those predicted from *in vivo* established tumors. We showed that EMT6 displayed the highest breadth and frequency of NARTs; despite CT26 having the highest TMB and predicted neoepitope load. Overall, we detected a total of 25-EMT6, 15-4T1, and 18-CT26 immunogenic neoepitopes in spleens and/or tumors. Interestingly, while all NARTs found in the CT26 model appeared similarly enriched, 1-2 NARTs dominated the $CD8^+$ T cell recognition of EMT6 and 4T1 neoepitopes. CPI therapy revealed very few NART responses otherwise absent in untreated mice. Likewise, some responses were solely found in spleens (where a higher breadth of NARTs was observed), which would have been missed if studying only the tumor compartment. We further showed that previously defined determinants of immunogenicity did not recapitulate the observed T cell recognition of neoepitopes. Lastly, we demonstrated the feasibility to engraft both Balb/c and C57BL/6 syngeneic tumor cell lines in the CB6F1 murine strain, which might be particularly helpful for preclinical investigation of neoepitope recognition.

Our observation that the predicted CT26 neoepitope candidates are conserved across different *in vitro* grown CT26 cell lines and *in vivo* established CT26 tumors, provides new insights to previous studies describing differences in certain immunological gene pathways (e.g., Ag presentation) in between tumors and cell lines [25]. Differences in the mutanome and transcriptome of *in vitro* grown tumor cell lines and *in vivo* established tumors are expected, as new mutations may arise during tumorigenesis and e.g., MHC-I expression might be downregulated during immunoediting [26]. However, neoepitopes appear to remain similar at the mutation and transcript level, indicating that they may not be a mechanism of immune evasion. It would be interesting to investigate whether they also remain constant at the surface presentation level through immunopeptidomics.

Mutation identification and neoepitope prediction with MuPeXi software revealed a higher TMB and neoepitope load for CT26, followed by EMT6 and 4T1. This observation is in line with previous studies [8], [9], [15] which have further shown that carcinogen-induced tumor cell lines such as CT26 bear higher TMBs than the virus-induced 4T1 and EMT6[25]. As shown for human cancers, a higher TMB yielded a higher number of predicted neoepitopes in these models [27], although it did not translate into a larger number of detected NARTs. Instead, EMT6 showed the largest breadth of detected NARTs, even though the total neoepitope-specific response was mainly dominated by the EMT6_171 neoepitope, which represented 40-50% of the EMT6-specific $CD8^+$ T cells. Interestingly, this dominant response was shared across all the analysed animals. The T cell recognized neoepitopes did not display differences in gene expression levels, suggesting that

transcript expression might not correlate with neoepitope presentation *in vivo* in these models. In this line, the detected responses did not display distinct characteristics previously used to describe patterns of immunogenicity [22], [24], [28]. As an example, it has been described that a higher proportion immunogenic neoepitopes arise from frameshift mutations in renal cell adenocarcinoma patients [29]. However, most of the responses found in the present study derived from mis-sense mutation events, followed by frameshift and indels, thus resembling the proportions in the selected library (refer to Figure 2F).

It should be noted that the high frequency of NARTs detected in these preclinical models contrast with the lower frequencies described in similar screenings in human cancers[24], [29]. One possible explanation is the higher TMB detected in the syngeneic cell lines compared to the respective human cancer they model, which have shown 5-10 order higher TMBs than the human counterpart [25]. This suggests that syngeneic tumor cell lines appear intrinsically more immunogenic than human tumors of the same type, which should be considered when interpreting translational results. Whether this translates into higher frequencies of NARTs in syngeneic tumors compared to human tumors cannot be concluded from this study in lack of a similar screening in the respective human cancer counterpart. In this line, NART screening of metastatic urothelial cancer patients showed that a broadening in the number of pre-existent NARTs after anti-PD-L1 treatment was predictive of CPI response [24].While we cannot draw a strong conclusion on this regard from our analysis because we did not screen the same animals prior and after treatment, CPI treatment appeared to enhance the number of responses in the majority of EMT6 mice, especially on the spleens. By contrast, no difference in the number of NARTs was observed between CT26 mice bearing growing tumors and CPI-induced regressing tumors. However, a lesser number of the NARTs detected in untreated CT26 mice was present in the CPI-treated animals undergoing tumor-rejection. Whether these NARTs are the ones driving tumor-rejection needs to be further studied. In view that the benefit of this dual CPI treatment in the CT26 model has been defined to be driven by anti-CTLA-4 depletion of Tregs [25], [30], further experiments are required to evaluate the contribution of NARTs to CT26 tumor-killing. This way, analysing NARTs present in animals with different tumor growth kinetics would be interesting to explore such contribution. Likewise, further experiments are required to validate the therapeutic potential of the detected responses through e.g., adoptive cell transfer into tumor-bearing mice, and assess the extent to which infiltrating cells are exhausted and dysfunctional.

Our observations of a larger breadth of NARTs in EMT6 and 4T1 spleens compared to tumors supports previous reports describing the relevance of analysing neoepitope recognition in the periphery rather than in tumors alone [25]. Owing to the role of cross-presentation in priming antitumor immunity, and the fact that many immune-evasion mechanisms could prevent NARTs from infiltrating the tumor or from being present in sufficient numbers to allow detection, relevant

NART responses could be missed when focusing the analyses on tumors alone. Along these lines, and additional evaluation of the NART landscape in tumor draining lymph nodes (dLN) could be interesting, due to being the source of cross-primed tumor-specific T cells and their relevance in reflecting response to CPI [31].

In addition, the absence of detection does not necessarily imply that the neoepitopes are not presented by the tumor. They might be presented below the required threshold levels to trigger priming of naïve $CD8^+$ T cells and instead, require vaccination to be recognized by memory $CD8^+$ T cells as suggested in [32]. In addition, focusing the selection on other parameters rather than binding affinity and expression levels alone might also broaden the detection of other immunogenic candidates.

Lastly, tumor establishment in the CB6F1 murine strain allowed recognition towards H-2^d and H-2^b neoepitopes, despite the latter not being expressed by the tumor cell line. This finding suggests cross-presentation of tumor-derived Ags by the host's APCs, and we believe it might comprise a valuable model for e.g., the study of cross-presentation in antitumor immunity. In addition, owing to the well-described type 1/type 2 $CD4^+$ T helper cells (T_H1/T_H2) bias between the C57BL/6 and Balb/c strains respectively [33] – and the implications of T_H1-$CD4^+$ T cells in the anti-tumor killing capacity of cytotoxic $CD8^+$ T cells [10], [34] – unifying the study of immunotherapeutic interventions in the T_H1/T_H2 balanced CB6F1 strain may prove of relevance. This might be of particular importance when comparing immunogenicity of tumor cell lines syngeneic to either Balb/c or C57BL/6, such as CT26 or MC38. On these grounds, it is hypothesized that a shift towards a T_H1 tumor microenvironment TME in the CB6F1 model compared to Balb/c (but not to C57BL/6) might be responsible for the delayed tumor growth seen in the CT26-CB6F1 model. However, a phenotypical analysis is required to evaluate the immunological differences between CT26-CB6F1 and CT26-Balb/c.

Overall, we define neoepitopes that are experimentally recognized by CD8+ T cells in relevantpreclinical models. In addition, we show that CPI does not significantly boost detection of otherwise absent NARTs. Instead, a lower fraction of the NARTs detected in untreated tumor-bearing mice was found in the CPI-induced regressing counterpart. Whether these NARTs are the ones driving therapeutic response to CPI remains to be defined. In addition, previously defined determinants of immunogenicity did not recapitulate the detected responses here. However, these neoepitopes may provide valuable knowledge to define patterns of immunogenicity when analysed on larger datasets. Given that preclinical tumor models are highly homogeneous in comparison to human tumors, we believe that mapping the neoepitope recognition landscape of such models will contribute to defining the determinants of neoepitope immunogenicity.

Furthermore, this complete mapping of T cell recognized neoepitopes in syngeneic tumor model can facilitate pre-clinical evaluation of neoepitope targeting immunotherapeutic strategies.

Materials and Methods

Mice

8 to 10 weeks old female Balb/cByJRj and C57BL/6JR were purchased from Janvier Labs (Le Genest-Saint-Isle, France). Age-matching female CB6F1 mice were purchased from Envigo (Netherlands). All animals were housed at the animal facility at the Technical University of Denmark and all experiments conducted in accordance with the Danish National Committee for the Protection of Animals used for Scientific Purposes. An amendment of such permit was filed allowing larger tumors in the EMT6 model. Each group was kept in separate cages with a maximum of six animals per cage. Different number of animals were used in different experiments and are specified in the figure legends.

Cell lines

Balb/c CT26 colon carcinoma cell line (ATCC, CRL-2638), and 4T1 (ATCC, CRL-2539) and EMT6 (ATCC, CRL-2755) breast cancer cell lines were cultured in R10/Pen-Strep medium (RPMI1640, Fischer Scientific, Cat. No. 61870044, 10% heat inactivated fetal calf serum (FCS, Fischer Scientific, Cat. No. 10500064) and 1% Penicillin-Streptomycin (Pen-Strep, Life Technologies, Cat. No. 15140122)). MC38 (Kerafast, Cat. No. ENH204-FP) was cultured following manufacturer's recommendations in Dulbecco's Modified MEM (DMEM, Cat. No. 11965084) supplemented with 10% FCS, 2mM glutamine (ThermoFisher, Cat. No. 25030081), 0.1mM non-essential amino acids (Thermo Fisher, Cat. No. 11140035), 1mM sodium pyruvate (Thermo Fisher, Cat. No. 11360039), 10mM Hepes (Thermo Fisher, Cat. No. 15630049), 50µg/mL gentamycin (Thermo Fisher, Cat. No. 15630049) and 1% Pen-Strep. Cells were mycoplasma-free. Cells were cultured at 37ºC and 5% CO_2 and split when confluent. Genomic DNA and total RNA were purified from CT26, 4T1 and EMT6 cell lines and CT26 tumors using AllPrep DNA/RNA Mini Kit (Qiagen, Cat. No. 80204).

Tumor models

Mice were anesthetized in a chamber under isoflurane and 2% oxygen and shaved on the back. Across all models, tumor cells in 150µl PBS were subcutaneously inoculated either in the right flank or in both flanks of the mice. Loaded syringes were kept on ice but adjusted to room temperature (RT) and mixed prior inoculation. Tumor growth was monitored three times a week using a digital caliper and tumor volume was calculated using the following formula: tumor volume = $\frac{\text{length x width}^2}{2}$. CT26 and MC38: $5x10^5$ cells (CT26) and $5x10^5$ cells (MC38) were inoculated on the right flank of Balb/c and C57BL/6 mice respectively. No tumors were collected from these mice in lack of digestion media *in house*. 4T1: $5x10^5$ cells were inoculated in both flanks of CB6F1 mice to increase the number of tumors while minimizing the number of animals used. All CT26, MC38 and 4T1 mice were euthanized when a single tumor reached the maximum allowed size of 12mm

in any diameter. EMT6: $2x10^5$ cells were inoculated in both flanks of CB6F1 mice. Due to strong side differences on tumor size in the 4T1 model, EMT6 tumor cells were loaded into syringes without a needle to prevent cell shearing. When two tumors were injected, needles were carefully changed in between injections. Mice were euthanized when tumors reached 20mm in any diameter or when showing signs of discomfort or tumor ulceration. CPI treatment comprised 200µg of anti-PD1 (Nordic BioSite, RMP1-14, Cat. No. BE0146) and 200µg of anti-CTLA-4 (Nordic BioSite, 9H10, Cat. No. BE0164) antibodies or 200µg of each relevant isotype control antibody (ISO); anti-IgG2a (Nordic BioSite, C1.18.4, Cat. No. BE0085) and anti-IgG2b (Nordic BioSite, MPC-11, Cat. No. BE0086) respectively. Antibodies were diluted in 200µl PBS per injection and administered intraperitoneally (i.p.) on days 7, 10, 13 and 16. Animals were randomized based on tumor volume on the day prior treatment initiation. For 4T1 and EMT6 the average of both sides was considered. Animals were assigned to CPI or the ISO control groups so that the difference on average of tumor size was kept to minimum. All mice were euthanized by cervical dislocation when reaching $2000mm^3$ in size. Some EMT6-bearing mice reached earlier humane endpoint due to tumor ulceration, thus tumor growth data is only shown and analysed for tumors reaching $350mm^3$ in volume. Regarding 4T1, variation in tumor size on the left side (first injection site) was minimal, while it markedly increased on the right side (second injection site, data not shown). Therefore, right-side tumors were excluded from analysis.

Generation of peptide-specific control samples

We generated samples with a known proportion of Ag specific $CD8^+$ T cells to act as internal controls of the binding of murine H-2 multimer libraries. For the different murine MHC-I monomers, the following Ag-specific responses were induced through intraperitoneal vaccination formulated in the CAF09b adjuvant (200µg/dose cationic lipid DDA, 40µg/dose mycobacterial cell wall lipid MMG-1, 40µg/dose toll like receptor-3 analogue Poly(I:C), kindly gifted by Dennis Christensen, Statens Serum Institute, Denmark): H2-Db: C57BL/6JRj mice were injected with 80µg HPV16 $E7_{49-57}$ (RAHYNIVTF [35]); H2-Kb: C57BL/6JRj mice were injected with 80µg $Ovalbumin_{257-264}$ (SIINFEKL [36]); H2-Dd: BALB/cJRj mice were injected with 80µg HIV Env $gp160_{311-320}$ (RGPGRAFVTI [37]); H2-Kd: BALB/cJRj mice were injected with 80µg Influenza $HA_{518-526}$ (IYSTVASSL, [38]H2-Ld: BALB/cJRj mice were injected with 80µg LCMV $NP_{118-126}$ (RPQASGVYM, [39]).

Cell isolation and preparation

Spleens and tumors were collected on ice in R10 or in complete DMEM (cDMEM, DMEM supplemented with 10% FCS) respectively. Spleens were mechanically disaggregated with a plunger and passed through a 70µm strainer on a 50mL Falcon tube. Tumors were cut in small pieces (~1mm in diameter) with scissors and scalpel and enzymatically digested in 4mL cDMEM supplemented with 5µg collagenase IV (Fisher Scientific, Cat. No. 17104019) and 100µg/mL

DNAse I (Fisher Scientific, Cat. No. 90083) for 45min at 37ºC 5% CO_2. The enzymatic mix was prepared prior use. Collagenase IV was kept refrigerated in powder, weighted, and sterile-filtered prior use. Cells were washed twice in R10 or cDMEM at 1500rpm for 5min at 4ºC. A maximum of $10x10^6$ cells per cryotube were cryopreserved in 1ml freezing media (FCS supplemented with 10% dimethyl sulfoxide (DMSO), Sigma-Aldrich, Cat. No. C6164) and stored at -80ºC in a Mr. Frosty (Corning, Cat. No. 432001) for 24h prior transfer to -180ºC nitrogen tank for long-term storage.

Neoepitope prediction and selection

Genomic DNA and total RNA were sequenced using a Hiseq NGS platform by CDGenomics (USA). To predicted potential neoepitopes, the Genome Analysis Tool Kit (GATK) best practice version 3.8.0 [40] have been used. The WES and RNA sequencing files were pre-processed with Trim Galore version 0.4.0 [41] and quality check with FastQC version 0.11.2 [42]. The trimmed WXS reads were aligned with Balb/c reference genome from Ensemble (release-89) [43] using Burrows-Wheeler Aligner version 0.7.1 [44] with default parameters. The aligned files were sorted with samtolls [45]Samtolls [45] version 0.1.18 and duplicated reads were marked with Picard-tools [46] version 2.9.1. Base-recalibration from GATK version 3.8.0 [47] were applied for all files and mutations called with MuTect2 [48] from GATK. The trimmed RNA sequencing reads were aligned with Kallisto [49] version 0.42.5 and ranscripts per million (TPM) for each transcript were obtained. The neoepitopes were predicted using MuPeXi 1.2.0 [50] with Mutect and Kallisto output as input files to following H-2 alleles: H-2D^d, H-2K^d, H-2L^d, H-2D^b, H-2K^b. Peptides were selected according to the expression from the corresponding transcript and the binding affinity to the corresponding MHC-I allele using netH2pan [51].NetH2pan [51]. Specifically, neoepitopes with eluted ligand (EL) %Rank score <0.5 were sorted based on decreasing TPM within each H-2 allele, and the top 100 chosen to be included in the neoepitope library.

***In vitro* folding and purification of murine H-2 monomers**

The *in vitro* folding of murine H-2 molecules was performed using photocleavable ligand as described above and previously [3]. To setup the refolding reaction, heavy chains (1 µM) and β2m (2 µM) were diluted in a folding buffer composed of 0.1M Tris pH 8.0, 500 mM L-Arginine-HCl, 2 mM EDTA, 0.5 mM oxidized glutathione and 5 mM reduced glutathione with 60 µM respective photocleavable peptide (H2-Db: ASNEN J ETM; H2-Kb: FAPGNY-J-AL; H2-Dd: RGPGRA-J-FVT, H2-Kd: IYSTV J SSL; H2-Ld: YPNVNIH J F). After folding for 3-5 days at 4°C, folded protein was upconcentrated with a 10KDa cut off membrane filters (Vivaflow-200, Sartorius, Cat. No. VS0601) and biotinylated using BirA biotin-protein ligase standard reaction kit (Avidity, Colorado). Finally, folded biotinylated monomer complexes were purified with size exclusion chromatography using HPLC (Waters Corporation, USA), and aliquots were stored at 80°C until further use.

Generation of pH-2 monomers

All peptides for pH-2 multimer libraries were purchased from Pepscan (Netherlands) and dissolved to 10mM in 100% DMSO. The five different murine H-2 monomers and their corresponding peptides were diluted in PBS. Monomers (50µg/mL final concentration) were added to the corresponding peptide (100µM final concentration) and placed under a 366 nm UV light for 1 hour at room temperature, to replace the UV ligand with the peptide of interest. A corresponding UV ligand control for each H-2 allele was in parallel incubated at RT on the bench.

Generation of DNA barcode labeled pH-2 multimers

Multimer libraries were prepared for each cell line independently comprising 100 predicted neoepitopes per H-2 allele. In addition, the following peptides were included in the library as functional controls: EMT6 library: H2-Db: HPV16 $E7_{49-57}$ (RAHYNIVTF); H2-Kb: $Ovalbumin_{257-264}$ (SIINFEKL); H2-Dd: HIV Env $gp160_{311-320}$ (RGPGRAFVTI); H2-Kd: Influenza $HA_{518-526}$ (IYSTVASSL); H2-Ld: LCMV $NP_{118-126}$ (RPQASGVYM). CT26 library: H2-Ld MuLV Env gp70 AH-1143-431 (SPSYVYHQF). Barcode panels were generated as described in previous publications. Briefly, pH-2 complexes (50µg/mL monomer and 100µM peptide) were prepared and coupled to PE-labeled dextran backbones loaded with a unique DNA barcode.

Before staining, MHC multimers were thawed on ice, centrifuged for 5 minutes at 3300g, and 1.5 µL (0.043 µg) of each distinct pMHC was taken from each well, avoiding potential aggregates in the bottom, and pooled. The volume of the reagent pool was reduced by ultrafiltration to obtain a final vol- ume of approximately 80 µL of pooled MHC multimers per staining. Centrifugal concentrators (Vivaspin 6, 100,000 Da, Sartorius) were saturated with BSA before use. Following ultrafiltration, the pool of multimers was spun at 10,000g for 2 minutes to sediment potential aggregates.

T cell staining with barcode-labeled pH-2 multimers

Splenocytes from tumor-bearing and immunized mice were thawed and washed twice in R10. Tumor infiltrating lymphocytes were positively selected with an EasySep $CD45^+$ selection kit (StemCell, Cat. No. 18945) following manufacturer's guidelines. 5-10x10^6 cells were plated into individual wells in a 96 well plate and washed with Barcode-Cytometry buffer (BCB, PBS with 0.5% BSA, 100µg/mL herring DNA, 2mM EDTA). Before staining, MHC multimers were thawed on ice, and centrifuged for 5 minutes at 3300g. A pool comprising 1.5µl (0.043 µg) of each pH-2 specificity was gathered and filtered through centrifugal concentrators (Vivaspin 6, 100,000 Da, Sartorius) to an approximate final volume of 70µl per sample. Following up-concentration, the pool of multimers was spun at 10,000g for 2 minutes to sediment potential aggregates. Cells were stained with the pool of the pH-2-multimers and with Near-IR LIVE/DEAD Fixable Dead Cell Staining kit (APC-Cy7, Biolegend, Cat. No. L10119) an antibody mix comprising: For control

samples: anti-CD3-BUV395 (BD, 145-2C11, Cat. No. 563565), anti-CD4-BV605 (BD, RM4-5, Cat. No. 563151), anti-CD8-BUV737 (BD, 53-6.7, Cat. No. 612759). For tumor model samples: the beforementioned and anti-CD45.2-A700 (Biolegend, 104, Cat. No. 109821), anti-CD11b-BV785 (BD, M1/70, Cat. No. 740861), anti-PD-1-PerCP-Cy5.5 (Biolegend, 29F.1A12, Cat. No. 109120), anti-TIM-3-BV711 (BD, 5D12, Cat. No. 747622), anti-CD39-PE-CF594 (Biolegend, Duha59, Cat. No. 143811), anti-CD44-FITC (BD, IM7, Cat. No. 553133), anti-CD62L-BV510 (BD, MEL-14, Cat. No. 563117)). Cells were acquired and sorted by FACS. pH-2 multimer-specific T cells were sorted based on live, singlets, lymphocytes, $CD3^+$, $CD8^+$, PE^+ cells. The sorted cells labeled with DNA barcoded pH-2 multimer reagents were centrifuged and pellets stored at -20°C. The DNA barcodes that were present in the samples at sorting were amplified along with triplicate full library baseline samples for comparison (aliquot of pH-2 multimer reagent pool). The amplified product was purified using QIAquick PCR Purification kit (Qiagen, Cat. No. 28104) and sequenced using an Ion Torrent PGM 316 or 318 chip (Life Technologies) at PrimBio Research Institute (USA).

Processing of barcode sequencing data

Data were processed by the publicly accessible software Barracoda developed at DTU (http://www.cbs.dtu.dk/services/barracoda). Barracoda calculates the total reads and clonally-reduced reads for each DNA barcode (relating to its coupled pH-2 specificity). Log2 fold changes in read counts linked to a given sample, related to the mean read counts, is compared to the baseline samples, and estimated with normalization factors determined by the trimmed mean of M-values method. False-discovery rates (FDRs) are estimated using the Benjamini–Hochberg method. A p-value is calculated based on the Log2 fold change distribution, determining the strength of the signal compared to the input. A $p < 0.001$ corresponding to FDR <0.1%, and Log2 fold change >=2, are established as the significance level determining a T cell response. Multimers with input counts <20 were excluded from analysis (CT26, 3 multimers; 4T1, 5 multimers).

Neoepitope re-stimulation and intracellular cytokine staining (ICS)

Splenocytes and target cells were co-cultured on a 3:1 ratio in U-bottom 96-well culture plates (Thermo Fisher Scientific Cat. No. 10360691) in a final volume of 200µl of protein transport blocking media (R10 with a final concentration of 2µM Monensin (GolgiStop, BD, Cat. No. 554724) and 10µg/ml Brefaldin-A (GolgiPlug, BD, Cat. No. 555029)). Protein transport blocking media was used as negative control to assess background cytokine production. Leukocyte activation cocktail (LAC, BD, Cat. No. 5120421E/550583) was used as stimulation positive control. Cells were stimulated for 4h at 37ºC 5% CO_2. Upon two washings with FACS buffer (PBS, 2% FCS), cells were incubated for 10min at 4ºC with 0.5µl anti-CD16/32 Fc receptor blocking antibody (Fc-block, Biolegend, Cat. No. 101301) and stained for 30min at 4ºC with Near-IR LIVE/DEAD Fixable Dead Cell Staining kit (APC-Cy7, Biolegend, Cat. No. L10119) and a surface antibody mix (anti-CD3-

FITC (Biolegend, 145-2C11, Cat. No. 100306), anti-CD4-BV605 (BD, RM4-5, Cat. No. 563151), anti-CD8-BUV737 (BD, 53-6.7, Cat. No. 612759)). Cells were washed twice, fixed and permeabilized (eBioscience, Cat. No. 88-8824-00) for 1h at RT and stained intracellularly for 30min at 4ºC (anti-INFγ-APC (BD, XMG1.2, Cat. No. 554413), anti-TNFα-PE-Cy7 (BD, MP6-XT22, Cat. No. 557644)). Samples were washed twice and fixed in 1% filtered paraformaldehyde (ThermoFisher, Cat. No. 11400580) for 1-24 hours.

Flow cytometry

All flow cytometry experiments were carried out on Fortessa and Aria instruments (BDBiosciences). Data were analyzed in FlowJo version 10.6.1 (TreeStar, Inc.).

Statistical analyses

R version 4.0.2 was used for graphing, statistical analyses, and tools. Statistical analyses are specified on the respective figure foot.

Acknowledgements

The authors would like to thank Bente Rotbøl, Anni Flarup Løye and Anna Gyllenberg Burkal for technical assistance.

Reference

[1] P. A. Monach, S. C. Meredith, C. T.Siegel, and H. Schreiber, “A unique tumor Ag produced by a single amino acid substitution,” *Immunity*, vol. 2, no. 1, pp. 45–59, Jan. 1995, doi: 10.1016/1074-7613(95)90078-0.

[2] E. S. Borden, K. H. Buetow, M. A. Wilson, and K. T. Hastings, “Cancer Neoantigens: Challenges and Future Directions for Prediction, Prioritization, and Validation,” *Frontiers in Oncology*, vol. 12. Frontiers Media S.A., Mar. 03, 2022. doi: 10.3389/fonc.2022.836821.

[3] B. J. Hos *et al.*, “Identification of a neo-epitope dominating endogenous CD8 T cell responses to MC-38 colorectal cancer,” *OncoImmunology*, vol. 00, no. 00, 2019, doi: 10.1080/2162402X.2019.1673125.

[4] M. Yadav *et al.*, “Predicting immunogenic tumor mutations by combining mass spectrometry and exome sequencing,” *Nature*, vol. 515, no. 7528, pp. 572–576, 2014, doi: 10.1038/nature14001.

[5] S. I. S. Mosely *et al.*, “Rational Selection of Syngeneic Preclinical Tumor Models for Immunotherapeutic Drug Discovery,” *Cancer Immunology Research*, vol. 5, no. 1, pp. 29–41, Jan. 2017, doi: 10.1158/2326-6066.CIR-16-0114.

[6] L. D. Wartman *et al.*, “Sequencing a mouse acute promyelocytic leukemia genome reveals genetic events relevant for disease progression,” *Journal of Clinical Investigation*, vol. 121, no. 4, pp. 1445–1455, Apr. 2011, doi: 10.1172/JCI45284.

[7] J. C. Castle *et al.*, “Exploiting the mutanome for tumor vaccination,” *Cancer Research*, vol. 72, no. 5, pp. 1081–1091, 2012, doi: 10.1158/0008-5472.CAN-11-3722.

[8] J. C. Castle *et al.*, “Immunomic, genomic and transcriptomic characterization of CT26 colorectal carcinoma,” *BMC Genomics*, vol. 15, no. 1, 2014, doi: 10.1186/1471-2164-15-190.

[9] B. Schrörs *et al.*, “Multi-Omics Characterization of the 4T1 Murine Mammary Gland Tumor Model,” *Frontiers in Oncology*, vol. 10, Jul. 2020, doi: 10.3389/fonc.2020.01195.

[10] S. Kreiter *et al.*, “Mutant MHC class II epitopes drive therapeutic immune responses to cancer,” *Nature*, vol. 520, no. 7549, pp. 692–696, 2015, doi: 10.1038/nature14426.

[11] L. Aurisicchio *et al.*, “Poly-specific neoantigen-targeted cancer vaccines delay patient derived tumor growth,” *Journal of Experimental and Clinical Cancer Research*, vol. 38, no. 1, pp. 1–13, 2019, doi: 10.1186/s13046-019-1084-4.

[12] E. Salvatori *et al.*, “Neoantigen cancer vaccine augments anti-CTLA-4 efficacy,” *npj Vaccines*, vol. 7, no. 1, p. 15, Dec. 2022, doi: 10.1038/s41541-022-00433-9.

[13] A. M. D’Alise *et al.*, “Adenoviral vaccine targeting multiple neoantigens as strategy to eradicate large tumors combined with checkpoint blockade,” *Nature Communications*, vol. 10, no. 1, pp. 1–12, 2019, doi: 10.1038/s41467-019-10594-2.

[14] M. Vormehr *et al.*, “A non-functional neoepitope specific CD8 $^{+}$ T-cell response induced by tumor derived Ag exposure *in vivo*,” *OncoImmunology*, vol. 8, no. 3, p. 1553478, Mar. 2019, doi: 10.1080/2162402X.2018.1553478.

[15] A.-H. Capietto *et al.*, “Mutation position is an important determinant for predicting cancer neoantigens,” *Journal of Experimental Medicine*, vol. 217, no. 4, Apr. 2020, doi: 10.1084/jem.20190179.

[16] L. Shen, J. Zhang, H. Lee, M. T. Batista, and S. A. Johnston, “RNA Transcription and Splicing Errors as a Source of Cancer Frameshift Neoantigens for Vaccines,” *Scientific Reports*, vol. 9, no. 1, pp. 1–13, 2019, doi: 10.1038/s41598-019-50738-4.

[17] A. K. Bentzen *et al.*, “Large-scale detection of Ag-specific T cells using peptide-MHC-I multimers labeled with DNA barcodes,” *Nature Biotechnology*, vol. 34, no. 10, pp. 1037–1045, Oct. 2016, doi: 10.1038/nbt.3662.

[18] A.-M. Bjerregaard, M. Nielsen, S. R. Hadrup, Z. Szallasi, and A. C. Eklund, “MuPeXI: prediction of neo-epitopes from tumor sequencing data,” *Cancer Immunology, Immunotherapy*, vol. 66, no. 9, pp. 1123–1130, Sep. 2017, doi: 10.1007/s00262-017-2001-3.

[19] V. Jurtz, S. Paul, M. Andreatta, P. Marcatili, B. Peters, and M. Nielsen, “NetMHCpan-4.0: Improved Peptide–MHC Class I Interaction Predictions Integrating Eluted Ligand and Peptide Binding Affinity Data,” *The Journal of Immunology*, vol. 199, no. 9, pp. 3360–3368, Nov. 2017, doi: 10.4049/jimmunol.1700893.

[20] Meldgaard T.S., Viborg N., TamhaneT., Suarez Hernandez S., Albacete D.V., and Hadrup S.R., “H-2 multimers for high-throughput T cell interrogation and description of novel conditional ligands for H-2Dd and H-2Kd,” *(manuscript submitted)*, 2019.

[21] A. Y. Huang *et al.*, “The immunodominant major histocompatibility complex class I-restricted Ag of a murine colon tumor derives from an endogenous retroviral gene product.,” *Proceedings of the National Academy of Sciences*, vol. 93, no. 18, pp. 9730–9735, Sep. 1996, doi: 10.1073/pnas.93.18.9730.

[22] F. Duan *et al.*, “Genomic and bioinformatic profiling of mutational neoepitopes reveals new rules to predict anticancer immunogenicity,” *Journal of Experimental Medicine*, vol. 211, no. 11, pp. 2231–2248, Oct. 2014, doi: 10.1084/jem.20141308.

[23] A.-M. Bjerregaard *et al.*, “An Analysis of Natural T Cell Responses to Predicted Tumor Neoepitopes,” *Frontiers in Immunology*, vol. 8, Nov. 2017, doi: 10.3389/fimmu.2017.01566.

[24] J. S. Holm *et al.*, “Neoantigen-specific CD8 T cell responses in the peripheral blood following PD-L1 blockade might predict therapy outcome in metastatic urothelial carcinoma,” *Nature Communications*, vol. 13, no. 1, p. 1935, Dec. 2022, doi: 10.1038/s41467-022-29342-0.

[25] W. Zhong *et al.*, “Comparison of the molecular and cellular phenotypes of common mouse syngeneic models with human tumors,” *BMC Genomics*, vol. 21, no. 1, p. 2, Dec. 2020, doi: 10.1186/s12864-019-6344-3.

[26] M. Campoli and S. Ferrone, “HLA Ag changes in malignant cells: epigenetic mechanisms and biologic significance,” *Oncogene*, vol. 27, no. 45, pp. 5869–5885, Oct. 2008, doi: 10.1038/onc.2008.273.

[27] T. N. Schumacher and R. D. Schreiber, “Neoantigens in cancer immunotherapy,” *Science (1979)*, vol. 348, no. 6230, pp. 69–74, Apr. 2015, doi: 10.1126/science.aaa4971.

[28] A.-M. Bjerregaard, T. K. Pedersen, A. M. Marquard, and S. R. Hadrup, “Prediction of neoepitopes from murine sequencing data,” *Cancer Immunology, Immunotherapy*, vol. 68, no. 1, pp. 159–161, Jan. 2019, doi: 10.1007/s00262-018-2254-5.

[29] U. K. Hansen *et al.*, “Tumor-Infiltrating T Cells From Clear Cell Renal Cell Carcinoma Patients Recognize Neoepitopes Derived From Point and Frameshift Mutations,” *Frontiers in Immunology*, vol. 11, Mar. 2020, doi: 10.3389/fimmu.2020.00373.

[30] C. A. Chambers, M. S. Kuhns, J. G. Egen, and J. P. Allison, “CTLA-4-mediated inhibition in regulation of T cell responses: mechanisms and manipulation in tumor immunotherapy,” *Annu Rev Immunol*, vol. 19, pp. 565–594, 2001, doi: 10.1146/ANNUREV.IMMUNOL.19.1.565.

[31] K. A. Connolly *et al.*, “A reservoir of stem-like CD8 $^{+}$ T cells in the tumor-draining lymph node preserves the ongoing antitumor immune response,” *Science Immunology*, vol. 6, no. 64, Oct. 2021, doi: 10.1126/sciimmunol.abg7836.

[32] F. Lang, B. Schrörs, M. Löwer, Ö. Türeci, and U. Sahin, “Identification of neoantigens for individualized therapeutic cancer vaccines,” *Nature Reviews Drug Discovery*, vol. 21, no. 4, pp. 261–282, Apr. 2022, doi: 10.1038/s41573-021-00387-y.

[33] J. Li, P. Scott, and J. P. Farrell, “In Vivo Alterations in Cytokine Production following Interleukin-12 (IL-12) and Anti-IL-4 Antibody Treatment of CB6F1 Mice with Chronic Cutaneous Leishmaniasis,” 1996.

[34] J. Borst, T. Ahrends, N. Bąbała, C. J. M. Melief, and W. Kastenmüller, “CD4+ T cell help in cancer immunology and immunotherapy,” *Nature Reviews Immunology*, vol. 18, no. 10, pp. 635–647, Oct. 2018, doi: 10.1038/s41577-018-0044-0.

[35] M. C. W. Feltkamp *et al.*, “Vaccination with cytotoxic T lymphocyte epitope-containing peptide protects against a tumor induced by human papillomavirus type 16-transformed cells,” *European Journal of Immunology*, vol. 23, no. 9, pp. 2242–2249, Sep. 1993, doi: 10.1002/eji.1830230929.

[36] F. R. Carbone, M. W. Moore, J. M. Sheil, and M. J. Bevan, “Induction of cytotoxic T lymphocytes by primary in vitro stimulation with peptides.,” *Journal of Experimental Medicine*, vol. 167, no. 6, pp. 1767–1779, Jun. 1988, doi: 10.1084/jem.167.6.1767.

[37] C. Bergmann, S. A. Stohlmann, and M. McMillan, “An endogenously synthesized decamer peptide efficiently primes cytotoxic T cells specific for the HIV-1 envelope glycoprotein,” *European Journal of Immunology*, vol. 23, no. 11, pp. 2777–2781, Nov. 1993, doi: 10.1002/eji.1830231109.

[38] J. L. Whitton *et al.*, “Molecular analyses of a five-amino-acid cytotoxic T-lymphocyte (CTL) epitope: an immunodominant region which induces nonreciprocal CTL cross-reactivity,” *Journal of Virology*, vol. 63, no. 10, pp. 4303–4310, Oct. 1989, doi: 10.1128/jvi.63.10.4303-4310.1989.

[39] K. KUWANO, T. J. BRACIALE, and F. A. ENNIS, “Cytotoxic T Lymphocytes Recognize a Cross-Reactive Epitope on the Transmembrane Region of Influenza H1 and H2 Hemagglutinins,” *Viral Immunology*, vol. 2, no. 3, pp. 163–173, Jan. 1989, doi: 10.1089/vim.1989.2.163.

[40] G. A. Auwera *et al.*, “From FastQ Data to High-Confidence Variant Calls: The Genome Analysis Toolkit Best Practices Pipeline,” *Current Protocols in Bioinformatics*, vol. 43, no. 1, Oct. 2013, doi: 10.1002/0471250953.bi1110s43.

[41] Felix Krueger, “TrimGalore https://github.com/FelixKrueger/TrimGalore.” 2021.

[42] S. Andrews, “FastQC: A Quality Control Tool for High Throughput Sequence [online] Data Available at: http://www.bioinformatics.babraham.ac.uk/projects/fastqc/.” 2010.

[43] F. Cunningham *et al.*, “Ensembl 2022,” *Nucleic Acids Research*, vol. 50, no. D1, pp. D988–D995, Jan. 2022, doi: 10.1093/nar/gkab1049.

[44] H. Li and R. Durbin, “Fast and accurate short read alignment with Burrows-Wheeler transform,” *Bioinformatics*, vol. 25, no. 14, pp. 1754–1760, Jul. 2009, doi: 10.1093/bioinformatics/btp324.

[45] P. Danecek *et al.*, “Twelve years of SAMtools and BCFtools,” *Gigascience*, vol. 10, no. 2, Feb. 2021, doi: 10.1093/gigascience/giab008.

[46] BroadInstitue, “Picard https://github.com/broadinstitute/picard.” BroadInstitue, 2021.

[47] G. A. van der Auwera *et al.*, “From fastQ data to high-confidence variant calls: The genome analysis toolkit best practices pipeline,” *Current Protocols in Bioinformatics*, no. SUPL.43, 2013, doi: 10.1002/0471250953.bi1110s43.

[48] K. Cibulskis *et al.*, “Sensitive detection of somatic point mutations in impure and heterogeneous cancer samples,” *Nature Biotechnology*, vol. 31, no. 3, pp. 213–219, Mar. 2013, doi: 10.1038/nbt.2514.

[49] N. L. Bray, H. Pimentel, P. Melsted, and L. Pachter, “Near-optimal probabilistic RNA-seq quantification,” *Nature Biotechnology*, vol. 34, no. 5, pp. 525–527, May 2016, doi: 10.1038/nbt.3519.

[50] A. M. Bjerregaard, T. K. Pedersen, A. M. Marquard, and S. R. Hadrup, “Prediction of neoepitopes from murine sequencing data,” *Cancer Immunology, Immunotherapy*, vol. 68, no. 1. Springer Science and Business Media Deutschland GmbH, pp. 159–161, Jan. 25, 2019. doi: 10.1007/s00262-018-2254-5.

[51] C. I. DeVette *et al.*, “NetH2pan: A computational tool to guide MHC peptide prediction on murine tumors,” *Cancer Immunology Research*, vol. 6, no. 6, pp. 636–644, Jun. 2018, doi: 10.1158/2326-6066.CIR-17-0298.

Supplementary material– Manuscript I

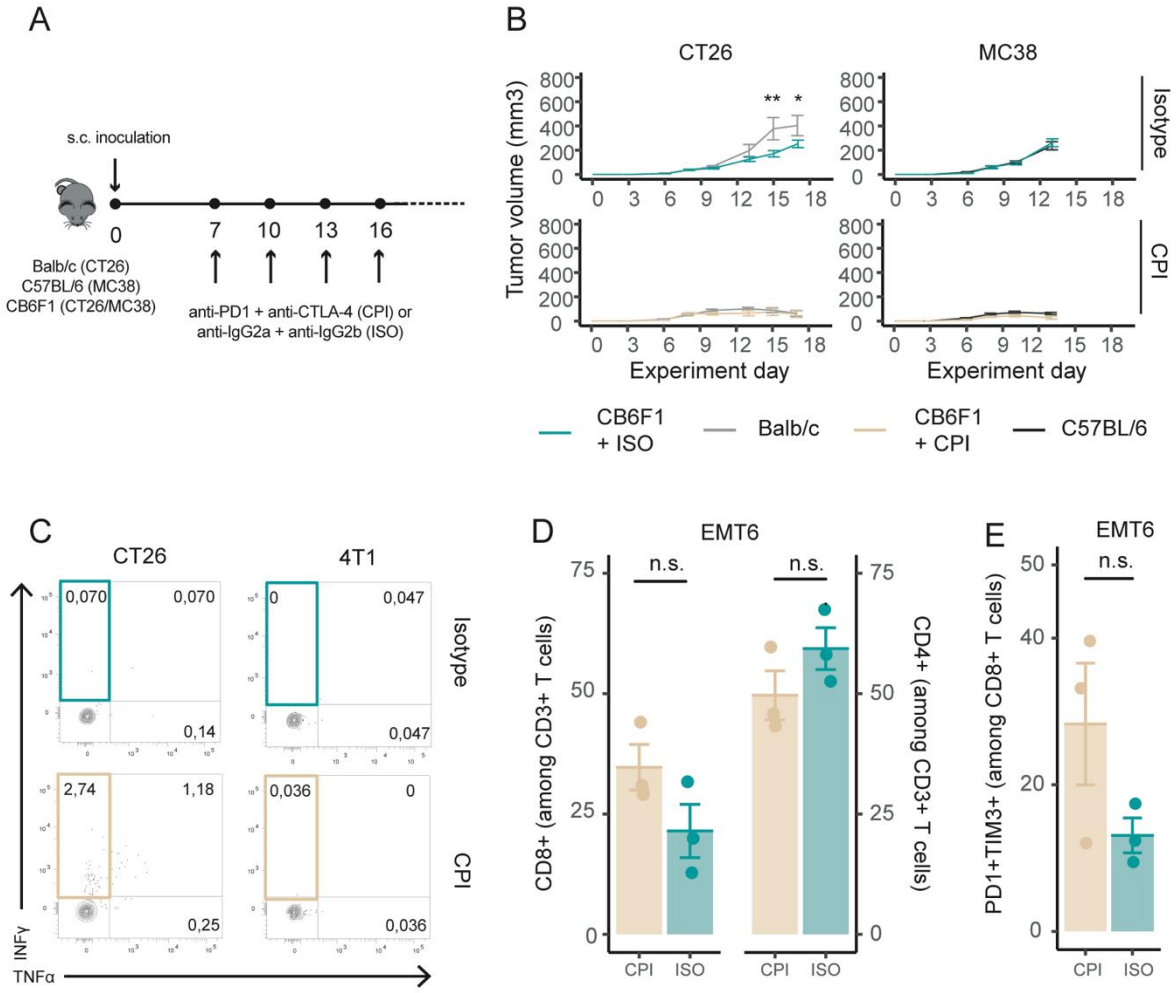

Supplementary Figure 1: Evaluation of CT26 and MC38 tumor establishment in CB6F1 mice, *in vitro* re-stimulation of splenocytes with CT26 and 4T1 tumor cell lines, and phenotype analysis of EMT6 TILs.

A) *In-vivo* therapy timeline. **B)** Average tumor growth of CT26 and MC38 implanted in CB6F1 and Balb/c or C57BL/6 respectively, receiving ISO (top) or CPI (bottom). N=3 mice per group. Error bars represent SEM. A mixed-efffect linear model considering tumors a random effect and Bonferroni-corrected denotes p-values <0.05, <0.01 * and ** respectively. **C)** *In vitro* restimulation of splenocytes from CT26 and 4T1 tumor-bearing mice with the respective tumor cell line (3:1 effector:target). **D-E)** Phenotype analysis of TILs in the EMT6 tumor model denoting $CD8^+$ and $CD4^+$ T cell proportions (D) and the proportion of exhausted CD8+ T cells expressing $PD\text{-}1^+$ and $TIM\text{-}3^+$ exhausted CD8+ T cells. Non-parametric Kruskal-Wallis t-test. N.s.: not significant.

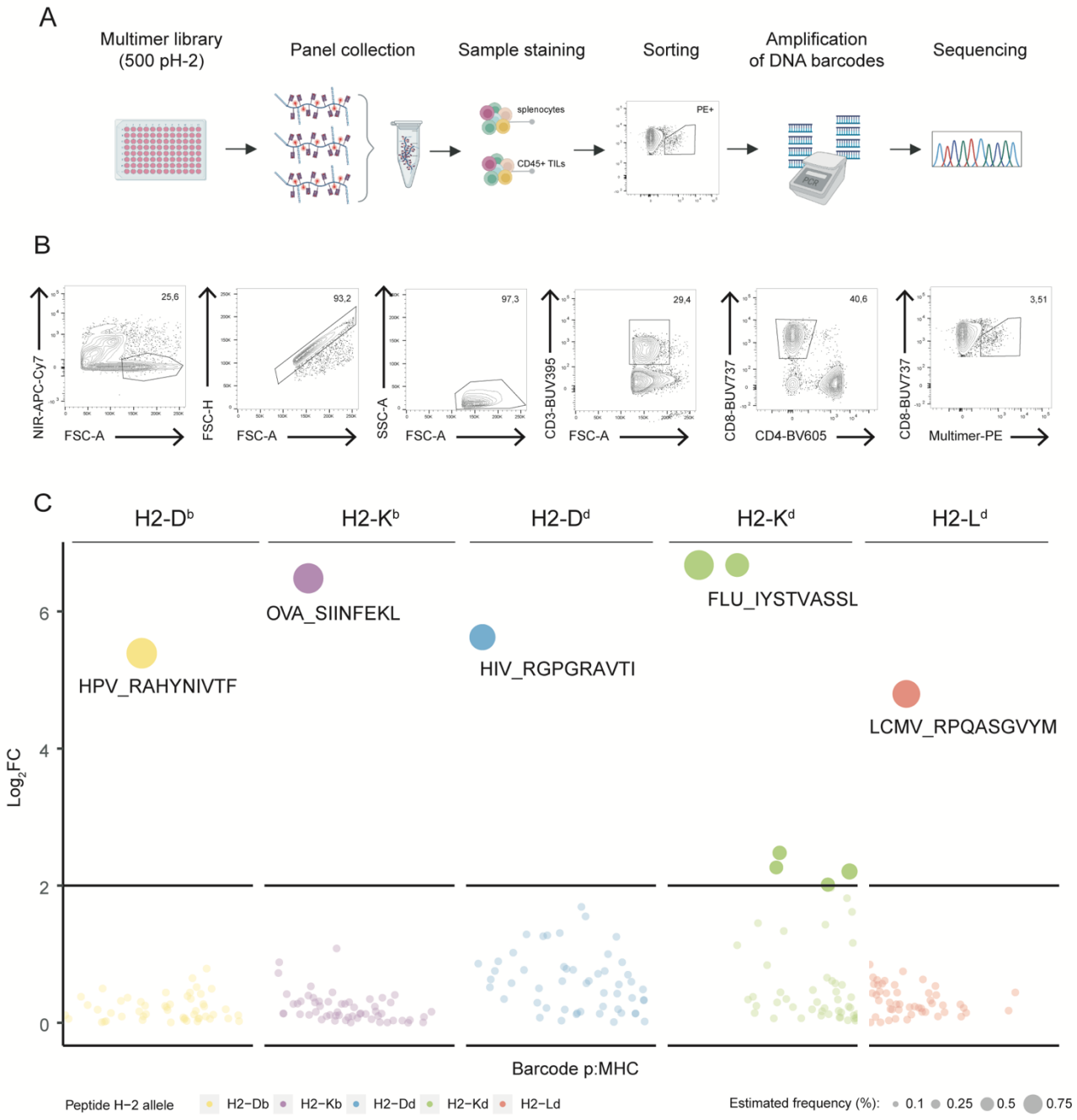

Supplementary Figure 2: Validation of the functionality of the EMT6 panel.

A) Overview of the workflow for detection of NARTs. **B)** Gating strategy of a spike-in mix sample containing known proportions of Ag-specific $CD8^+$ T cells. **C)** Log_2 of sequenced pMHC associated barcodes enriched over the input library. Labelled dots represent the Ag-specific $CD8^+$ T cells comprising the spike-in mix. Size represents the estimated frequency of the Ag-specific response among $CD8^+$ T cells. All Ag-specific responses were retrieved in similar frequencies as they were spiked-in, demonstrating the functionality of the panel. Horizontal bar represents significantly enriched barcodes within the sorted population (log_2 FC ≥2, p-value <0.001, read counts in input triplicates >20). Figure A created with Biorender.com.

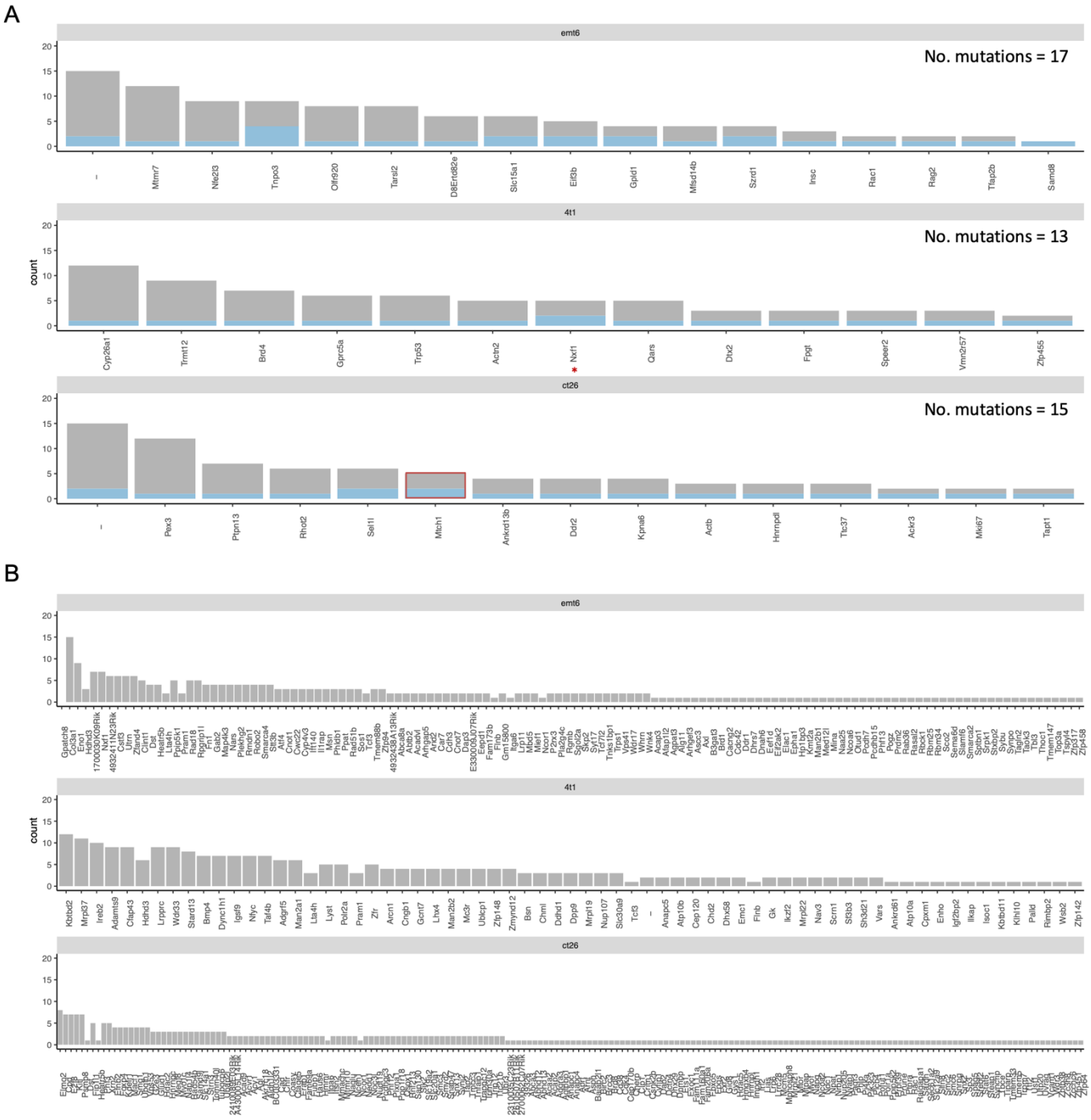

Supplementary Figure 3: T cell recognition of mutations covered in the libraries.

A) Mutations with ≥1 detected NARTs. B) Mutations with undetected NARTs. *A different mutation on the same gene has been described as an immunogenic neoepitope on the EMT6 model [15]. Red border: previously validated as an immunogenic response [13].

Supplementary Table 1: Overview of the detected neoepitopes. n represents the total number of detected neoepitopes. Underline indicates the mutated residue.

Treatment	Organ	Gene	Peptide name	H-2 allele	Sequence	Mutation consequence	Binding affinity (%EL Rank)	Expression level (TPM)
EMT6 (n=25)								
ISO	tumor	-	EMT6_139	H2-Kb	VSYLEFVYNLT	M	0.4297	0.120705
		Szrd1	EMT6_178	H2-Kd	EYAEARRPI	M	0.1257	31.26955
		Szrd1	EMT6_241	H2-Kd	AEYAEARRPI	M	0.7232	31.26955
	spleen	Slc15a1	EMT6_169	H2-Kd	SYCGMRALL	M	0.0097	0.236976
		Rag2	EMT6_221	H2-Kd	SYMPSTQRN	M	0.4872	0.138189
		Mtmr7	EMT6_335	H2-Dd	ISIENIHVM	M	0.0367	0.965453
		Insc	EMT6_398	H2-Kd	VYSMSVRL	M	0.7209	1.456698
ISO+CPI	spleen+tumor	Gpld1	EMT6_171	H2-Kd	NYLSLRWYV	M	0.0389	1.185526
		Samd8	EMT6_207	H2-Kd	AYHQSRRAKI	M	0.3834	7.058012
		Gpld1	EMT6_239	H2-Kd	FNYLSLRWYV	M	0.7214	1.185526
		Eif3b	EMT6_337	H2-Dd	VGPDRLDKL	M	0.0083	162.7098
		Olfr920	EMT6_350	H2-Dd	IPKMLMSF	M	0.5986	0.122325
		Mfsd14b	EMT6_362	H2-Dd	SAPLIGTL	M	0.0848	15.8984
		Tnpo3	EMT6_401	H2-Kd	LNYCRIFTKL	M	0.4847	36.13217
	spleen	Slc15a1	EMT6_206	H2-Kd	SYCGMRALLVL	M	0.3822	0.236976
		Tnpo3	EMT6_212	H2-Kd	VLNYCRIFTKL	M	0.4116	36.13217
		D8Ertd82e	EMT6_338	H2-Dd	SQYRMFDEF	M	0.0085	14.16352
		Tnpo3	EMT6_340	H2-Kd	NYCRIFTKL	M	0.01	36.13217
		Tarsl2	EMT6_400	H2-Db	STHILGEAM	M	0.4831	5.830485
		Tnpo3	EMT6_403	H2-Kd	YCRIFTKL	M	0.5634	36.13217
		Eif3b	EMT6_95	H2-Dd	QVGPDRLDKL	M	0.4858	162.7098
CPI	spleen	Nfe2l3	EMT6_214	H2-Kd	SFNSMLSRYYM	M	0.4179	0.127951
		Rac1	EMT6_349	H2-Dd	VSPASFEKV	M	0.0391	207.4471
		-	EMT6_354	H2-Dd	SYLEFVYNL	M	0.0597	0.120705
		Tfap2b	EMT6_63	H2-Db	AAIMLWKLL	M	0.5772	0.117629
CT26 (n=18)								
ISO	spleen	Mki67	CT26_124	H2-Kb	VTIDELVRL	M	0.1367	58.31735
		-	CT26_178	H2-Kd	IYVALLRVM	I	0.0464	200.7828
		Rhot2	CT26_220	H2-Kd	AHPLAPQAL	M	0.465	27.82658
		-	CT26_229	H2-Kd	VYLYMATYA	M	0.2614	21.61154
		Ackr3	CT26_236	H2-Kd	KYSAKTGFTKL	M	0.33	18.73706
ISO	spleen	Kpna6	CT26_298	H2-Ld	VPPCLPVL	M	0.3111	23.3545
		Actb	CT26_356	H2-Dd	ASLSTFHQM	M	0.2055	2876.865
		Ttc37	CT26_363	H2-Dd	KSFMKTSEL	M	0.4978	18.45046
ISO+CPI	spleen	Ddr2	CT26_125	H2-Kb	IVVRFVRLI	M	0.2452	56.69061
		Sel1l	CT26_148	H2-Kb	ILGYRYWTGI	M	0.3207	18.29106
		Mtch1	CT26_175	H2-Kd	WKYLSVQSQL	M	0.1569	207.7357
		Ankrd13b	CT26_235	H2-Kd	IFHILNTRI	M	0.2722	20.45385
		Ptpn13	CT26_410	H2-Kd	VPYFRLEHYL	M	0.2547	15.29317
CPI	spleen	Mtch1	CT26_174	H2-Kd	KYLSVQSQL	M	0.0029	207.7357
		Hnrnpdl	CT26_187	H2-Kd	SWDTSKKNL	M	0.3546	96.31966
		Tapt1	CT26_206	H2-Kd	NFVEIKESV	M	0.1251	50.18922
		Pex3	CT26_361	H2-Kd	IYQVFNTSL	F	0.0719	17.63604
		Sel1l	CT26_364	H2-Kb	LGYRYWTGI	M	0.0648	18.29106
4T1 (n=15)								
ISO	tumor	Dtx2	4T1_244	H2-Kb	TGPPASRL	M	0.5221	5.051263
	spleen	Fpgt	4T1_105	H2-Kd	FYMDQKSAKKL	M	0.3955	8.42116
		Trmt12	4T1_262	H2-Dd	RSPLFFIKCM	F	0.1673	1.783477
		Vmn2r57	4T1_297	H2-Kd	KWPTQFTKI	M	1.1266	0.166462
		Nxf1	4T1_45	H2-Dd	KGRCFYFL	M	0.3147	53.49932
ISO+CPI	spleen+tumor	Zfp455	4T1_151	H2-Kd	SLLITRRRI	M	2.2259	1.94566
		Actn2	4T1_53	H2-Dd	RKGLKLMLLL	M	1.144	2.621732
	spleen	Trmt12	4T1_262	H2-Kb	RSPLFFIKCM	F	0.7073	1.783477
		Nxf1	4T1_315	H2-Ld	VKGRCFYFL	M	2.6513	53.49932
CPI	tumor	Gprc5a	4T1_264	H2-Kb	AHALNLIKL	M	1.8065	79.86488
		Speer2	4T1_320	H2-Kb	STFHEESLL	M	1.2656	0.258735
	spleen	Cyp26a1	4T1_267	H2-Dd	AATSLITYI	M	0.8198	0.444871
		Qars	4T1_290	H2-Kb	RGFPPDAI	M	2.1421	111.702
		Trp53	4T1_293	H2-Kb	RRYPAITSL	F	0.7081	53.01564
		Brd4	4T1_91	H2-Kb	KTVFNSRF	M	1.8772	3.864229

Chapter 6: Manuscript 2

Neoepitope immunogenicity: rules or chaos?

With the advent of neoepitopes as potent targets for immunotherapy, preclinical studies and early clinical data evidenced that a very little proportion of the predicted candidates is recognized by T cells. This observation motivated various studies aiming to define what characteristics determine neoepitope immunogenicity. Here, we rationally selected CT26 neoepitopes showing previously hypothesized immunogenic characteristics; and conducted a vaccination study in Balb/c mice. However, in view of the few detected responses, we would require larger peptide pools to evaluate potential differences across the studied neoepitope immunogenic features.

The research presented in Manuscript II requires further data for submission. It has been formatted as a Letter article for the purpose of this thesis, comprising a unique body text, two figures, and three Supplementary tables describing the peptide sequences.

Neoepitope immunogenicity: rules or chaos?

Authors: Sara Suarez Hernandez[1], Annie Borch[1], Tripti Tamhane[1], Sine Reker Hadrup[1]

Affiliations:

[1]Department of Health Technology, Technical University of Denmark, Lyngby, Denmark

Financial support: This research was funded in part by The Danish Innovation Fund (project NeoPepVac).

Neoepitopes are cancer Ags caused by somatic mutations occurring during tumor development, thus being fully tumor specific. Therefore, they have paved the way towards the emergence of personalized cancer immunotherapies, such as patient-specific therapeutic cancer vaccines. However, only 1-2% of a tumor's mutations are giving rise to spontaneous T cell recognition and may potentially elicit antitumor responses [1]. The identification of the few neoepitopes that are immunogenic in the terms of raising T cell recognition, is crucial to therapeutic development aiming to enhance such neoepitope-directed T cell responses e.g., through vaccination. Understanding the characteristics of immunogenic neoepitopes will allow us to determine relevant neoepitopes more precisely, and to build computational models for predicting those [2]. Here we experimentally examine the influence of key parameters, previously hypothesized to influence neoepitope immunogenicity: 1) MHC-I binding capacity; 2) dis-similarity to self; 3) with a missense or frame-shift mutation origin; and 4) in absence of a strong MHC-II binding motif within the long peptide sequence. We did not observe any significant influence of the studied parameters upon vaccination of naïve mice, which may have been influenced by a limited number of studied neoepitopes. These results exemplify the current limitation to prioritize predicted immunogenic candidates and the difficulty to study neoepitope T cell responses to peptide-vaccination in pre-clinical tumor-free settings.

In this study, we immunized naïve Balb/c mice with candidate neoepitopes predicted from the murine CT26 colon carcinoma cell line (Figure 1A). All neoepitopes were predicted using whole exome sequencing (WES) and RNA-seq from the CT26 cell line. The Balb/c reference genome was used to identify single nucleotide variants and indels/frameshifts on the tumor cell line using the *in-silico* neoepitope prediction software MuPeXi [3]. Predicted MHC-I binding capacity provided by NetMHCpan [4], transcription of the corresponding gene (transcripts per million, TPM) and self-similarity scores to the corresponding or nearest unmutated epitope were used to rank and select 5 neoepitopes per experimental group (see Table 1 and Methods for details).

MHC binding affinity is a key parameter in neoepitope discovery. This is not only necessary for Ag presentation and T cell recognition, but also, neoepitopes with stronger MHC-I binding capacity (eluted (EL) %Rank score < 0.5) and high affinity scores (half-maximal inhibition (IC_{50}) < 50nM) have generally been associated with immunogenic responses [4], [5]. However, neoepitopes classified as MHC-I non-binders based on binding affinity (IC_{50} > 200nM) showed convincing $CD8^+$ T cell activation and tumor growth control on a murine fibrosarcoma tumor model [6]. Further analysis on what characteristic made these predicted non-binders immunogenic, revealed that significant binding affinity differences between a given neoepitope and their unmutated normal or self- version – defined as the differential agretopic index (DAI) – was a predictor of neoepitopes immunogenicity on their data. On the other hand, in contexts where the mutation does not favour higher affinity or stronger binding to MHC-I molecules, neoepitopes' dis-

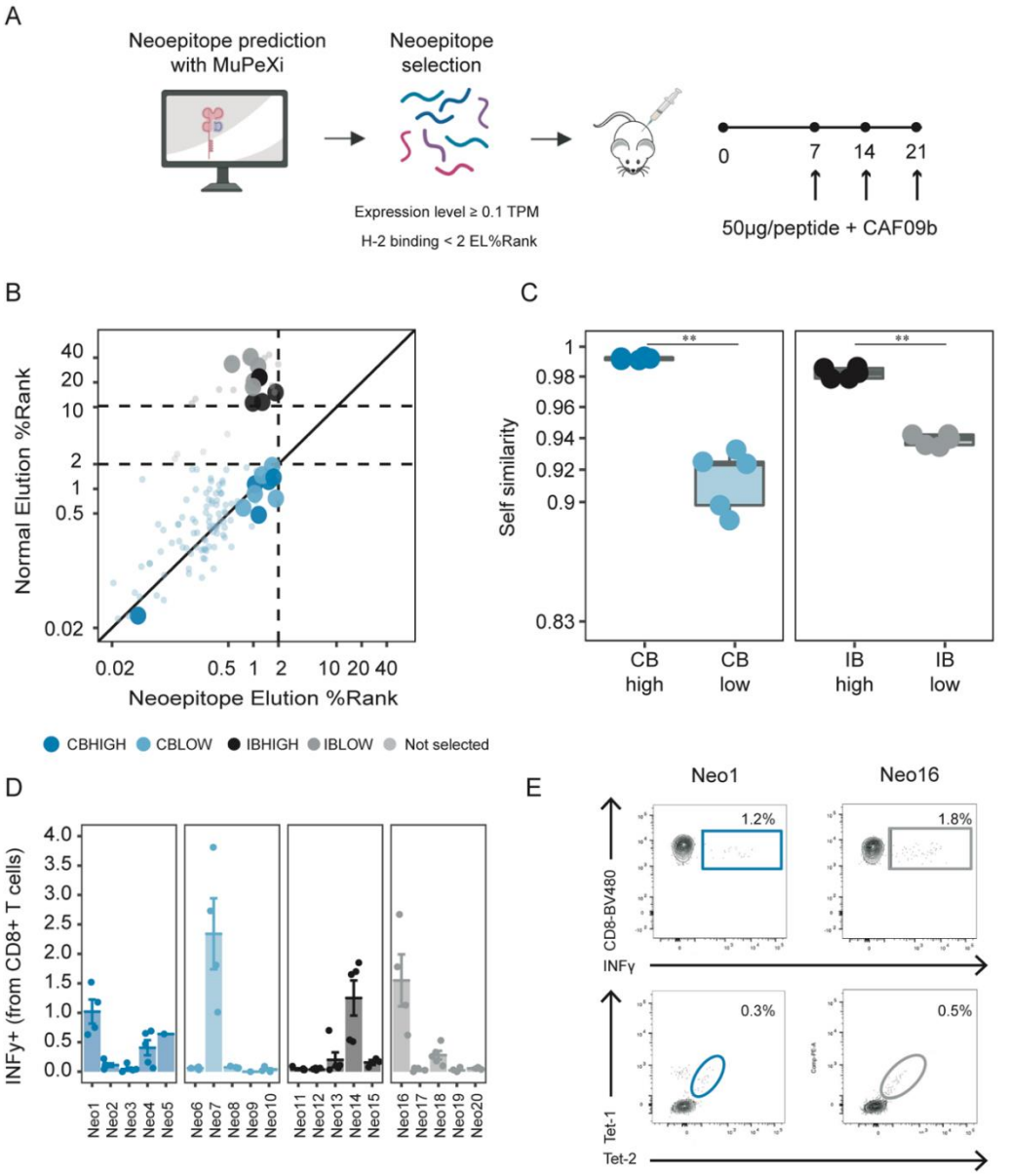

Figure 1: Analysis of immunogenicity based on MHC-I binding affinity and self-similarity scores.

A) Experimental workflow. Neoepitopes were predicted and selected based on predicted MHC-I binding affinity (EL %Rank <2) and expression level (TPM >0.1). **B)** EL %Rank score for normal unmutated epitope and neoepitope of conserved (CB) and improved binders (IB). Dotted lines represent a predicted MHC-I binding score (EL %Rank <2) or predicted non binders (EL %Rank >10). **C)** Self-similarity scores of high and low groups among conserved binders (blue) and improved binders (black). Statistical analysis comprised a non-parametric Kruskal-Wallis t-test, denoting p-value <0.01, as **. **D)** Proportion of INFγ-producing $CD8^+$ T cells. Statistical analysis consisted on a multi-comparison ANOVA with Bonferroni correction, showing no significant differences across neoepitopes. No background signal was detected on experimental controls, represented with dotted line**. E)** Representative FACS plots of the two INFγ responses (top) confirmed by tetramer staining (bottom).

similarity to the respective self-peptide allowed discrimination between immunogenic and non-immunogenic responses in [7]. Therefore, both improved MHC-I binding capacity and neoepitopes' dis-similarity to self, seem to overcome potential tolerization of $CD8^+$ T cells towards the self-epitope. Hence, these neoepitope-specific $CD8^+$ T cells potentially harbour high-affinity TCRs capable of triggering strong anti-tumor responses, justifying the growing interest in neoepitopes as immunotherapy targets. To further study the implication of these characteristics in neoepitopes' immunogenicity, here we classify CT26 predicted H2-K^d binding neoepitopes as conserved binders when EL %Rank score values of the neo- and normal epitopes were below 2; or as improved binders when the normal epitope EL %Rank score value was greater than 10 (Figure 1B). Within each of the groups, we ranked the selected neoepitopes for self-similarity scores, selecting the top and bottom five as high and low self-similarity groups respectively. This way, we forced a significant difference between the two groups (Figure 1C). Despite no $CD8^+$ T cell responses were induced to the majority of the studied neoepitopes, four candidates spread over the four vaccination groups triggered activation of $CD8^+$ T cells by means of INFγ production (Figure 1D). However, no significant differences were seen across, nor within vaccination groups; and we could only validate two of these neoantigen-reactive $CD8^+$ T cells (NARTs) by tetramer staining (Figure 1E). Overall, the heterogenous levels of INFγ produced between neoepitopes within the same experimental group (e.g., Neo2 responses in CBlow group) difficult comparing immunogenicity across groups. In other words, the prioritized neoepitopes seem to represent per-peptide levels of immunogenicity rather than the immunogenic potential of the shared characteristics.

On the other hand, insertion-and-deletion (indel) mutations causing changes in the translation reading frame have gained interest over recent years as a source of immunogenic neoepitopes [8]. A higher density of $CD8^+$ T cells in the tumor infiltrate has been shown to correlate with the number of frameshift (FS) mutations in microsatellite instability-high colorectal cancer [9]; and with the generation of higher numbers of neoepitopes with a greater proportion of strong binders in a pan cancer analysis [8]. On these grounds, FS mutations may comprise a greater source of completely new MHC-I binding neoepitopes with high degrees of self-dissimilarity compared to missense (MS) single nucleotide variants (SNVs). On this study, we used self-similarity scores to prioritize potential immunogenic frameshift mutations, hypothesizing that highly dis-similar neoepitopes might be more likely to be recognized by non-tolerized T cells. All chosen neoepitopes were expressed and predicted conserved binders to minimize bias between groups (Figure 2A). It should be noted that MuPeXi annotations of the normal counterpart of FS-derived neoepitopes are approximations based on sequence similarity to the self-peptidome, which unlikely represents the original unmutated peptide. However, we used this approximated self-similarity score to maximize the likelihood of choosing FS mutations generating new $H2^d$-restricted binders, selecting five FS neoepitopes with the lowest self-similarity scores. By contrast,

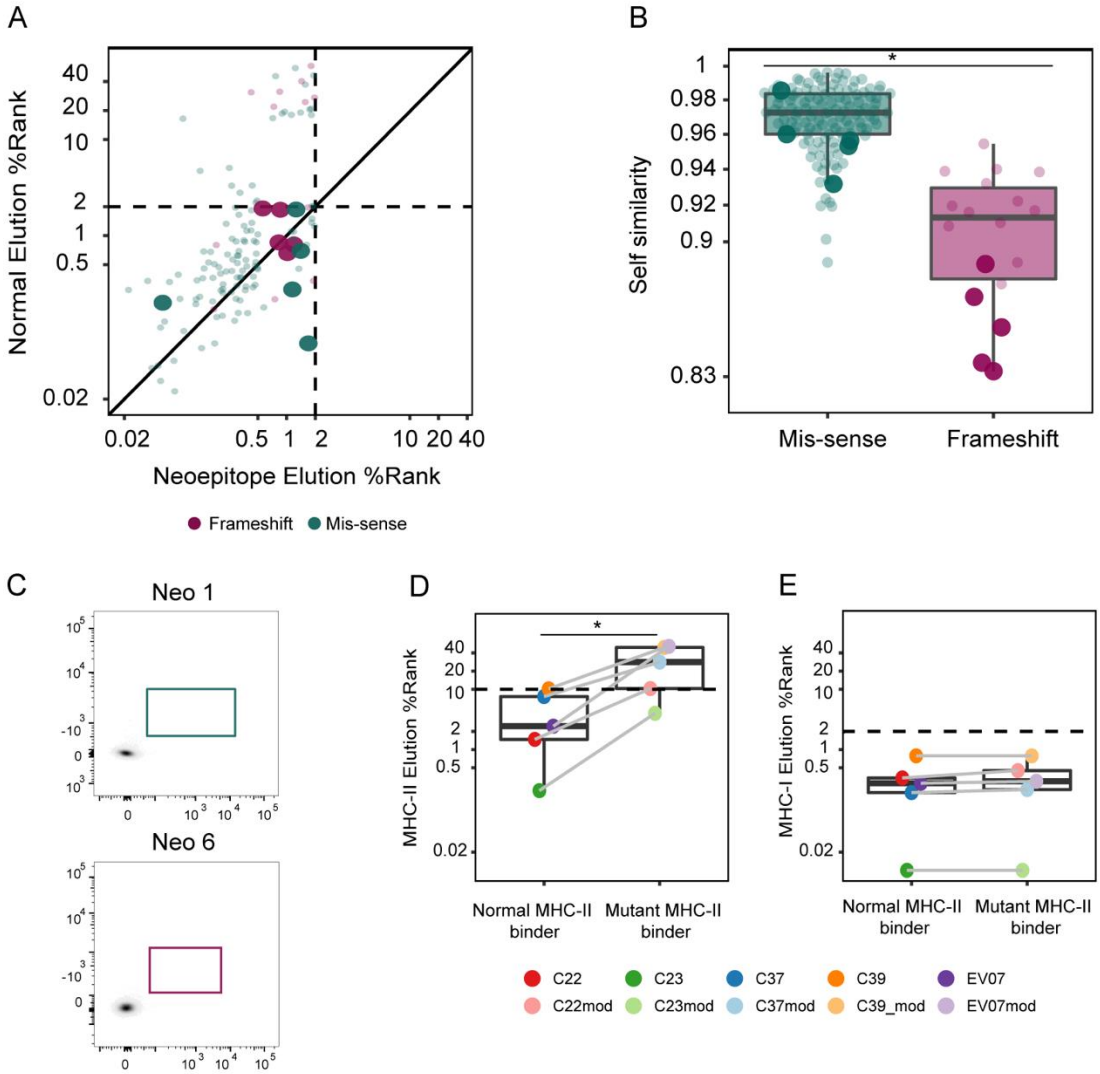

Figure 2: Analysis of immunogenicity based on mutation origin or disruption if the MHC-II motif.

A) EL %Rank score for normal unmutated epitope and neoepitope, showing no bias in MHC-I binding affinity across selected neoepitopes. **B)** Mis-sense and frameshift neoepitopes were selected to show a significant difference in self-similarity scores. **C)** Representative FACS plots of the tetramer staining illustrating the lack of response across both groups**. D)** MHC-II binding affinity and **E)** MHC-I binding affinity between long peptides with a normal or mutated disrupted MHC-II binding motif. F) KFKASRASI-tetramer staining (short C22 peptide) of splenocytes vaccinated with non modified a modified peptides. Statistical analysis comprised a non-parametric Kruskal-Wallis t-test, denoting p-value <0.05 as *. N.s.: not significant.

five MS neoepitopes were randomly chosen to represent average self-similarity scores within the MS group (Figure 2B). However, due to a complete lack of detection of vaccine induced $CD8^+$ T cells by tetramer staining, functional responses upon neoepitope restimulation were not studied (a representative neoepitope-tetramer staining from each group is deployed on Figure 2C).

Lastly, advantages of long-peptide (SLP) vaccination (22-45 amino acids in length) over short peptide formulations (8-11 amino acids) have been extensively revised [10]. On the other hand, while $CD4^+$ T cell help for efficient $CD8^+$ T cell priming and activation has been demonstrated [11], [12], the benefits on cytotoxic T cell activation of including both $CD4^+$ and $CD8^+$ T cell epitopes within SLP sequences is yet somewhat controversial. While the initial success of a short lymphocytic choriomeningitis virus (LCMV) $CD8^+$ T cell epitope vaccine was due to the presence of a helper $CD4^+$ T cell epitope within the sequence [13]; another study including both ovalbumin $OVA_{(257-264)}$ $CD8^+$ and $OVA_{(323-339)}$ $CD4^+$ T cell epitopes within a SLP, showed strong $CD8^+$ T cell activation even in absence of $CD4^+$ T cells and MHC-II expression [14]. To further study the impact of MHC-I and MHC-II binders on neoepitopes immunogenicity, we analysed differences in $CD8^+$ T cell induction in between SLPs carrying a strong MHC-I binder together with: a strong MHC-II binder (e.g., C22); or a mutation-induced MHC-II non binder (C22mod, see Table 3 for full list of neoantigens). Impact of the mutation in impairing predicted MHC-II binding while leaving intact the predicted MHC-I binding capacity is deployed on Table 3 and illustrated on Figure 2D, E. In lack of functional data, induction of neoepitope-specific $CD8^+$ T cells shows opposite trends when vaccinating with single or pooled peptides (Figure 2E). Absence of a strong MHC-II binder in neopeptide C22mod seems to enhance priming of KFKASRASI-specific $CD8^+$ T cells, despite not significant. However, the opposite effect on the %KFKASRASI-specific $CD8^+$ T cells is observed when vaccinating the five modified neoepitopes together (termed “Poolmod” on Figure 2E). In lack of information for C23mod-, C37mod-, C39mod- or EV07mod-specific $CD8^+$ T cells, conclusions cannot be drawn on whether the absence of the MHC-II binding motif affects immunogenicity differently across the studied neopeptides.

Overall, we only observed T cell responses towards a small fraction of all the studied neoepitopes, implying the need to evaluate larger peptide pools to fully reveal patterns driving immunogenicity. However, despite the limitation in size, our study also reveals a challenge in segregating characteristics affecting immunogenicity, since such many factors are influencing the capacity to raise a T cell response. Thus, in the current setting we could not establish if self-dissimilarity among conserved MHC-I neoepitopes contributes to NART recognition. If proven relevant, considering self-similarity scores in conjunction with MHC-I binding affinity when prioritizing neoepitopes might boost selection of immunogenic candidates.

A limitation of our study is lacking an evaluation of NARTs present prior vaccination. In the absence of a tumor presenting mutation-derived neoantigens in this setup, NART responses would comprise spontaneously occurring naïve $CD8^+$ T cells capable of recognizing such neoepitopes. Such knowledge could elucidate any biases generated by the naïve T cell repertoire, e.g., clarify whether the observed per-peptide immunogenicity rather than the immunogenic potential of the shared characteristics correlate to varying numbers of pre-existing NARTs across the different specificities. Additionally, to improve T cell detection, an earlier readout after vaccine boost, could be relevant. A similar study describing neoepitopes' immunogenicity in tumor-free mice follows a prime-boost strategy with rationally designed SLPs, analysing reactivity in splenocytes two days after boosting [15]. Owing to the contracting kinetics of memory T cells following vaccination priming and clonal expansion [16], we hypothesize that an earlier readout could potentially improve T cell detection.

Additionally, whether the mutations disrupting the MHC-II binding motif of SLPs had a different impact across the analysed neoantigens remains to be defined. In view that MHC-I neoepitopes require expression of at least an additional MHC-II binder for successful antitumor immunity in preclinical mouse models [17], the presented approach might enlighten how to rationally place MHC-I and MHC-II binders within the long peptide sequence for successful $CD8^+$ and $CD4^+$ T cell priming. In addition, given the defined requirement of $CD4^+$ T cell activation for successful $CD8^+$ T cell priming and response to vaccination ([18], [19]), utilizing SLPs to evaluate short peptide immunogenicity might be of relevance [15].

Overall, while MHC binding is the first requirement for neoepitopes immunogenicity, very few neoepitopes selected on the bases of predicted binding affinity or elution rank scores result in immunogenic responses in mice [15], [20]–[23]. Likewise, ruling out predicted non binders has also been questioned by diverse studies in mouse [6], [24], [25], and man [26]–[28], where they have proven to be experimentally immunogenic. Therefore, major efforts are being made to understand the determinants of neoepitope immunogenicity [2], [29]. Yet, there is still no consensus of clear patterns across immunogenic neoepitopes for such characteristics, although substantial amounts of data are being generated currently from cancer patients treated with immunotherapy, elucidating the role of NART and their characteristics. Such 'real life' data may eventually provide us with sufficient information to allow reliable prediction and assessments of characteristics of relevance for neoepitope immunogenicity. In this multi-causal space, real life data may prove to best source, despite the great heterogeneity among cancer patients.

Materials and Methods

Mice

8 to 10 weeks old female Balb/cByJRj were purchased from Janvier Labs (France) and housed at the Department of Health Technology, Technical University of Denmark. Mice were acclimated for one week prior to initiation of experiments. Mice were euthanized by cervical dislocation. All experiments were conducted in accordance with the Danish Animal Experimentation Act, making all efforts to minimize animal discomfort and suffering.

Cell lines

Balb/c CT26 colon carcinoma cell line (ATCC, #CRL2638) was purchased from ACTT and cultured in R10/Pen-Strep medium (RPMI1640, Fischer Scientific, Cat. No. 61870044, 10% heat inactivated fetal calf serum (FCS, Fischer Scientific, Cat. No. 10500064) and 1% Penicillin-Streptomycin (Pen-Strep, Life Technologies, Cat. No. 15140122)) at 37ºC and 5% CO_2. Cells were split when confluent.

Neoepitope prediction and selection

Neoepitopes were predicted from the CT26 cell line as presented in Chapter 3. From the MuPeXi predicted neoepitopes, expressed and predicted MHC-I binders (>0.1 transcripts per million and neoepitope %EL Rank score ≤ 2 respectively) were filtered from the MuPeXi output file and the following selection criteria applied for the different immunization experiments. Self-similarity: They were classified as conserved binders when the normal counterpart was also a predicted binder normal epitope %EL Rank score ≤ 2) or as improved binders when normal epitope %EL Rank score was ≥ 10. On each of the groups, candidates were ranked based on self-similarity scores: the top 5 selected as “high” and the bottom five as “low” self-similarity. Missense and frameshift: mutations**:** five neoepitopes arising from mis-sense mutations were randomly chosen to represent the average self-similarity score for the “MS” immunization group. For frameshift candidates, they were ranked based on decreasing self-similarity score and the bottom five chosen as “FS” group. MHC-II binding motif: 27-mer neopeptide sequences shown in Table 3 were kindly provided by Evaxion Biotech (Denmark). Lyophilized 8-11mer neoepitopes were purchased from Pepscan (Netherlands) and reconstituted in dimethyl sulfoxide (DMSO, Sigma-Aldrich, Cat. No. C6164) to a concentration of 10mg/ml. Peptides were stored at -20 ºC and thawed at room temperature (RT) prior use.

Neoepitope immunization and splenocyte preparation

Mice were immunized a total of three times (prime-boost-boost) with a weekly interval. Vaccines comprised a single or five pooled neoepitopes as outlined on results section Supplementary Table 1-3. 50µg/dose of each 27-mer or 8-10-mer neoepitopes were dissolved in Tris buffer (9% sucrose, pH 7.4) in a total volume of 120µl; and added dropwise to 80µl of CAF09b adjuvant

(200µg/dose cationic lipid DDA, 40µg/dose mycobacterial cell wall lipid MMG-1, 40µg/dose toll like receptor-3 analogue Poly(I:C), kindly gifted by Dennis Christensen, Statens Serum Institute, Denmark). Mixes were vortexed for 30 seconds and kept at RT for 30min before injection. 200µl per injection were given intraperitoneally (i.p.).

Cell isolation and preparation

Spleens were harvested in R10 and kept on ice. Splenocyte single cell suspensions were obtained through mechanical disaggregation on a 70µm strainer (Corning, Cat. No. 43175) and 50ml Falcon tube using a syringe plunger. Strainers were flushed with 10ml R10 to filter the dissociated splenocytes. Cells were washed twice in 10ml R10 by centrifugation at 1500rpm for 5min at 4ºC. A maximum of 10 x 10^6 cells per cryotube were cryopreserved in 1ml freezing media (FCS, 10% DMSO) and stored at -80ºC in a Mr. Frosty (Corning, Cat. No. 432001) for 24h prior transfer to -180ºC nitrogen tank for long-term storage. Splenocytes were thawed in 10ml R10 adjusted to 37 ºC and washed twice by centrifugation at 1500rpm for 5min at 4ºC.

Neoepitope re-stimulation and intracellular cytokine staining (ICS)

2x10^6 splenocytes were stimulated with 2µg/ml final concentration of each 8-11mer neoepitope in a final volume of 200µl. Cells were plated in U-bottom 96-well culture plates (Thermo Fisher Scientific Cat. No. 10360691) and rested in 100µl R10 in the incubator at 37ºC 5% CO_2 during stimuli preparation. Neoepitopes were dissolved in protein transport blocking media (R10 with a final concentration of 2µM Monensin (GolgiStop, BD, Cat. No. 554724) and 10µg/ml Brefaldin-A (GolgiPlug, BD, Cat. No. 555029)). Protein transport blocking media was used as negative control to assess background cytokine production. Leukocyte activation cocktail (LAC, BD, Cat. No. 5120421E/550583) was used as stimulation positive control. Cells were stimulated overnight (O/N, 10-13h) at 37ºC 5% CO_2. Upon two washings with FACS buffer (PBS, 2% FCS), cells were incubated for 10min at 4ºC with 0.5µl anti-CD16/32 Fc receptor blocking antibody (Fc-block, Biolegend, Cat. No. 101301) and stained for 30min at 4ºC with Near-IR LIVE/DEAD Fixable Dead Cell Staining kit (APC-Cy7, Biolegend, Cat. No. L10119) and a surface antibody mix (anti-CD3-FITC (Biolegend, 145-2C11, Cat. No. 100306), anti-CD4-BV605 (BD, RM4-5, Cat. No. 563151), anti-CD8-BUV737 (BD, 53-6.7, Cat. No. 612759)). Cells were washed twice, fixed and permeabilized (eBioscience, Cat. No. 88-8824-00) for 1h at RT and stained intracellularly for 30min at 4ºC (anti-INFγ-APC (BD, XMG1.2, Cat. No. 554413), anti-TNFα-PE-Cy7 (BD, MP6-XT22, Cat. No. 557644)). Samples were washed twice and fixed in 1% filtered paraformaldehyde (ThermoFisher, Cat. No. 11400580) for 1-24 hours.

Peptide-MHC (pMHC) tetramer preparation

Murine MHC-I molecules stabilized with a UV-photocleavable ligand were produced *in-house* as described in [30]. Briefly, neoepitopes and the respective histocompatibility-2 (H-2) MHC-I molecules (see Supplementary Table 1-3 for details) were diluted in PBS and mixed to a final concentration of 200µM and 100µM respectively. Next, the mix was placed under a 366nm UV light for 1h at RT to allow exchange of the UV-photocleavable ligand by the neoepitope of interest. A UV ligand control for each H-2 molecule was incubated at RT on the bench. The 100µg/ml pMHC product was loaded onto 1.804µg of fluorochrome-labeled streptavidin complexes (PE-SV (Biolegend, Cat. No. 405204), APC-SV (Biolegend, Cat. No. 405207), BV421-SV (BD, Cat. No. 563259), BUV395-SV (BD, Cat. No. 564176), PE-Cy7-SV (Biolegend, Cat. No. 405206), BUV737-SV (BD, Cat. No. 612775), BV650-SV (BD, Cat. No. 563855)) and incubated for 30min at 4ºC. If two-colour combinations were used as described on [31], [32], one half of the pMHC product was stained with colour1-SV and the other half with colour2-SV and the respective combinations merged upon incubation. D-biotin (Avidity, Cat. No. BIO200) was added to a final concentration of ~30µM to block free streptavidin. Tetramers were stored at -20ºC on a 10X freezing media (PBS with 5% bovine serum albumin (BSA) and 50% glycerol, being 0.5% and 5% the respective final concentrations).

Staining of neoepitope-specific $CD8^+$ T cells

3-5x10^6 splenocytes were plated in U-bottom 96-well culture plates. Tetramers were thawed on ice and centrifuged at 10000rcf for 2min at 4ºC to remove aggregates. Unspecific binding was blocked with anti-CD16/32 antibody (Fc-block, Biolegend, Cat. No. 101301) for 10min at 4ºC. 1µl of each specificity were collected in FACS buffer in a final volume of 50µl per staining, containing 10µl 10X BV Buffer (BD, Cat. No. 566385) and 0.5nM Dasatinib and incubated for 15 minutes at 37°C. Cells were stained with Near-IR LIVE/DEAD Fixable Dead Cell Staining kit (APC-Cy7, Biolegend, Cat. No. L10119) and a surface antibody mix (anti-CD3-FITC (Biolegend, 145-2C11, Cat. No. 100306), anti-CD4-BV605 (BD, RM4-5, Cat. No. 563151), anti-CD8-BV480 (BD, 53-6.7, Cat. No. 566096)).

Flow cytometry

All flow cytometry experiments were carried out on Fortessa instruments (BD Biosciences). Data were analysed in FlowJo version 10.6.1 (TreeStar, Inc.).

Statistical analyses

R version 4.0.2 was used for graphing and statistical analyses. Statistical analyses are specified on the Figure foots.

Acknowledgements

The authors would like to thank Dennis Christensen for kindly providing the CAF09b adjuvant. In addition, special thanks Bente Rotbøl, Anni Flarup Løye and Anna Gyllenberg Burkal for technical assistance.

References

[1] F. Lang, B. Schrörs, M. Löwer, Ö. Türeci, and U. Sahin, “Identification of neoantigens for individualized therapeutic cancer vaccines,” *Nature Reviews Drug Discovery*, vol. 21, no. 4, pp. 261–282, Apr. 2022, doi: 10.1038/s41573-021-00387-y.

[2] E. S. Borden, K. H. Buetow, M. A. Wilson, and K. T. Hastings, “Cancer Neoantigens: Challenges and Future Directions for Prediction, Prioritization, and Validation,” *Frontiers in Oncology*, vol. 12. Frontiers Media S.A., Mar. 03, 2022. doi: 10.3389/fonc.2022.836821.

[3] A.-M. Bjerregaard, M. Nielsen, S. R. Hadrup, Z. Szallasi, and A. C. Eklund, “MuPeXI: prediction of neo-epitopes from tumor sequencing data,” *Cancer Immunology, Immunotherapy*, vol. 66, no. 9, pp. 1123–1130, Sep. 2017, doi: 10.1007/s00262-017-2001-3.

[4] V. Jurtz, S. Paul, M. Andreatta, P. Marcatili, B. Peters, and M. Nielsen, “NetMHCpan-4.0: Improved Peptide–MHC Class I Interaction Predictions Integrating Eluted Ligand and Peptide Binding Affinity Data,” *The Journal of Immunology*, vol. 199, no. 9, pp. 3360–3368, Nov. 2017, doi: 10.4049/jimmunol.1700893.

[5] M. Nielsen and M. Andreatta, “NetMHCpan-3.0; improved prediction of binding to MHC class I molecules integrating information from multiple receptor and peptide length datasets,” *Genome Medicine*, vol. 8, no. 1, p. 33, Dec. 2016, doi: 10.1186/s13073-016-0288-x.

[6] F. Duan *et al.*, “Genomic and bioinformatic profiling of mutational neoepitopes reveals new rules to predict anticancer immunogenicity,” *Journal of Experimental Medicine*, vol. 211, no. 11, pp. 2231–2248, Oct. 2014, doi: 10.1084/jem.20141308.

[7] A.-M. Bjerregaard *et al.*, “An Analysis of Natural T Cell Responses to Predicted Tumor Neoepitopes,” *Frontiers in Immunology*, vol. 8, Nov. 2017, doi: 10.3389/fimmu.2017.01566.

[8] S. Turajlic *et al.*, “Insertion-and-deletion-derived tumor-specific neoantigens and the immunogenic phenotype: a pan-cancer analysis,” *The Lancet Oncology*, vol. 18, no. 8, pp. 1009–1021, Aug. 2017, doi: 10.1016/S1470-2045(17)30516-8.

[9] P. Maby *et al.*, “Correlation between Density of CD8 $^{+}$ T-cell Infiltrate in Microsatellite Unstable Colorectal Cancers and Frameshift Mutations: A Rationale for Personalized Immunotherapy,” *Cancer Research*, vol. 75, no. 17, pp. 3446–3455, Sep. 2015, doi: 10.1158/0008-5472.CAN-14-3051.

[10] C. J. M. Melief and S. H. van der Burg, “Immunotherapy of established (pre)malignant disease by synthetic long peptide vaccines,” *Nature Reviews Cancer*, vol. 8, no. 5, pp. 351–360, May 2008, doi: 10.1038/nrc2373.

[11] J. Borst, T. Ahrends, N. Bąbała, C. J. M. Melief, and W. Kastenmüller, “CD4+ T cell help in cancer immunology and immunotherapy,” *Nature Reviews Immunology*, vol. 18, no. 10, pp. 635–647, Oct. 2018, doi: 10.1038/s41577-018-0044-0.

[12] S. P. Schoenberger, R. E. M. Toes, E. I. H. van der Voort, R. Offringa, and C. J. M. Melief, “T-cell help for cytotoxic T lymphocytes is mediated by CD40–CD40L interactions,” *Nature*, vol. 393, no. 6684, pp. 480–483, Jun. 1998, doi: 10.1038/31002.

[13] M. Schulz, R. M. Zinkernagel, and H. Hengartner, “Peptide-induced antiviral protection by cytotoxic T cells.,” *Proceedings of the National Academy of Sciences*, vol. 88, no. 3, pp. 991–993, Feb. 1991, doi: 10.1073/pnas.88.3.991.

[14] M. S. Bijker, S. J. F. van den Eeden, K. L. Franken, C. J. M. Melief, R. Offringa, and S. H. van der Burg, "CD8 + CTL Priming by Exact Peptide Epitopes in Incomplete Freund's Adjuvant Induces a Vanishing CTL Response, whereas Long Peptides Induce Sustained CTL Reactivity," *The Journal of Immunology*, vol. 179, no. 8, pp. 5033–5040, Oct. 2007, doi: 10.4049/jimmunol.179.8.5033.

[15] A.-H. Capietto *et al.*, "Mutation position is an important determinant for predicting cancer neoantigens," *Journal of Experimental Medicine*, vol. 217, no. 4, Apr. 2020, doi: 10.1084/jem.20190179.

[16] E. Blass and P. A. Ott, "Advances in the development of personalized neoantigen-based therapeutic cancer vaccines," *Nature Reviews Clinical Oncology*, vol. 18, no. 4, pp. 215–229, Apr. 2021, doi: 10.1038/s41571-020-00460-2.

[17] E. Alspach *et al.*, "MHC-II neoantigens shape tumor immunity and response to immunotherapy," *Nature*, vol. 574, no. 7780, pp. 696–701, Oct. 2019, doi: 10.1038/s41586-019-1671-8.

[18] S. Kreiter *et al.*, "Mutant MHC class II epitopes drive therapeutic immune responses to cancer," *Nature*, vol. 520, no. 7549, pp. 692–696, 2015, doi: 10.1038/nature14426.

[19] S. T. Ferris *et al.*, "cDC1 prime and are licensed by CD4+ T cells to induce anti-tumor immunity," *Nature*, vol. 584, no. 7822, pp. 624–629, Aug. 2020, doi: 10.1038/s41586-020-2611-3.

[20] J. C. Castle *et al.*, "Exploiting the mutanome for tumor vaccination," *Cancer Research*, vol. 72, no. 5, pp. 1081–1091, 2012, doi: 10.1158/0008-5472.CAN-11-3722.

[21] M. Yadav *et al.*, "Predicting immunogenic tumor mutations by combining mass spectrometry and exome sequencing," *Nature*, vol. 515, no. 7528, pp. 572–576, 2014, doi: 10.1038/nature14001.

[22] M. Vormehr *et al.*, "A non-functional neoepitope specific CD8 + T-cell response induced by tumor derived Ag exposure in vivo," *OncoImmunology*, vol. 8, no. 3, pp. 1–14, 2019, doi: 10.1080/2162402X.2018.1553478.

[23] M. M. Gubin *et al.*, "Checkpoint blockade cancer immunotherapy targets tumor-specific mutant Ags," *Nature*, vol. 515, no. 7528, pp. 577–581, Nov. 2014, doi: 10.1038/nature13988.

[24] H. Ebrahimi-Nik *et al.*, "Mass spectrometry–driven exploration reveals nuances of neoepitope-driven tumor rejection," *JCI Insight*, vol. 4, no. 14, Jul. 2019, doi: 10.1172/jci.insight.129152.

[25] S. D. Martin *et al.*, "Low Mutation Burden in Ovarian Cancer May Limit the Utility of Neoantigen-Targeted Vaccines," *PLOS ONE*, vol. 11, no. 5, p. e0155189, May 2016, doi: 10.1371/journal.pone.0155189.

[26] E. Ghorani *et al.*, "Differential binding affinity of mutated peptides for MHC class I is a predictor of survival in advanced lung cancer and melanoma," *Annals of Oncology*, vol. 29, no. 1, pp. 271–279, Jan. 2018, doi: 10.1093/annonc/mdx687.

[27] A. J. Rech *et al.*, "Tumor Immunity and Survival as a Function of Alternative Neopeptides in Human Cancer," *Cancer Immunology Research*, vol. 6, no. 3, pp. 276–287, Mar. 2018, doi: 10.1158/2326-6066.CIR-17-0559.

[28] J. S. Holm *et al.*, "Neoantigen-specific CD8 T cell responses in the peripheral blood following PD-L1 blockade might predict therapy outcome in metastatic urothelial carcinoma," *Nature Communications*, vol. 13, no. 1, p. 1935, Dec. 2022, doi: 10.1038/s41467-022-29342-0.

[29] S. Kim *et al.*, "Neopepsee: accurate genome-level prediction of neoantigens by harnessing sequence and amino acid immunogenicity information," *Annals of Oncology*, vol. 29, no. 4, pp. 1030–1036, Apr. 2018, doi: 10.1093/annonc/mdy022.

[30] Meldgaard T.S., Viborg N., TamhaneT., Suarez Hernandez S., Albacete D.V., and Hadrup S.R., "H-2 multimers for high-throughput T cell interrogation and description of novel conditional ligands for H-2Dd and H-2Kd," *(manuscript submitted)*, 2019.

[31] S. R. Hadrup *et al.*, "Parallel detection of Ag-specific T-cell responses by multidimensional encoding of MHC multimers," *Nature Methods*, vol. 6, no. 7, pp. 520–526, Jul. 2009, doi: 10.1038/nmeth.1345.

[32] R. S. Andersen *et al.*, "Parallel detection of Ag-specific T cell responses by combinatorial encoding of MHC multimers," *Nature Protocols*, vol. 7, no. 5, pp. 891–902, May 2012, doi: 10.1038/nprot.2012.037.

Supplementary Material

Supplementary Table 1: Neoepitopes used to study characteristics 1) MHC-I binding capacity; and 2) Self dis-similarity.

EL %Rank was predicted with NetH2Pan. EL%Rank <0.5 denotes MHC-I strong binder; <2 weak binder; and >2 non-binder.

Neoepitope	MHC-I	Neoepitope sequence	EL %Rank Neoepitope	EL %Rank Normal epitope	Self similarity	Mutation consequence	Expression level
Conserved binders – High self similarity (CBHigh)							
Neo1	H2-Kd	IYLESVAIM	0.04	0.03	0.99	M	129.82
Neo2	H2-Kd	GFTATLKNV	1.16	0.48	0.99	M	0.39
Neo3	H2-Kd	AYVNAIEKIF	1.05	1.14	0.99	M	160.6
Neo4	H2-Kd	SFLAARGINV	1.53	1.24	0.99	M	3.33
Neo5	H2-Kd	YYDILKQIC	1.75	1.38	0.99	M	6.16
Conserved binders – Low self similarity (CBLow)							
Neo6	H2-Kd	QHSLGGDLL	0.76	0.59	0.9	M	9.72
Neo7	H2-Kd	VFPIAWHRL	1.04	0.87	0.89	M	16.94
Neo8	H2-Kd	KQTENRYPL	1.68	1.91	0.92	M	1.24
Neo9	H2-Kd	KGMILPGTQL	1.86	0.76	0.93	M	9.31
Neo10	H2-Kd	IFWNAGWQM	0.76	0.59	0.9	M	9.72
Improved binders – High self similarity (IBHigh)							
Neo11	H2-Kd	IHLHISALI	0.99	11.28	0.99	M	88.94
Neo12	H2-Kd	FHLLNREQRI	1.19	23	0.98	M	0.61
Neo13	H2-Kd	YFLESTMNEYI	1.28	11.51	0.98	M	0.17
Neo14	H2-Kd	VYEHLLYLSI	1.17	23.15	0.98	M	3.73
Neo15	H2-Kd	FYPPDEALEI	1.85	15.07	0.99	M	0.37
Improved binders – Low self similarity (IBLow)							
Neo16	H2-Kd	TYGPSEFSCM	0.55	33.55	0.94	M	7.15
Neo17	H2-Kd	VYCQIPLFGIM	1.01	20.49	0.94	M	23.28
Neo18	H2-Kd	VYCQIPLFGI	0.93	40.94	0.94	M	23.28
Neo19	H2-Kd	KWSMSRLEL	0.99	17.57	0.94	M	14.8
Neo20	H2-Kd	AYQPPFAF	1.14	31.48	0.93	M	2.79

Supplementary Table 2: Neoepitopes used to study characteristic 3) Mutation origin.

EL %Rank was predicted with NetH2Pan. EL%Rank <0.5 denotes MHC-I strong binder; <2 weak binder; and >2 non-binder.

Neoepitope	MHC-I	Neoepitope sequence	EL %Rank Neoepitope	EL %Rank Normal epitope	Self similarity	Mutation consequence	Expression level
Mis-sense (MS)							
Neo1	H2-Dd	NMFEFPPHL	0.05	0.2	0.93	M	18.02
Neo2	H2-Dd	KKFSHCVNL	1.26	1.87	0.96	M	0.13
Neo3	H2-Dd	TIFKDVYEL	1.15	0.28	0.95	M	0.52
Neo4	H2-Dd	GSGSPLDFM	1.41	0.7	0.99	M	0.26
Neo5	H2-Dd	NGARLKSLV	1.69	0.08	0.96	M	3.72
Frameshift (FS)							
Neo6	H2-Dd	VSTALWPAL	0.86	1.86	0.89	F	9.1
Neo7	H2-Dd	DGPLHGQHDL	1.19	0.81	0.83	F	22.02
Neo8	H2-Dd	TPGPLQGVTL	0.83	0.85	0.84	F	22.02
Neo9	H2-Dd	AAFQHDAAV	1.02	0.66	0.85	F	22.02
Neo10	H2-Dd	LNPHCFLKSL	0.56	1.92	0.87	F	10.93

Supplementary Table 3: Long peptides used to study charactesitic 4) absence of a strong MHC-II binding motif

EL %Rank long peptide was calculated with NetMHCIIPan. EL %Rank long peptide <2 denotes MHC-II strong binder; <10 weak binder; and >10 non-binder. EL %Rank short peptide was predicted with NetH2Pan. EL%Rank <0.5 denotes MHC-I strong binder; <2 weak binder; and >2 non-binder. In red: introduced point mutation disrupting the MHC-II binding motif. In green: MHC-I binding motif no affected by the point mutation.

Neopeptide	Long peptide (20-25mer)	MHC-II	MHC-II binder	EL %Rank long peptide	MHC-I	MHC-I binder	EL %Rank short peptide
C22	QIETQQRKFKASRASILSEMKMLKEKR	H2-IAd	QRKFKASRASILSEM	1.48	H2-Kd	KFKASRASI	0.34
C22mod	QIETQQRKFKASRASIWSEMKMLKEKR	H2-IAd	QRKFKASRASIWSEM	10.29	H2-Kd	KFKASRASI	0.45
C23	VILPQAPSGPSYATYLQPAQAQMLTPP	H2-IAd	GPSYATYLQPAQAQM	0.21	H2-Dd	SGPSYATYL	0.12
C23mod	VILPQAPSGPSYATYLQPAQWQMLTPP	H2-IAd	GPSYATYLQPAQWQM	3.99	H2-Dd	SGPSYATYL	0.12
C37	GEVPPQKLQALQRALQSEFCNAVREVY	H2-IAd	PPQKLQALQRALQSE	7.57	H2-Ld	VPPQKLQAL	0.19
C37mod	GEVPPQKLQALRRALQSEFCNAVREVY	H2-IAd	VPPQKLQALRRALQS	28.20	H2-Ld	VPPQKLQAL	0.22
C39	KKFMERDPDELRFNTIALSA	H2-IAd	RDPDELRFNTIALSA	10.16	H2-Kd	KFMERDPDEL	0.79
C39_mod	KKFMERDPDELRFNTIALFA	H2-IAd	RDPDELRFNTIALFA	49.31	H2-Kd	KFMERDPDEL	0.79
EV07	GDVKIHAHKVVLANISPYFKAMFTGNL	H2-IAd	IHAHKVVLANISPYF	2.45	H2-Dd	ISPYFKAMF	0.28
EV07mod	GDVKIHAHKVVLWNISPYFKAMFTGNL	H2-IAd	KVVLWNISPYFKAMF	51.40	H2-Dd	ISPYFKAMF	0.30

Chapter 7: Pilot study

B16BL6-OVA as a mouse model for validation of *in vitro* expanded $CD8^+$ T cells

This Chapter outlines a pilot study aiming to establish a workflow for the future investigation of the *in vivo* tumor-killing capacity (via ACT) of the neoepitope-specific $CD8^+$ T cells defined in Manuscript I. For such system, *in vitro* expansion of the desired ACT product is required to get sufficient cell numbers for transfer. Here, we established a B16BL6-OVA melanoma model to evaluate the use of Ag-scaffolds to expand $CD8^+$ T cells in an Ag-specific manner. This model permits the use of the transgenic OT-I T cell clone as a positive control for ACT, simplifying the optimization of experiments.

However, evaluating the effect of ACT was challenging, potentially explained by a highly immunosuppressive TME. Further studies are required, potentially establishing OVA expression in a more immunogenic model instead such as the colon carcinoma MC38.

Introduction

Ovalbumin-expressing tumor cell lines are an efficient tool to study T cell recognition in preclinical tumor models. Stable OVA expression offers an immunological target to explore T cell recognition of cancer, while the TCR transgenic OT-I mice – which all TCRs are monoclonal for the $OVA_{257-264}$ epitope SIINFEKL [1] – provide an optimal high-affinity T cell clone. Adoptive transfer of OT-I cells into OVA-expressing tumor-bearing mice has paved the way towards understanding mechanisms behind sensitivity of tumor models to e.g., CPI antibodies [2] or tumor irradiation [3]. In addition, such models have further contributed to define key factors to overcome resistance to ACT interventions by e.g., modulating immunosuppressive tumor microenvironments (TME, [4]). Surprisingly, even when using the OT-I T cell clone, some reports required large numbers of cells to slow tumor growth, while tumor regression has only been achieved when combining 2-20 million OT-I ACT with other immunomodulatory agents such as TGF-β [4], anti-CD137 [5] or tumor irradiation [2], [3]. Therefore, getting enough numbers of Ag-specific cells ensures a challenge to study functionality of low-frequent NART populations via ACT in murine syngeneic tumor models.

In a clinical context, ACT of tumor-recognizing T cells has proven clinical efficacy for metastatic melanoma patients [6]. In this regard, the standard method for large-scale *in vitro* expansion of tumor infiltrating lymphocytes (TILs) was pioneered on TILs from such patients. This method implies culturing TILs isolated from a biopsy with high doses of IL-2 for 2-3 weeks to eradicate tumor cells, followed by a rapid expansion process (REP) of pure TIL cultures using: i) Irradiated feeder cells allowing Ag presentation; ii) anti-CD3 antibody for TCR stimulation and T cell activation; and iii) high dose of IL-2. This way, both tumor-specific and bystander TILs present in the biopsied tissue are non-specifically expanded (reviewed in [7]). Recently, various reports highlighted the advantages of characterizing tumor-reactive TILs prior infusion [8], and the relevance of NARTs within TIL infusion products to modulate patients' response to ACT [9].

In view of this, NART enrichment within TIL infusion products may benefit response to ACT in the clinic. The so called "Ag-scaffold" technology recently developed in our lab allows expansion and enrichment of Ag-specific T cells within two weeks of *in vitro* culture (manuscript in preparation). Ag-scaffolds comprise a polysaccharide dextran backbone with covalently bound streptavidin conjugates, which allow the attachment of biotinylated peptide-MHC complexes and co-stimulatory molecules providing essential T cell survival and differentiation signals. This way, these scaffolds mimic the immunological synapse provided by professional Ag-presenting cells (APCs) and can be customized to expand T cells of a certain specificity while modulating the phenotype depending on the chosen cytokines (Figure 1A).

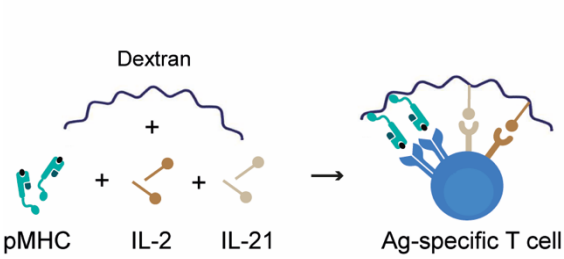

Figure 1: Schematic drawing of the Ag-scaffold construct.
Ag-scaffolds comprise a streptavidin-conjugated dextran backbone to which a biotinylated peptide-MHC complex (pMHC) and co-stimulatory molecules or cytokines can be attached. An IL-2 and IL-21 construct was used in this study. Ag-scaffolds bind T cells via pMHC-TCR interactions mimicking the immunological synapse with APCs.

In the present study, I generated a B16BL6-OVA melanoma model to evaluate the *in vivo* killing capacity of Ag-scaffold-expanded SIINFEKL-specific $CD8^+$ T cells as a control system. This pilot study follows the purpose of defining the requirements of Ag-scaffold expansion of murine T cells, to use them for studying NARTs in the context of a relevant preclinical model such as CT26 (see Chapter 5).

The standard scaffold construct used in the lab for expansion of human T cells comprises IL-2 and IL-21 cytokines, which are crucial for T cell proliferation and differentiation (reviewed in [10]). However, several reports evidence the need of IL-2 and IL-7 to ensure survival of murine T cells [11]–[13]. Therefore, I performed a series of optimization experiments to establish their optimal expansion conditions, reproducing the findings of [12] and concluding on the IL-7 requirement to expand OT-I T cells (data not shown). As IL-21 in combination with IL-2 and IL-7 has proven beneficial for the expansion of murine T cells [13], I kept IL-2 and IL-21 as the Ag-scaffold co-stimulatory molecules while supplementing the cultures with soluble IL-7. I further performed expansions on splenocytes from OVA-vaccinated mice following the rationale that the high affinity TCRs from OT-I cells might drive more efficient expansions than the low affinity TCRs characterizing NARTs. In addition, culturing isolated $CD8^+$ T cells with SIINFEKL-scaffolds resulted in higher yields of expanded cells by minimizing the high numbers of scaffold non-targeted cells present in splenocyte cultures from mice (data not shown).

To validate the functionality of Ag-scaffold-expanded OVA-specific $CD8^+$ T cells *in vivo*, I established a preclinical syngeneic B16BL6-OVA tumor model. The B16BL6 cell line is a metastatic melanoma murine cell line with enhanced tissue-invading capacity. It is characterized by little immune cell infiltration, hence being classified as a “cold tumor” reverted by OVA expression. Therefore, B16BL6-OVA *in vivo* tumor models allow the evaluation of the tumor-killing capacity of OVA-specific $CD8^+$ T cells through ACT experiments.

This way, the research presented in this chapter comprised a pilot study with the following aims:

- Aim 1: Establish the B16BL6-OVA tumor cell line *in vivo* in CB6F1 mice.
- Aim 2: Compare Ag-scaffold expansion of SIINFEKL-specific $CD8^+$ T cells to the standard free-peptide approach. Within this objective, several parameters were investigated.
    - Aim 2.1: Assess *in vitro* SIINFEKL-$CD8^+$ T cell expansion yield and phenotype.
    - Aim 2.2: Evaluate *in vivo* the tumor-killing capacity of Ag-scaffold vs free-peptide expanded $CD8^+$ T cells.
    - Aim 2.3: Study whether anti-PD-1 and anti-CTLA-4 treatment boost response to ACT.
    - Aim 2.4: Dose-scalation of Ag-scaffold expanded ACT.

Regarding the experimental procedure followed, it should be mentioned that scheduling vaccination of C57BL/6 donor mice and tumor engraftment of CB6F1 mice was essential for collecting Ag-specific expanded CD8+ T cells on the desired day for ACT into tumor-bearing mice. This is visualized in Figure 2. In addition, inclusion of CPI- and ISO-treated mice receiving 5 x 10^6 pre-activated OT-I T cells provided an ACT control group receiving a defined number of an optimal SIINFEKL-specific $CD8^+$ T cell clone (refer to Methods for details). Furthermore, the number of cells for the dose escalation were assessed based on the frequency of Ag-specific $CD8^+$ T cells achieved in previous expansion optimization experiments (data not shown). These cultures yielded ~20% Ag-specific $CD8^+$ T cells after Ag-scaffold expansion, so ACT doses of $20x10^6$, $10x10^6$, and $5x10^6$ expanded cells (corresponding to ~$4x10^6$, $2x10^6$, and $1x10^6$ estimated SIINFEKL-specific $CD8^+$ T cells) were chosen for Aim 2.4.

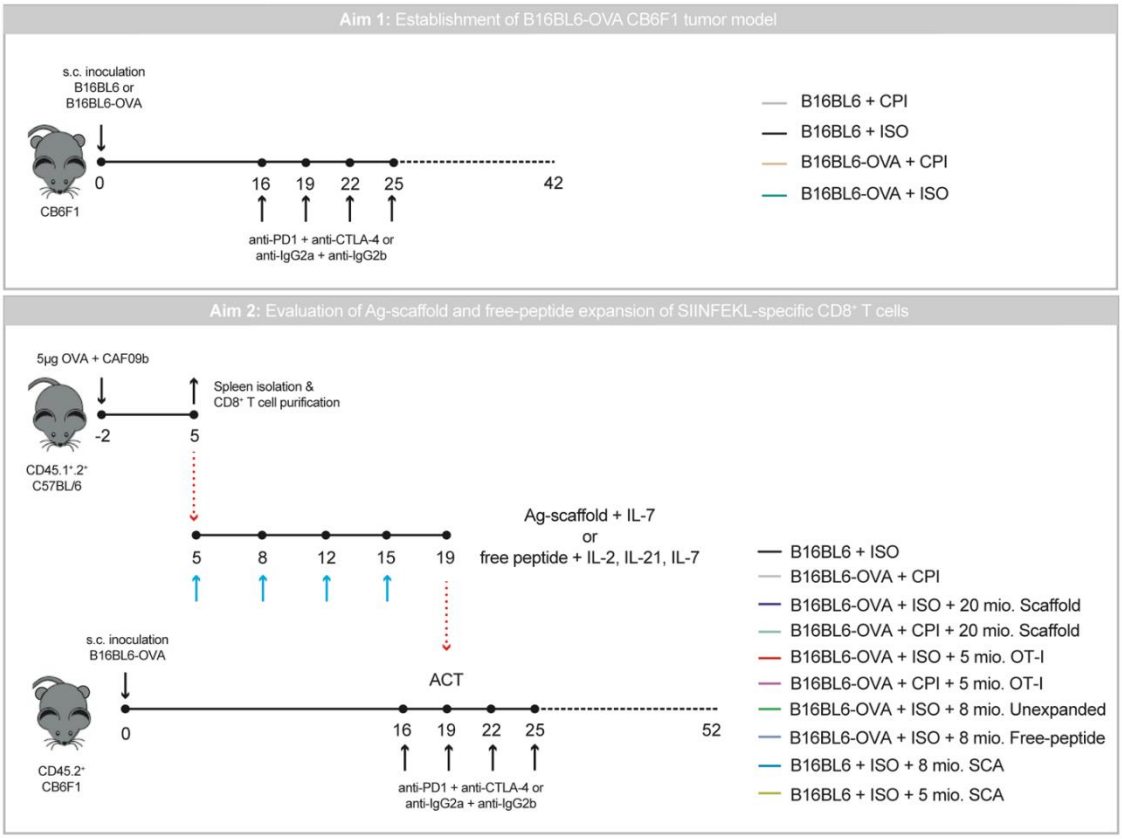

Figure 2: Overview of the *in vivo* experiments in the context of the study aims.
Aim 1: To validate the engraftment of the transfected B16BL6-OVA cell line, CB6F1 mice were subcutaneously (s.c.) inoculated with $0.5x10^6$ B16BL6-OVA or un-transfected B16BL6 cells as control. Mice received 200µg anti-PD-1 and 200µg anti-CTLA-4 checkpoint inhibitor antibodies (CPI) or the respective anti-IgG2a or anti-IgG2b isotype controls (ISO) to evaluate the different sensitivity of the models to CPI treatment. **Aim 2.1-2.2:** To evaluate *in vivo* the tumor killing capacity of Ag-specific expanded cells with free peptide or Ag-scaffolds, B16BL6-OVA tumor-bearing CB6F1 mice were intravenously (i.v.) infused with $8x10^6$ free peptide or Ag-scaffold expanded $CD8^+$ T cells on day 19 upon tumor establishment. As control, Unexpanded $CD8^+$ T cells (green) were isolated on the ACT day from splenocytes of mice vaccinated with 5µg OVA in the adjuvant CAF09b seven days prior ACT. **Aim 2.3:** To evaluate the synergistic effect of ACT and CPI therapy, a group of mice received the highest Ag-scaffold-expanded dose ($20x10^6$) together with CPI treatment (light blue). As controls, mice receiving $5x10^6$ pre-activated OT-I cells with ISO (red) or CPI (pink); and mice receiving ISO (black) or CPI (grey) without ACT were included. **Aim 2.4**: To define the optimal dose of Ag-scaffold-expanded $CD8^+$ T cells two groups of mice received $20x10^6$ (dark purple) or $5x10^6$ cells (yellow). All groups comprised 5 mice except for the following groups: ISO + $8x10^6$ free peptide (n=2), ISO + $5x10^6$ OT-I cells (n=4). Dotted lines represent the time during which mice with tumors reaching 2000mm3 in volume were sacrificed. The congenic CD45.1.2 and CD45.2 mice were used to distinguish cells from the ACT donor and recipient mice in future studies analyzing isolated tumors.

Results

OVA expression delays tumor onset

To evaluate the tumor establishment capacity of the transfected cell line, I generated B16BL6 and B16BL6-OVA tumor models on the CB6F1 hybrid murine strain. CPI treatment was given to further assess a potential synergistic effect with the ACT product as stated in Aim 2.3.

OVA expression markedly delayed tumor onset as visualized in Figure 3A, with tumors taking significantly longer times to reach 1600mm^3 in volume in both ISO- and CPI- treated groups. Of note, B16BL6 mice did not complete CPI treatment due to reaching humane endpoint before treatment completion. As previously described for B16F10 [15] B16BL6 was refractory to CPI treatment, independently of OVA expression (Figure 3A). Interestingly, CPI-treated B16BL6-OVA mice slowed tumor growth (Figure 3A), taking a significantly longer time to reach a size of 1600mm^3 compared to the CPI-treated B16BL6 cell line (Figure 3B).

Therefore, OVA expression sensitizes the B16BL6 cell line to endogenous T cell control, as previously defined in other melanoma models [2]. This enhanced immunogenicity seems to render the model responsive to CPI treatment when targeting PD-1 and CTLA-4 receptors.

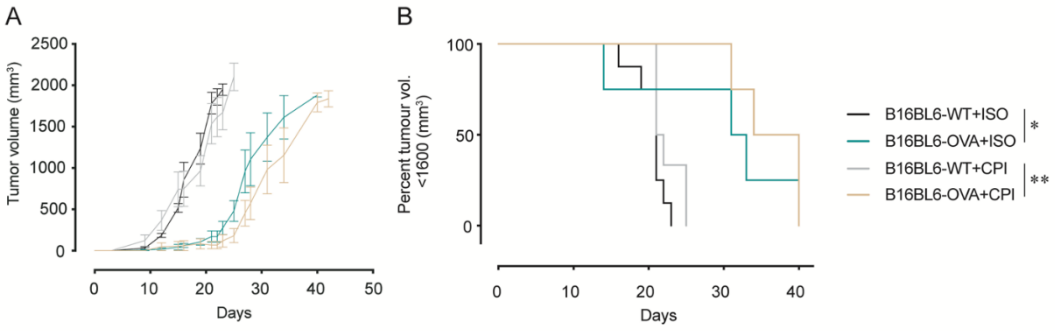

Figure 3: OVA expression by the B16BL6 melanoma cell line delays tumor onset.
A-B) B16BL6 engrafted CB6F1 received 200µg anti-IgG2a and 200µg anti-IgG2b isotype controls (ISO, black) or a similar dose of anti-PD-1 and anti-CTLA-4 checkpoint inhibitor antibodies (CPI, grey). B16BL6-OVA engrafted CB6F1 mice received ISO (green) or CPI (yellow). **A)** Tumor volume from engraftment of B16BL6 and B16BL6-OVA cells showing mean and mean standard error (SEM). **B)** Kaplan-Meier curves representing the probability of tumors to reach a volume of 1600mm^3. Log-Rank (Mantel-Cox) test (B) represents $p < 0.05$ as *, and $p < 0.01$ as **. B16BL6+ISO (n=6), B16BL6+CPI (n=8), B16BL6-OVA+ISO (n=4), B16BL6-OVA+CPI (n=4).

Ag-scaffold expansion results in higher yields of SIINFEKL-specific CD8$^+$ T cells

Ag-scaffolds restrict cytokine stimulation to the Ag-specific CD8$^+$ T cells by mimicking the immunological synapse provided by professional Ag-presenting. This allows activation and proliferation of Ag-specific CD8$^+$ T cell clones over bystander subsets. By contrast, standard Ag-specific T cell expansion methods require supplementing the culture media with cytokines and the peptide of interest, thus promoting proliferation of all T cells in the culture irrespectively of specificity. To evaluate the different efficacy to promote T cell expansion between Ag-scaffolds and free-peptide, parallel cultures were setup with CD8$^+$ T cells from OVA-vaccinated CD45.1.2 C57BL/6 mice (refer to Figure 2 for details).

Due to a higher number of mice receiving Ag-scaffold-expanded- compared to free-peptide-expanded SIINFEKL-specific CD8$^+$ T cells, Ag-scaffold cultures started with approximately 50x10^6 CD8$^+$ T cells while free-peptide cultures comprised ~ 10x10^6 seeded CD8$^+$ T cells. Per well, a total of 3x10^6 CD8$^+$ T cells were seeded. To compare culture yields and cell numbers, results depicted in Figure 4A-C are normalized to the number of cultured wells on each condition. This means that the "Unexpanded" product comprises the 3x10^6 seeded CD8$^+$ T cells and the free-peptide and Ag-Scaffold numbers are divided by the number of wells on each condition (refer to "*Preparation of adoptive cell transfer product" in* Methods section for details).

Ag-scaffold CD8$^+$ T cell expansion yielded higher number of total live cells compared to using free-peptide (expansion) (Figure 4A), resulting in a ~100 fold-expansion from 0.15x10^6 seeded SIINFEKL-specific CD8$^+$ T cells to 17x10^6 Ag-scaffold-expanded SIINFEKL-specific CD8$^+$ T cells (Figure 4B). Expansion of Ag-specific CD8+ T cells using free-peptide condition yielded lower expansion efficiency, resulting in 5.8 x 10^6 SIINFEKL-specific CD8$^+$ T cells and a ~37 fold-expansion. Moreover, Ag-scaffold expansion resulted in approximately 90% of SIINFEKL-specific CD8$^+$ T cells compared to 77% using the free-peptide condition (Figure 4C). These results strongly show a superior capacity of the Ag-scaffolds to expand SIINFEKL-specific CD8$^+$ T cells over bystander cells compared to using the free-peptide expansion method.

T cell differentiation and exhaustion phenotypes assessed for both Ag-scaffold- and free-peptide-expanded SIINFEKL-specific CD8$^+$ T cells by multi-colour flow cytometry were visualized using Uniform Manifold Approximation and Projection (UMAP) dimensionality reduction. When faceting UMAPs by expansion condition, unexpanded cells all clustered within the same population (Supplementary Figure 1C) characterized by a CD44$^+$CD62L$^-$ effector-memory phenotype lacking expression of the exhaustion markers CD39, PD-1 and LAG-3 (Figure 4D, black population). This phenotype is consistent with the non-sustained exposure to OVA, as cells were not re-exposed to OVA upon collection seven days after OVA-vaccination of donor mice. Of note, due to the low efficiency of free-peptide expansion for ACT, only 242 SIINFEKL-specific CD8$^+$ T cells were

analysed per condition. Therefore, phenotypic observations should only be taken as descriptive of the ACT products, as further replicates of these expansions are needed to confirm these observations.

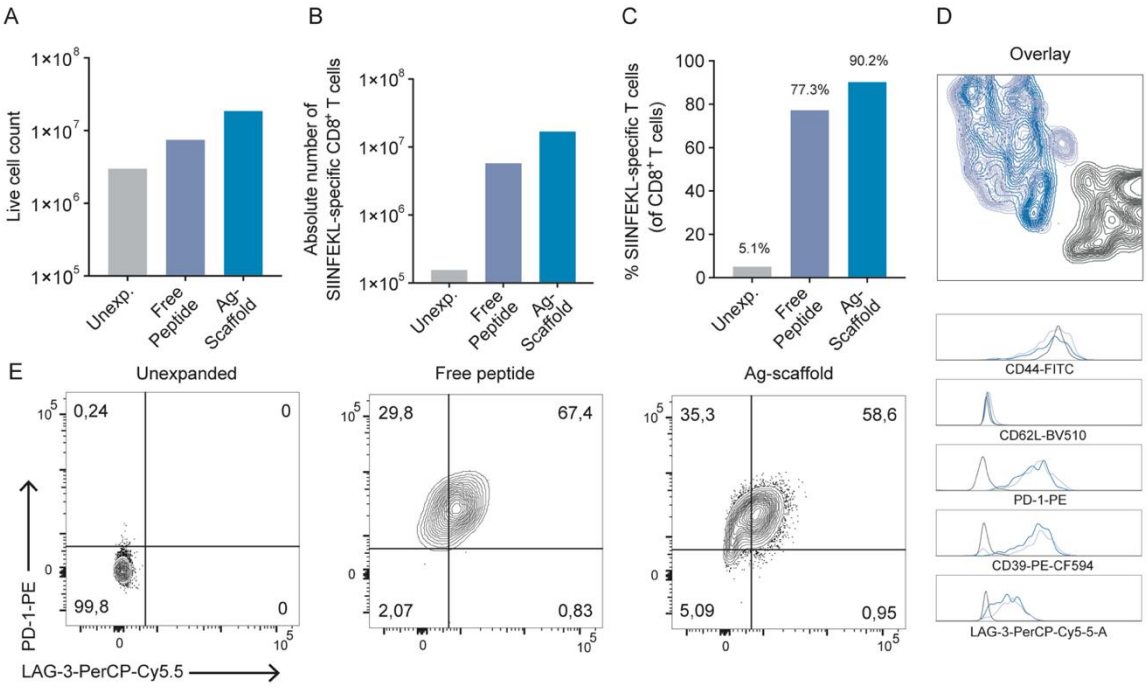

Figure 4: Ag-scaffolds efficiently expand SIINFEKL-specific CD8$^+$ T cells.
A) Number of viable cells when seeding the culture (Unexp.) and after two weeks of expansion with free peptide or Ag-scaffolds. Free peptide comprised SIINFEKL, IL-2, IL-21 and IL-7 in solution. Ag-scaffolds carried SIINFEKL:H2-K^b, IL-2 and IL-21 attached to the backbone and IL-7 was added in solution. **B)** Number and **C)** frequency of SIINFEKL-specific CD8$^+$ T cells after two weeks of expansion. **D)** Overlay of UMAP clustering analysis of the unexpanded (grey), free peptide- (purple) and Ag-scaffold-expanded (blue) SIINFEKL-specific CD8$^+$ T cells ACT products. SIINFEKL-specific CD8$^+$ T cells were identified by tetramer staining and characterized with a phenotyping panel including differentiation (CD44 and CD62L) and exhaustion markers (PD-1, CD39, LAG-3). Expression level of these markers are represented with MFI histograms. **E)** FACS plots showing proportions of PD-1$^+$ and LAG-3$^+$ CD8$^+$ T cells across unexpanded and expanded cells. Data is representative of one experiment.

Ag-scaffold-expanded CD8$^+$ T cells show superior tumor control over free-peptide-expanded SIINFEKL-specific CD8$^+$ T in B16BL6-OVA engrafted CB6F1 mice

Upon ACT on day 19 after tumor establishment, tumors from mice receiving Ag-scaffold-expanded CD8$^+$ T cells showed significantly smaller volumes on day 26 compared to tumors from mice receiving free-peptide-expanded CD8$^+$ T cells (Figure 5 A, B). This observed difference might be influenced by a 90.2% SIINFEKL-specific Ag-scaffold-expanded CD8$^+$ T cell product compared to the 70.3% of free-peptide-expanded CD8+ T cells (refer to Figure 4B), which

translates into mice receiving approximately 1.5 x 10^6 Ag-specific $CD8^+$ T cells more for the group of Ag-scaffold compared to free-peptide group. On this line, it should be noted that, the ability of Ag-scaffolds to generate ACT products with a higher proportion of Ag-specific $CD8^+$ T cells is an intrinsic advantage of this expansion method. Therefore, these results show an advantage of Ag-scaffold over free-peptide expanded CD8+ T cells to limit tumor growth within the first 26 days of tumor development.

Nevertheless, there were no significant differences in tumor growth between Ag-scaffold-expanded and unexpanded SIINFEKL-specific $CD8^+$ T cell injected groups, in part due to increased variation between tumors in the unexpanded group (Figure 5 A, B).

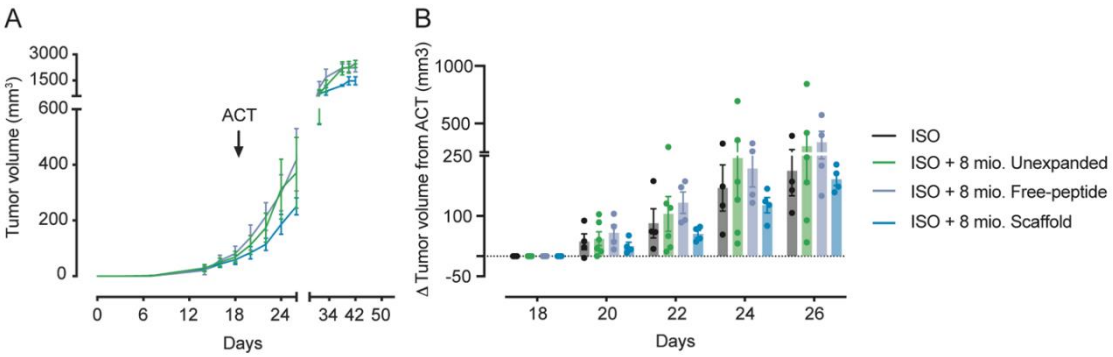

Figure 5: Ag-scaffold-expanded $CD8^+$ T cells delay tumor growth in B16BL6-OVA engrafted CB6F1 mice.

A-B) B16BL6-OVA tumor-bearing CB6F1 mice received intravenously 8x10^6 free peptide- (purple) or Ag-scaffold-expanded (blue) $CD8^+$ T cells. As control, mice received the same dose of Unexpanded (green) $CD8^+$ T cells isolated from C57BL/6 mice one week upon vaccination with 5µg OVA in CAF09b adjuvant. **A)** Tumor volume from B16BL6-OVA inoculation showing mean and mean standard error (SEM). **B)** Difference in tumor volume between the specified timepoints and measurements on the ACT infusion day. Error bars represent SEM. A mixed-effect linear model considering tumors a random effect and Bonferroni-corrected denotes differences of means between treatments on each day, with p-values < 0.05 represented as *.

Checkpoint inhibitor treatment masks the effect of transferred SIINFEKL-specific CD8+ T cell product

To evaluate the synergistic effect between ACT and CPI treatment, ACT was given together with the second administration of CPI or ISO antibodies. Growth curves and differences in tumor volume from ACT illustrated in Figure 6A, B clearly show how CPI controls tumor growth significantly in both groups receiving $5x10^6$ pre-activated OT-I T cells and $20x10^6$ Ag-scaffold-expanded SIINFEKL-specific CD8+ T cells. CPI treatment of mice with or without ACT (Figure 6B) showed similar tumor growth control, suggesting that the mechanisms by which anti-PD-1 and anti-CTLA-4 slower B16BL6-OVA tumor growth are independent of the transferred SIINFEKL-specific $CD8^+$ T cells. In addition, $5x10^6$ pre-activated OT-I T cells do not seem sufficient to induce tumor growth control. This observation is in line with previous literature showing tumor-slowing responses to $10x10^6$ pre-activated OT-I cells [4]. However, a limited number of cells prevented us from increasing the OT-I dose to $10x10^6$ cells. Moreover, $20x10^6$ Ag-scaffold-expanded cells did not further improve tumor-growth control seen by the $8x10^6$ Ag-scaffold-expanded product (Figure 6 C, D).

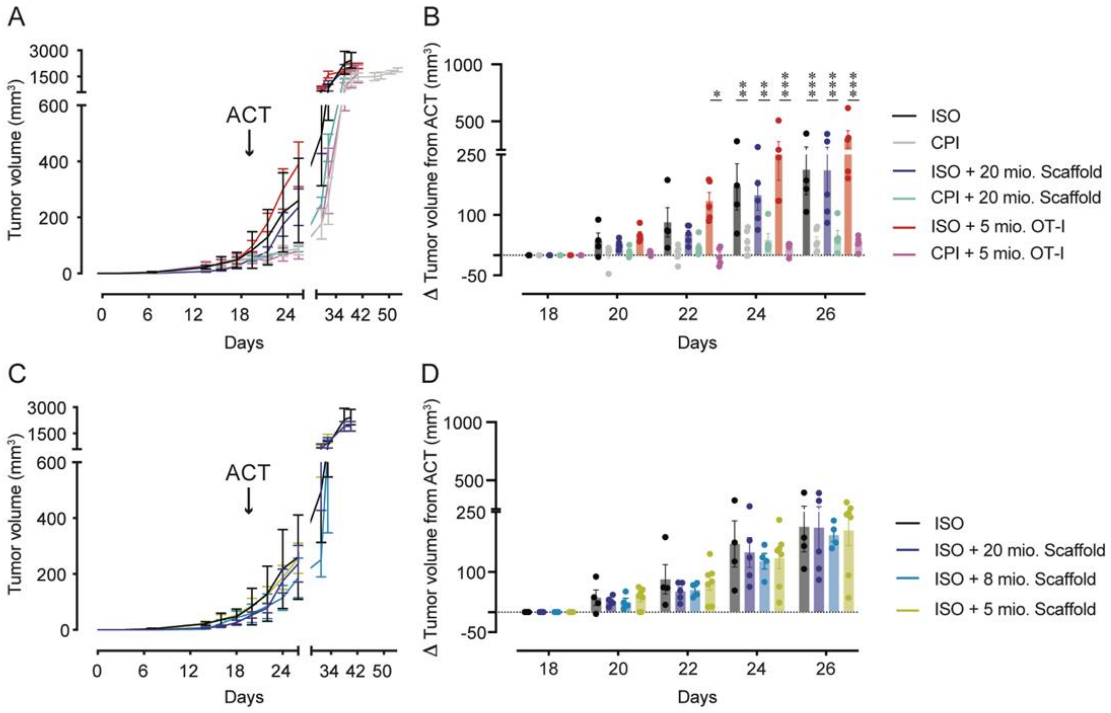

Figure 6. CPI treatment masks the effect of transferred SIINFEKL-specific CD8+ T cell product, with no apparent benefit of upscaling the ACT dose to 20x10^6 cells.

A-B) B16BL6-OVA engrafted CB6F1 mice received intravenously 20x10^6 Ag-Scaffold expanded cells while treated with 200µg anti-IgG2a and 200µg anti-IgG2b isotype controls (ISO, purple) or a similar dose of anti-PD-1 and anti-CTLA-4 checkpoint inhibitor antibodies (CPI, light blue). As controls, mice received 5x10^6 pre-activated OT-I cells with ISO (red) or CPI (pink) were included; and ISO (black) or CPI alone (grey). C-D) B16BL6-OVA engrafted BB6F1 mice receiving ISO antibodies were intravenously injected with 20x10^6 (purple, same animal group as in A-B), 8x10^6 (blue, same animal group as in Figure 5), or 5x10^6 (yellow) with ISO antibodies. **A-C)** Tumor volume from B16BL6-OVA inoculation showing mean and mean standard error (SEM). **B-D)** Difference in tumor volume between the specified timepoints and measurements on the ACT infusion day. Error bars represent SEM. A mixed-effect linear model considering tumors a random effect and Bonferroni-corrected denotes differences of means between treatments on each day, with p-values < 0.05, <0.01, <0.001 represented as *, ** and *** respectively. Multiple comparisons showed no significant differences in D**.**

Discussion

Firstly, we show how OVA expression slows tumor growth of the B16BL6 tumor mode. In addition, we demonstrate the advantage of using Ag-scaffolds to drive a 100-fold expansion of SIINFEKL-specific CD8$^+$ T cells in a short time frame of 2 weeks of culture. The Ag-scaffold-expanded SIINFEKL-specific CD8$^+$T cells slowed tumor growth to a greater extent than free-peptide-expanded SIINFEKL-specific CD8$^+$ T cells. Lastly, we show that CPI treatment alone slowed tumor growth longer than ACT of either free-peptide-expanded OT-I cells or Ag-scaffold-expanded SIINFEKL-specific CD8$^+$T cells. And interestingly, our observations indicate no benefit of combining CPI therapy with ACT on this model – not even when upscaling the ACT dose to 20x10^6 cells.

Regarding the expanded SIINFEKL-specific CD8$^+$ T cell culture, both Ag-scaffold- and free-peptide-expanded cells were mainly PD1$^+$LAG-3$^+$. Co-expression of these markers is linked to terminally exhausted CD8$^+$ T cells (Tex) lacking proliferative capacity. Instead, memory-like precursor exhausted CD8$^+$ T cells (Tpe) expressing the transcription factor TCF-1 and the surface receptor PD-1 have self-renewal properties and the capacity to differentiate into effector-like transitory cells responsive to CPI, being able to mount strong anti-tumor responses (revised in [16], [17]). A more extensive phenotypic analysis is required to evaluate whether the higher expansion yields of Ag-scaffold-expanded cells correlate to a higher proportion of Tpe cells. Preclinical melanoma tumor models have proven useful to evaluate the efficacy and untangle mechanisms of relevant therapeutic interventions in patients [18]. To our knowledge, the B16F10 cell line is the most widely characterized while the B16BL6 metastatic melanoma model has not been as extensively explored. In addition, we believe that the present study is novel in the use of

B16BL6-OVA, so our observations may not translate to findings described in B16F10-OVA models.

Previous studies on B16BL6 preclinical models demonstrate the need to inhibit its immunosuppressive TME for successful immune-mediated tumor elimination in response to immunotherapeutic interventions. This tumor has been observed to specifically recruit Tregs to mediate immune suppression. Prophylactic administration of the regulatory-T cell (Treg)-depleting anti-CD25 antibody prior to tumor establishment was demonstrated to coincide with activation of the tumor vasculature and tumor-rejection [19]. In absence of prophylactic Treg cell depletion, histological analysis showed how $CD8^+$ T cells failed to infiltrate the tumor. However, this situation was reverted in a later study when anti-CTLA-4+Gvax administration was combined with lymphodepleting irradiation and ACT of melanoma-specific “pmel” T cell clones from pre-vaccinated donor mice [20]. Therefore, T cell-driven slowing of tumor-growth in a therapeutical setting was only achieved in this model when the tumor-bearing hosts were irradiated and infused with ACT from pre-vaccinated donor mice, while also receiving booster anti-CTLA-4 and Gvax vaccinations [20]. This approach induced $CD8^+$ T cell infiltration of the tumor otherwise absent.

Another report describing an algorithm to model *in silico* induced immune responses in B16-melanoma preclinical models [5], further shows how activation of the vasculature by anti-CD137 antibodies – which target the CD137 receptor expressed in endothelial tumor cells – is needed to achieve tumor-regression by preactivated OT-I cells. Ligand-binding of CD137 receptors result in a pro-inflammatory switch allowing T cell infiltration [21], supporting the observations described on [20] of poor T cell infiltration in a B16 model even when expressing OVA.

These observations suggest the need of alternative interventions in this model (e.g., tumor irradiation prior ACT transfer [3]) to boost its immunogenicity and be able to draw conclusions on the effectivity of ACT. With this, we wonder whether the lack of a synergistic effect between CPI and ACT on the B16BL6-OVA model was propitiated by a non-permeable vasculature and immunosuppressive TME. However, CPI do mediate tumor growth delay, most likely due to activation of endogenous TILs and Treg depletion following anti-CTLA-4 administration [22], [23]. In this regard, we hypothesize that early OVA expression in the B16BL6-OVA model allows endogenous tumor infiltration until a certain timepoint, after which it becomes “immune-excluded”. To elucidate this, immunohistochemistry analysis of tumor sections may pinpoint whether adoptively transferred cells managed to infiltrate the tumor or if all TILs are endogenous CD45.2 expressing OVA-specific $CD8^+$ T cells.

With this pilot work, we have realized the challenges with the B16BL6 tumor model to evaluate ACT strategies, and hence we will introduce alternative models to allow for such pre-clinical

evaluations of ACT anti-tumor efficacy. Alternatively, infusion of free-peptide and Ag-scaffold expanded SIINFEKL-specific $CD8^+$ T cells prior tumor cell inoculation – and evaluation of its capacity to delay tumor onset – might serve to validate *in vivo* the expanded T cell product functionality while overcoming the suppressive TME of established tumors.

Materials and Methods

Mice

All animals Ire housed at the animal facility at the Technical University of Denmark and all experiments conducted in accordance with the Danish National Committee for the Protection of Animals used for Scientific Purposes. CD45.1.2 C57BL6 female mice were bred *in house* and kindly provided by Associate Professor Katharina Lahl (Department of Health Technology, Technical University of Denmark, Denmark). Transgenic OT-I female mice were kindly provided by Professor William Agace (Department of Experimental Medicine Science, BMC Biomedical Center, Sweden). CB6F1 female mice Ire purchased from Envigo (Horst, Netherlands). Female, 8 to 11 weeks old mice were used in all experiments. Each group was kept in separate cages with a maximum of six animals per cage.

Cell lines

The B16BL6 cell line was kindly provided by Dr. Sergio Quezada (University College London Cancer Institute, United Kingdom). These cells Ire transduced with a lentivirus vector encoding expressing full length ovalbumin, click bettle green luciferace and a green fluorescent protein (GFP) tag for easy detection (data not published). OVA-expressing transduced cells Ire selected by Fluorescence Activated Cell Sorting (FACS) based on GFP signal. Cells Ire cultured in Dulbecco's Modified MEM (DMEM, Cat. No. 11965084) supplemented with 10% heat inactivated fetal calf serum (FCS, Fischer Scientific, Cat. No. 10500064) and 1% Penicillin-Streptomycin (Pen-Strep, Life Technologies, Cat. No. 15140122). Cells Ire kept at 37ºC and 5% CO_2 and split when confluent. Stable OVA-expression by cultured cells was inferred based on GFP signal by FACS analysis at random timepoints before tumor inoculation.

Tumor models

Mice Ire anesthetized in a chamber under isoflurane and 2% oxygen and shaved on the back. Tumor cells in 150µl PBS Ire subcutaneously inoculated in both flanks of the mice. Loaded syringes Ire kept on ice but adjusted to room temperature (RT) and mixed prior to inoculation. Tumor growth was monitored three times a Iek using a digital caliper and tumor volume was calculated using the following formula: tumor volume = $\frac{\text{length} \times \text{width}^2}{2}$. The number of cells inoculated are specified in the legend of each Figure. Animals were euthanized by cervical dislocation when they showed signs of distress, tumors reached ≥2000mm^3, or ulcerated. Tumors that did not reach a volume of 1000mm^3 due to earlier termination because of e.g., ulceration or endpoint size of the contralateral tumor, Ire excluded. Figure 1: 10 mice Ire inoculated with B16BL6 and B16BL6-OVA cells. Six B16BL6-OVA tumors did not establish. Figures 3-5: Fifty mice Ire inoculated with B16BL6-OVA cells. HoIver, three mice Ire found dead, and four tumors did not establish. The number of tumors included on each experiment are specified on the figure legends.

Immunization of ACT donor mice and CD8$^+$ T cell isolation

CD45.1.2 mice were vaccinated with 5µg OVA formulated in CAF09b adjuvant (200µg/dose cationic lipid DDA, 40µg/dose mycobacterial cell wall lipid MMG-1, 40µg/dose toll like receptor-3 analogue Poly(I:C), kindly gifted by Dennis Christensen, Statens Serum Institute, Denmark). OVA was diluted in 100µl Tris-buffer (9% sucrose, pH 7.4) and added drop-wise to 100µl CAF09b. The mix was vortexed for 30 seconds and kept at room temperature (RT) for 30min prior to injection. Vaccines Ire injected intraperitoneally in a volume of 200µl. A week later, spleens Ire isolated in R10 (RPMI1640, Fischer Scientific, Cat. No. 61870044 supplemented with 10% FCS) and kept on ice. Single cell suspensions Ire obtained through mechanical disaggregation on a 70µm strainer (Corning, Cat. No. 43175) and 50ml Falcon tube using a syringe plunger. Strainers Ire flushed with 10mL R10. CD8+ T cells Ire isolated from splenocytes by negative selection using the EasySep Mouse CD8+ T cell Isolation Kit (Cat. No. 19854, Stemcell Technologies).

Generation of peptide-MHC molecules

Lyophilized SIINFEKL was purchased from Pepscan (Netherlands), and reconstituted in dimethyl sulfoxide (DMSO, Sigma-Aldrich, Cat. No. C6164) to a concentration of 10mg/ml. Aliquots Ire stored at -20 ºC and thawed at RT before use. Murine MHC-I molecules stabilized with a UV-photocleavable ligand were produced *in house* as described in [14]. Briefly, SIINFEKL and the murine MHC-I molecule H2-Kb Ire diluted in PBS and mixed to a final concentration of 200µM and 100µM, respectively. Next, the mix was placed under a 366nm UV light for 1h at RT to allow exchange of the UV-photocleavable ligand by SIINFEKL. Upon centrifugation at 3300g for 5min at 4ºC, the exchanged supernatant was transferred to a new plate to discard aggregates in the pellet. Plates were kept refrigerated in the dark until use no later than 24 hours.

Ag scaffold preparation

Titration of the different Ag-scaffolds' components showed improved expansion capacity when prepared in a ratio 1:24:6:6 (dextran:pMHC:IL-2:IL-21, data not shown). For this, biotinylated human IL-2 (hIL-2, Avitag, Cat. No. IL2-H82F3, AcroBiosystems) and biotinylated human IL-21 (hIL-21, Avitag, Cat. No. IL2-H82F7, AcroBiosystems) Ire thawed on ice. Cytokines and the exchanged SIINFEKL-H2K^b complexes were mixed in PBS to a final concentration of 4.58µM and 2.22µM respectively. The streptavidin-conjugated phycoerythrin (PE)-labeled dextran (160nM stock, Fina Biosolutions, USA) was centrifuged at 10000rpm for 5min at 4ºC and added to the mix at a 0.6µM final concentration. Upon incubation for 30min on ice in the dark, D-biotin was added to a final concentration of 5.76µM to block the remaining streptavidin free binding sites. Assembled Ag-scaffolds Ire centrifuged at 3000g for 5min at 4ºC and the supernatant transferred to a Vivaspin 6 Centrifugal Concentrator (100KDa, Fisher Scientific, Cat. No. 10120901) for up-concentration of the Ag-scaffold stimulations. Columns Ire pre-saturated with 2% Bovine Serum

Albumin (BSA, Cat.No. A7906, Sigma-Aldrich) by centrifugation at 3000g. After two PBS washes, Ag-scaffolds Ire loaded and up-concentrated to a final volume of 2µl per stimulation. Freezing media was added to a final concentration of 0.5% BSA and 5% glycerol, considering 2µl/stimulation as the final volume. The final Ag-scaffold solution was aliquoted and stored at -20ºC.

Detection of SIINFEKL-specific T cells

Allophycocyanin labeled streptavidin (SV-APC, Biolegend, Cat. No. 405207) was loaded with exchanged pMHC for 30 minutes on ice (1.804µg SV-APC/100µl pMHC). 500µM D-biotin (Avidity, Cat. No. BIO200) was added and incubated 20 minutes on ice, and the final product was stabilized using a 10x freezing media (PBS with 0.5% BSA and 5% glycerol) and stored at -20°C. 5 x 10^5 splenocytes Ire plated in U-bottom 96-Ill culture plates. Tetramers were thawed on ice and centrifuged at 10000rcf for 2min at 4ºC to remove aggregates. Unspecific binding was blocked with anti-CD16/32 antibody (Fc-block, Biolegend, Cat. No. 101301) for 10min at 4ºC. 1µl of tetramer was collected in FACS buffer in a final volume of 50µl per staining, containing 10µl 10X BV Buffer (BD, Cat. No. 566385) and 0.5nM Dasatinib and incubated for 15 minutes at 37°C. Cells were stained with Near-IR LIVE/DEAD Fixable Dead Cell Staining kit (APC-Cy7, Biolegend, Cat. No. L10119) and a surface antibody mix (anti-CD3-BUV395 (BD, 145-2C11, Cat. No. 563565), anti-CD4-BV605 (BD, RM4-5, Cat. No. 563151), anti-CD8-BUV737 (BD, 53-6.7, Cat. No. 612759), anti-CD223-PerCP-Cy5.5 (LAG-3, C9B7W, Cat. No. 564673), anti-PD-1-PE (BD, J43, Cat. No. 561788), CD39-PE-CF594 (Biolegend, Duha59, Cat. No. 143811), anti-CD44-FITC (BD, IM7, Cat. No. 553133), anti-CD62L-BV510 (BD, MEL-14, Cat. No. 563117)), for 30 minutes at 4°C. After two washes in FACS buffer the cells were either filtered using blue cap FACS tubes (Falcon, Cat#352235) and acquired directly on the flow cytometer or fixed using 1% filtered paraformaldehyde (ThermoFischer, Cat# 11400580) for 1–24 hours before acquision.

Preparation of adoptive cell transfer product

3 x 10^6 million cells were distributed per well in a G-rex cell culture 24-well plate (Cat. No. KDW0024). Sixteen wells received Ag-scaffold culture media while three wells received free-peptide stimulation. All cells were cultured on a 5mL final volume as follows: Ag-scaffold expansion: cells were first resuspended in 1mL complete culture media (R10 supplemented with 1% Penicillin-Streptomycin (Pen-Strep, Life Technologies, Cat. No. 15140122), 1% Insulin-Transferrin-Selenium (ITS, Gibco, Cat. No. 41400-045), 0.1% 2-Mercaptoethanol (55mM stock, Gibco, Cat. No. 21984-025)) supplemented with 2 stimulations/mL and human IL-7 (hIL-7, Prepotech, Cat. No. 200-07) at 10ng/mL final concentration. Cells were cultured for 1 hour to promote interaction between Ag-scaffolds and $CD8^+$ T cells, after which wells were topped up to 5mL final volume. Free-peptide: cells were directly cultured in 5mL complete culture media containing 2µM SIINFEKL, 10ng/mL hIL-7, 40IU/mL hIL-2 (Prepotech, Cat. No. 200-02) and

10ng/mL hIL-21. Half of the media was exchanged every second day without disturbing cells at the bottom, adding fresh Ag-scaffolds/peptide and cytokines on days 3, 7, and 10 after seeding the cultures. OT-I cells: frozen OT-I splenocytes were thawed and $CD8^+$ T cells purified two days before ACT administration. They were pre-activated for 48 hours following the free-peptide stimulation protocol. Unexpanded cells: CD45.1.2 donor mice were vaccinated one-week before ACT. On the same day as ACT, spleens were collected, single cell suspensions made and $CD8^+$ T cells purified as previously described. Cells were collected and counted four days upon last stimulation. Cytokines were diluted following manufacturer's recommendations, stored at -20ºC and thawed on ice before use. They were kept refrigerated for a maximum period of one week upon thawing.

Checkpoint inhibitor treatment and ACT

Immune checkpoint inhibitor (CPI) treatment comprised 200µg of anti-PD1 (Nordic BioSite, RMP1-14, Cat. No. BE0146) and 200µg of anti-CTLA-4 (Nordic BioSite, 9H10, Cat. No. BE0164) antibodies or 200µg of each relevant isotype control antibody (ISO); anti-IgG2a (Nordic BioSite, C1.18.4, Cat. No. BE0085) and anti-IgG2b (Nordic BioSite, MPC-11, Cat. No. BE0086) respectively. Antibodies Ire diluted in 200µl PBS per injection and administered intraperitoneally (i.p.) on days 16, 19, 22 and 25. Cells for ACT Ire washed three times in PBS, diluted to the optimal dose and injected in 100µl volume. Each treatment group comprised a total of five mice. However, due to insufficient free-peptide-expanded and pre-activated OT-I cells, only two and four mice were included in the FP+ISO and OT-I+ISO group, respectively.

Flow cytometry

Flow cytometry data were analyzed using FlowJo version 10.7.1 (TreeStar, Inc.). For UMAP dimensionality reduction, 242 live, $CD3^+$, $CD8^+$, $SIINFEKL^+$ cells were concatenated from each sample (n = 3) and plotted using the UMAP plugin in FlowJo. UMAP was run for the following parameters: CD44, CD62L, CD39, PD-1 and LAG-3. Unsupervised clustering was performed with the FlowSom algorithm in FlowJo, where the 8 default clusters were selected. All flow cytometry experiments were carried out on Fortessa instruments (BD Biosciences).

Statistical analyses

GraphPad Prism 7 for Mac OS X was used for graphing. Statistical analysis was performed in R version 4.0.2.

Acknowledgements

We would like to thank Christoph Hillisch for his dedication to optimizing the Ag-scaffold cultures of murine T cells during his MSc thesis. We also thank Maria Ormhøj for the transfection of the B16BL6-OVA cell line. We thank Katharina Kahl and William Agace for providing $CD45.1^+.2^+$ mice

and OT-I splenocytes respectively. In addition, we thank Katrine Fog Starup and Isabel Ulmert for support with the CD45.1^{+}.2^{+} mice breeding. And lastly, special thanks to Marcus Svensson Frej and Siri Amanda Tvingsholm for the very needed support with animal handling.

References

[1] F. R. Carbone, S. J. Sterry, J. Butler, S. Rodda, and M. W. Moore, “T cell receptor α-chain pairing determines the specificity of residue 262 within the K^{b} -restricted, ovalbumin $_{257–264}$ determinant,” *International Immunology*, vol. 4, no. 8, pp. 861–867, 1992, doi: 10.1093/intimm/4.8.861.

[2] E. J. Lelliott *et al.*, “A novel immunogenic mouse model of melanoma for the preclinical assessment of combination targeted and immune-based therapy,” *Scientific Reports*, vol. 9, no. 1, p. 1225, Dec. 2019, doi: 10.1038/s41598-018-37883-y.

[3] J.-Z. Lai, Y.-Y. Zhu, M. Ruan, L. Chen, and Q.-Y. Zhang, “Local Irradiation Sensitized Tumors to Adoptive T Cell Therapy via Enhancing the Cross-Priming, Homing, and Cytotoxicity of Ag-Specific CD8 T Cells,” *Frontiers in Immunology*, vol. 10, Dec. 2019, doi: 10.3389/fimmu.2019.02857.

[4] A. Wallace *et al.*, “Transforming Growth Factor-β Receptor Blockade Augments the Effectiveness of Adoptive T-Cell Therapy of Established Solid Cancers,” *Clinical Cancer Research*, vol. 14, no. 12, pp. 3966–3974, Jun. 2008, doi: 10.1158/1078-0432.CCR-08-0356.

[5] F. Pappalardo, I. M. Forero, M. Pennisi, A. Palazon, I. Melero, and S. Motta, “SimB16: Modeling Induced Immune System Response against B16-Melanoma,” *PLoS ONE*, vol. 6, no. 10, p. e26523, Oct. 2011, doi: 10.1371/journal.pone.0026523.

[6] L. T. Nguyen *et al.*, “Phase II clinical trial of adoptive cell therapy for patients with metastatic melanoma with autologous tumor-infiltrating lymphocytes and low-dose interleukin-2,” *Cancer Immunology, Immunotherapy*, vol. 68, no. 5, pp. 773–785, May 2019, doi: 10.1007/s00262-019-02307-x.

[7] Ö. Met, K. M. Jensen, C. A. Chamberlain, M. Donia, and I. M. Svane, “Principles of adoptive T cell therapy in cancer,” *Seminars in Immunopathology*, vol. 41, no. 1, pp. 49–58, Jan. 2019, doi: 10.1007/s00281-018-0703-z.

[8] E. Tran *et al.*, “Cancer Immunotherapy Based on Mutation-Specific CD4+ T Cells in a Patient with Epithelial Cancer,” *Science (1979)*, vol. 344, no. 6184, pp. 641–645, May 2014, doi: 10.1126/science.1251102.

[9] N. P. Kristensen *et al.*, “Neoantigen-reactive CD8+ T cells affect clinical outcome of adoptive cell therapy with tumor-infiltrating lymphocytes in melanoma,” *Journal of Clinical Investigation*, vol. 132, no. 2, Jan. 2022, doi: 10.1172/JCI150535.

[10] G. C. Sim and L. Radvanyi, “The IL-2 cytokine family in cancer immunotherapy,” *Cytokine & Growth Factor Reviews*, vol. 25, no. 4, pp. 377–390, Aug. 2014, doi: 10.1016/j.cytogfr.2014.07.018.

[11] A. Drake, M. Kaur, B. P. Iliopoulou, R. Phennicie, A. Hanson, and J. Chen, “Interleukins 7 and 15 Maintain Human T Cell Proliferative Capacity through STAT5 Signaling,” *PLOS ONE*, vol. 11, no. 11, p. e0166280, Nov. 2016, doi: 10.1371/journal.pone.0166280.

[12] M. D. Lewis, E. de Leenheer, S. Fishman, L. K. Siew, G. Gross, and F. S. Wong, “A reproducible method for the expansion of mouse CD8 + T lymphocytes,” *Journal of Immunological Methods*, vol. 417, pp. 134–138, Feb. 2015, doi: 10.1016/j.jim.2015.01.004.

[13] C. Zoon, W. Wan, L. Graham, and H. Bear, “Expansion of T Cells with Interleukin-21 for Adoptive Immunotherapy of Murine Mammary Carcinoma,” *International Journal of Molecular Sciences*, vol. 18, no. 2, p. 270, Jan. 2017, doi: 10.3390/ijms18020270.

[14] Meldgaard T.S., Viborg N., TamhaneT., Suarez Hernandez S., Albacete D.V., and Hadrup S.R., “H-2 multimers for high-throughput T cell interrogation and description of novel conditional ligands for H-2Dd and H-2Kd,” *(manuscript submitted)*, 2019.

[15] J. F. Grosso and M. N. Jure-Kunkel, “CTLA-4 blockade in tumor models: an overview of preclinical and translational research.,” *Cancer Immun*, vol. 13, p. 5, 2013.

[16] J. D. Chan, J. Lai, C. Y. Slaney, A. Kallies, P. A. Beavis, and P. K. Darcy, “Cellular networks controlling T cell persistence in adoptive cell therapy,” *Nature Reviews Immunology*, vol. 21, no. 12, pp. 769–784, Dec. 2021, doi: 10.1038/s41577-021-00539-6.

[17] G. Escobar, D. Mangani, and A. C. Anderson, “T cell factor 1: A master regulator of the T cell response in disease,” *Science Immunology*, vol. 5, no. 53, Nov. 2020, doi: 10.1126/sciimmunol.abb9726.

[18] K. Nakamura, N. Yoshikawa, Y. Yamaguchi, S. Kagota, K. Shinozuka, and M. Kunitomo, “Characterization of mouse melanoma cell lines by their mortal malignancy using an experimental metastatic model,” *Life Sciences*, vol. 70, no. 7, pp. 791–798, Jan. 2002, doi: 10.1016/S0024-3205(01)01454-0.

[19] S. A. Quezada, “CTLA4 blockade and GM-CSF combination immunotherapy alters the intratumor balance of effector and regulatory T cells,” *Journal of Clinical Investigation*, vol. 116, no. 7, pp. 1935–1945, Jul. 2006, doi: 10.1172/JCI27745.

[20] S. A. Quezada, K. S. Peggs, T. R. Simpson, Y. Shen, D. R. Littman, and J. P. Allison, “Limited tumor infiltration by activated T effector cells restricts the therapeutic activity of regulatory T cell depletion against established melanoma,” *Journal of Experimental Medicine*, vol. 205, no. 9, pp. 2125–2138, Sep. 2008, doi: 10.1084/jem.20080099.

[21] A. Palazón *et al.*, “Agonist Anti-CD137 mAb Act on Tumor Endothelial Cells to Enhance Recruitment of Activated T Lymphocytes,” *Cancer Research*, vol. 71, no. 3, pp. 801–811, Feb. 2011, doi: 10.1158/0008-5472.CAN-10-1733.

[22] M. Fehlings *et al.*, “Checkpoint blockade immunotherapy reshapes the high-dimensional phenotypic heterogeneity of murine intratumoral neoantigen-specific CD8 + T cells,” *Nat Commun*, vol. 8, no. 1, Dec. 2017, doi: 10.1038/S41467-017-00627-Z.

[23] M. M. Gubin *et al.*, “High-Dimensional Analysis Delineates Myeloid and Lymphoid Compartment Remodeling during Successful Immune-Checkpoint Cancer Therapy,” *Cell*, vol. 175, no. 4, pp. 1014-1030.e19, Nov. 2018, doi: 10.1016/J.CELL.2018.09.030.

Epilogue

The research presented in this thesis is tied together by the purpose of defining the neoepitope features that facilitate $CD8^+$ T cell recognition in preclinical syngeneic murine models.

Vast screenings for neoepitope-specific $CD8^+$ T cells in preclinical and clinical immunotherapy studies have shown that a very small fraction of the predicted neoepitope candidates are immunogenic. This has motivated great interest in the field to define the characteristics determining $CD8^+$ T cell recognition [57], [64] (referred as T cells for the remaining of the Section). Finding patterns of immunogenicity among the highly individual and heterogenous human tumors and HLAs further complicates the matter, making immunocompetent syngeneic tumor mouse models an attractive tool to explore “the common factor” behind neoepitopes’ immunogenicity.

While several neoepitopes have been investigated in preclinical syngeneic models in the context of immunization, only few studies have characterized spontaneously occurring neoepitope-specific T cells in tumor-bearing mice [65], [108]. **Manuscript I** mapped the $CD8^+$ T cell neoepitope-recognition landscape of commonly used preclinical syngeneic models of mammary (EMT6 and 4T1) and colon (CT26) carcinomas. Utilizing a library of 500 DNA barcode-labeled pMHC multimers, 25, 15, and 18 responses were detected in the respective models (refer to Manuscript I). Anti-PD-1 and anti-CTLA-4 CPI treatment did not significantly foster their discovery, as most of the responses (84%, 60%, and 72%) were found in isotype-treated animals. Whether other tumor-mediated T cell suppressive mechanisms in these models prevents the priming and/or detection of more neoepitope-specific T cells was not explored. Even though these experiments require replication and fluorescent-based tetramer staining to validate each response individually, the number of responses detected are not negligible if proven reproducible. For comparison, a study identifying 1290 neoepitopes from a colon carcinoma MC38 syngeneic murine model only validated 7 pMHCs through mass spectrometry, from which 3 were immunogenic [65]. This exemplifies how the majority of predicted neoepitopes might not even reach the surface of tumor cells. Therefore, the main limitation of this study is lacking experimental validation of surface presentation of the selected neoepitopes. However, the fact that current prediction algorithms are trained on immunopeptidomics data, meaning on experimentally validated MHC-I binders, justifies the widely established use of transcript expression and predicted eluted MHC-binding affinity for selection of neoepitope candidates. While this has proven useful to deconvolute immunopeptidomics results [109], and to predict immunogenicity and response to immunotherapy across various preclinical and clinical studies [65], [110], the opposite has also been described [108], [111]. Therefore, researchers are exploring other

parameters that are predictable of neoepitope immunogenicity, such as, dis-similarity to self-epitopes [112], [113].

Manuscript II investigated the immunogenicity of different characteristics previously hypothesized to drive T cell recognition. Naïve Balb/c mice were vaccinated with neoepitopes predicted from the CT26 tumor cell line rationally selected to represent: 1) MHC-I binding capacity; 2) dis-similarity to self; 3) a mutation of missense or frameshift origin; and 4) absence of a strong MHC-II binding motif within the long neopeptide sequence. T cell recognition was studied in splenocytes through *in vitro* re-stimulation with the vaccine neoepitopes and/or tetramer staining. A small fraction of the studied neoepitopes triggered T cell responses, demonstrating the need to evaluate larger peptide pools to reveal patterns of immunogenicity. In addition, an insufficient presentation of neoepitopes to T cells could also explain the observed limited recognition. While formulation of the vaccine in the CAF09b adjuvant promotes activation and cross-presentation of the vaccine neoepitopes by professional dendritic cells DCs to T cells, presentation alone is not sufficient for T cell recognition of the neoepitope. Additionally, neoepitopes need to be exposed in sufficient amounts to be detected by the naïve T cell repertoire of tumor-free mice. Upscaling the dose of the neoepitopes in the vaccine or using long peptide sequences instead, might circumvent this limitation. On the other hand, a TCR capable of recognizing such neoepitopes needs to be present within the murine T cell repertoire. Therefore, mapping the CT26 neoepitopes presented in the context of MHC-I molecules through immunopeptidomics, prior to the sequential high-throughput screening of the recognizing T cells in CT26-tumor bearing mice, will pinpoint what T cell clones endure TCRs capable of *"seeing"* the CT26 "neopeptidome". This would narrow down the selection to neoepitopes that are both presented by the tumor cells; and in sufficient amounts to be immunogenic. Then they can be sorted by different characteristics and used as an optimized immunization approach to find patterns of immunogenicity. However, in view of the limited number of immunogenic neoepitopes confirmed by immunopeptidomics previously outlined, such sorting will unlikely be possible.

Together, both research projects reflect the (unexpected) difficulty to study neoepitope immunogenicity in preclinical syngeneic mouse tumor models. It is hypothesized that the great overlap between the predicted neoepitopes in CT26 tumors and cell lines reflects a conserved mutanome of such models, with little editing in the presence of immune pressure. Therefore, tumor rejection by neoepitope-specific T cells in these models might be limited to recognition of a few numbers of mutations driving the intrinsic tumorigenesis of the cell lines. This goes in line with their short therapeutic window, which upon a fast tumor onset (after establishment of the cell line) show rapid tumor-regression to e.g., CPI therapy. In this regard, the recurrent validation of the dominant CT26 endogenous response to the retroviral AH-1 epitope [114] might exemplify the little immunogenic variation of such models to immune pressure.

Lastly, **Chapter 7** outlined a pilot work conceived with the final purpose of validating the tumor-rejection capacity of the previously studied NARTs through ACT. The study was designed to circumvent the difficulties of potential limited neoepitope presentation and poor immunogenicity. The establishment of a melanoma B16BL6-OVA model was envisioned as a suitable system to optimize the ACT framework using Ag-scaffold- or free-peptide-expanded OVA-specific T cells. In spite of B16BL6-OVA expression transforming B16BL6 responsive to CPI, it proved as a challenging model to evaluate ACT strategies. Based on previous reports describing a poorly permeable vasculature of such model [101], we hypothesized that the established tumors became "immune-excluded", thus preventing infiltration of the ACT product. For the purpose of having a control model, establishing OVA expression in a more immunogenic syngeneic cell line (e.g., MC38), will allow the evaluation of the advantages of Ag-scaffold-expanded T cells over standard procedures. However, this model exemplifies how preclinical syngeneic murine models do not fully recapitulate the reality of human tumors, where melanoma is highly immunogenic and is showing clinical benefit in clinical trials of ACT of autologous TILs [96].

Overall, the present work exemplifies the multifactorial complexity of understanding cancer immunogenicity, even when stepping down its heterogeneity by using homogenous murine tumor models. In addition, it also points out that clinical translation of preclinical findings – at least from syngeneic models – must be critically assessed. Humanized PDX models are arising as the "hotspot model", as they better contextualize the microenvironment of a patient's tumor. Therefore, they minimize translational challenges such as different TMBs between syngeneic cell lines and human primary tumors. However, while my research has primarily focused on the neoepitope contribution to the crosstalk between cancer and the immune system, further challenges await on the T cell site. The stochastic character and high variability of the TCR repertoire adds another layer of complexity when aiming to model the immune response against a highly individual disease such as cancer. On these basis, I believe that the advent of single cell technologies and the interrogation of TCR:pMHC pairs will foster the revolution that neoepitope prediction algorithms have already granted to the field of immunotherapy, allowing the prediction of what patients will benefit from such treatments. Finally, if a better model was to be found for preclinical investigation of cancer, one could envision a future in which tumors and organs-on-a-chip succeeded to reproduce a person's tumor and immune system. Improvements on such *ex vivo* systems will pave the way towards minimizing the knowledge lost in translation.

References

[1] J. Parkin and B. Cohen, “An overview of the immune system,” *The Lancet*, vol. 357, no. 9270, pp. 1777–1789, Jun. 2001, doi: 10.1016/S0140-6736(00)04904-7.

[2] N. Jain, “The early life education of the immune system: Moms, microbes and (missed) opportunities,” *Gut Microbes*, vol. 12, no. 1, p. 1824564, Nov. 2020, doi: 10.1080/19490976.2020.1824564.

[3] C. A. Janeway, “Pillars article: approaching the asymptote? Evolution and revolution in immunology. Cold spring harb symp quant biol. 1989. 54: 1-13.,” *J Immunol*, vol. 191, no. 9, pp. 4475–87, Nov. 2013.

[4] N. K. Crellin, S. Trifari, C. D. Kaplan, N. Satoh-Takayama, J. P. di Santo, and H. Spits, “Regulation of Cytokine Secretion in Human CD127+ LTi-like Innate Lymphoid Cells by Toll-like Receptor 2,” *Immunity*, vol. 33, no. 5, pp. 752–764, Nov. 2010, doi: 10.1016/j.immuni.2010.10.012.

[5] M. Kende, “Role of macrophages in the expression of immune responses.,” *J Am Vet Med Assoc*, vol. 181, no. 10, pp. 1037–42, Nov. 1982.

[6] R. M. Steinman and M. D. Witmer, “Lymphoid dendritic cells are potent stimulators of the primary mixed leukocyte reaction in mice.,” *Proc Natl Acad Sci U S A*, vol. 75, no. 10, pp. 5132–6, Oct. 1978, doi: 10.1073/pnas.75.10.5132.

[7] J. Banchereau and R. M. Steinman, “Dendritic cells and the control of immunity,” *Nature*, vol. 392, no. 6673, pp. 245–252, Mar. 1998, doi: 10.1038/32588.

[8] D. Schenten and R. Medzhitov, “The control of adaptive immune responses by the innate immune system.,” *Adv Immunol*, vol. 109, pp. 87–124, 2011, doi: 10.1016/B978-0-12-387664-5.00003-0.

[9] F. Sallusto and A. Lanzavecchia, “The instructive role of dendritic cells on T-cell responses.,” *Arthritis Res*, vol. 4 Suppl 3, pp. S127-32, 2002, doi: 10.1186/ar567.

[10] D. I. Godfrey, A. P. Uldrich, J. McCluskey, J. Rossjohn, and D. B. Moody, “The burgeoning family of unconventional T cells,” *Nature Immunology*, vol. 16, no. 11, pp. 1114–1123, Nov. 2015, doi: 10.1038/ni.3298.

[11] K. Shortman and L. Wu, “Early T Lymphocyte Progenitors,” *Annual Review of Immunology*, vol. 14, no. 1, pp. 29–47, Apr. 1996, doi: 10.1146/annurev.immunol.14.1.29.

[12] R. Ahmed and D. Gray, “Immunological Memory and Protective Immunity: Understanding Their Relation,” *Science (1979)*, vol. 272, no. 5258, pp. 54–60, Apr. 1996, doi: 10.1126/science.272.5258.54.

[13] M. Fabbi, O. Acuto, J. E. Smart, and E. L. Reinherz, “Homology of Ti α-subunit of a T-cell Ag–MHC receptor with immunoglobulin,” *Nature*, vol. 312, no. 5991, pp. 269–271, Nov. 1984, doi: 10.1038/312269a0.

[14] Y. Li, Y. Yin, and R. A. Mariuzza, “Structural and Biophysical Insights into the Role of CD4 and CD8 in T Cell Activation,” *Frontiers in Immunology*, vol. 4, 2013, doi: 10.3389/fimmu.2013.00206.

[15] S. T. Ferris *et al.*, “cDC1 prime and are licensed by CD4+ T cells to induce anti-tumor immunity,” *Nature*, vol. 584, no. 7822, pp. 624–629, Aug. 2020, doi: 10.1038/s41586-020-2611-3.

[16] Z. Fan and Q. Zhang, “Molecular mechanisms of lymphocyte-mediated cytotoxicity.,” *Cell Mol Immunol*, vol. 2, no. 4, pp. 259–64, Aug. 2005.

[17] T. Shiina, K. Hosomichi, H. Inoko, and J. K. Kulski, “The HLA genomic loci map: expression, interaction, diversity and disease,” *Journal of Human Genetics*, vol. 54, no. 1, pp. 15–39, Jan. 2009, doi: 10.1038/jhg.2008.5.

[18] D. Di, J. M. Nunes, W. Jiang, and A. Sanchez-Mazas, “Like Wings of a Bird: Functional Divergence and Complementarity between HLA-A and HLA-B Molecules,” *Molecular Biology and Evolution*, vol. 38, no. 4, pp. 1580–1594, Apr. 2021, doi: 10.1093/molbev/msaa325.

[19] P. Kisielow, H. S. Teh, H. Blüthmann, and H. von Boehmer, “Positive selection of Ag-specific T cells in thymus by restricting MHC molecules,” *Nature*, vol. 335, no. 6192, pp. 730–733, Oct. 1988, doi: 10.1038/335730a0.

[20] P. Marrack, J. P. Scott-Browne, S. Dai, L. Gapin, and J. W. Kappler, “Evolutionarily Conserved Amino Acids That Control TCR-MHC Interaction,” *Annual Review of Immunology*, vol. 26, no. 1, pp. 171–203, Apr. 2008, doi: 10.1146/annurev.immunol.26.021607.090421.

[21] M. S. Anderson *et al.*, “Projection of an Immunological Self Shadow Within the Thymus by the Aire Protein,” *Science (1979)*, vol. 298, no. 5597, pp. 1395–1401, Nov. 2002, doi: 10.1126/science.1075958.

[22] P. G. Ashton-Rickardt *et al.*, “Evidence for a differential avidity model of T cell selection in the thymus,” *Cell*, vol. 76, no. 4, pp. 651–663, Feb. 1994, doi: 10.1016/0092-8674(94)90505-3.

[23] R. M. Steinman and M. C. Nussenzweig, “Avoiding horror autotoxicus: The importance of dendritic cells in peripheral T cell tolerance,” *Proceedings of the National Academy of Sciences*, vol. 99, no. 1, pp. 351–358, Jan. 2002, doi: 10.1073/pnas.231606698.

[24] M. S. Jordan *et al.*, “Thymic selection of CD4+CD25+ regulatory T cells induced by an agonist self-peptide,” *Nature Immunology*, vol. 2, no. 4, pp. 301–306, Apr. 2001, doi: 10.1038/86302.

[25] D. Hanahan, “Hallmarks of Cancer: New Dimensions,” *Cancer Discovery*, vol. 12, no. 1, pp. 31–46, Jan. 2022, doi: 10.1158/2159-8290.CD-21-1059.

[26] G. P. Dunn, L. J. Old, and R. D. Schreiber, “The Immunobiology of Cancer Immunosurveillance and Immunoediting,” *Immunity*, vol. 21, no. 2, pp. 137–148, Aug. 2004, doi: 10.1016/j.immuni.2004.07.017.

[27] V. Shankaran *et al.*, “IFNγ and lymphocytes prevent primary tumor development and shape tumor immunogenicity,” *Nature*, vol. 410, no. 6832, pp. 1107–1111, Apr. 2001, doi: 10.1038/35074122.

[28] J. A. Joyce and D. T. Fearon, “T cell exclusion, immune privilege, and the tumor microenvironment,” *Science (1979)*, vol. 348, no. 6230, pp. 74–80, Apr. 2015, doi: 10.1126/science.aaa6204.

[29] O. Kourko, K. Seaver, N. Odoardi, S. Basta, and K. Gee, “IL-27, IL-30, and IL-35: A Cytokine Triumvirate in Cancer,” *Frontiers in Oncology*, vol. 9, Oct. 2019, doi: 10.3389/fonc.2019.00969.

[30] A. E. Vilgelm and A. Richmond, “Chemokines Modulate Immune Surveillance in Tumorigenesis, Metastasis, and Response to Immunotherapy,” *Frontiers in Immunology*, vol. 10, Feb. 2019, doi: 10.3389/fimmu.2019.00333.

[31] D. I. Gabrilovich, T. Ishida, S. Nadaf, J. E. Ohm, and D. P. Carbone, “Antibodies to vascular endothelial growth factor enhance the efficacy of cancer immunotherapy by improving endogenous dendritic cell function.,” *Clin Cancer Res*, vol. 5, no. 10, pp. 2963–70, Oct. 1999.

[32] S. H. Wrzesinski, Y. Y. Wan, and R. A. Flavell, “Transforming Growth Factor-β and the Immune Response: Implications for Anticancer Therapy,” *Clinical Cancer Research*, vol. 13, no. 18, pp. 5262–5270, Sep. 2007, doi: 10.1158/1078-0432.CCR-07-1157.

[33] D. I. Gabrilovich and S. Nagaraj, “Myeloid-derived suppressor cells as regulators of the immune system,” *Nature Reviews Immunology*, vol. 9, no. 3, pp. 162–174, Mar. 2009, doi: 10.1038/nri2506.

[34] B. Huang *et al.*, “Gr-1 $^{+}$ CD115 $^{+}$ Immature Myeloid Suppressor Cells Mediate the Development of Tumor-Induced T Regulatory Cells and T-Cell Anergy in Tumor-Bearing Host,” *Cancer Research*, vol. 66, no. 2, pp. 1123–1131, Jan. 2006, doi: 10.1158/0008-5472.CAN-05-1299.

[35] Y. Zhang, X. Guan, and P. Jiang, “Cytokine and Chemokine Signals of T-Cell Exclusion in Tumors,” *Frontiers in Immunology*, vol. 11, Dec. 2020, doi: 10.3389/fimmu.2020.594609.

[36] D. S. Chen and I. Mellman, “Oncology Meets Immunology: The Cancer-Immunity Cycle,” *Immunity*, vol. 39, no. 1, pp. 1–10, Jul. 2013, doi: 10.1016/j.immuni.2013.07.012.

[37] R. Noubade, S. Majri-Morrison, and K. v. Tarbell, “Beyond cDC1: Emerging Roles of DC Crosstalk in Cancer Immunity,” *Frontiers in Immunology*, vol. 10, May 2019, doi: 10.3389/fimmu.2019.01014.

[38] E. W. Roberts *et al.*, “Critical Role for CD103+/CD141+ Dendritic Cells Bearing CCR7 for Tumor Ag Trafficking and Priming of T Cell Immunity in Melanoma,” *Cancer Cell*, vol. 30, no. 2, pp. 324–336, Aug. 2016, doi: 10.1016/j.ccell.2016.06.003.

[39] H. Salmon *et al.*, “Expansion and Activation of CD103 + Dendritic Cell Progenitors at the Tumor Site Enhances Tumor Responses to Therapeutic PD-L1 and BRAF Inhibition,” *Immunity*, vol. 44, no. 4, pp. 924–938, Apr. 2016, doi: 10.1016/j.immuni.2016.03.012.

[40] B. W. MacNabb *et al.*, “Dendritic cells can prime anti-tumor CD8+ T cell responses through major histocompatibility complex cross-dressing,” *Immunity*, vol. 55, no. 6, pp. 982-997.e8, Jun. 2022, doi: 10.1016/j.immuni.2022.04.016.

[41] S. Kaczanowska, A. M. Joseph, and E. Davila, “TLR agonists: our best *frenemy* in cancer immunotherapy,” *Journal of Leukocyte Biology*, vol. 93, no. 6, pp. 847–863, Jun. 2013, doi: 10.1189/jlb.1012501.

[42] R. E. Tay, E. K. Richardson, and H. C. Toh, “Revisiting the role of CD4+ T cells in cancer immunotherapy—new insights into old paradigms,” *Cancer Gene Therapy*, vol. 28, no. 1–2, pp. 5–17, Feb. 2021, doi: 10.1038/s41417-020-0183-x.

[43] M. Hashimoto *et al.*, “CD8 T Cell Exhaustion in Chronic Infection and Cancer: Opportunities for Interventions,” *Annual Review of Medicine*, vol. 69, no. 1, pp. 301–318, Jan. 2018, doi: 10.1146/annurev-med-012017-043208.

[44] J. A. Hollenbaugh, J. Reome, M. Dobrzanski, and R. W. Dutton, “The Rate of the CD8-Dependent Initial Reduction in Tumor Volume Is Not Limited by Contact-Dependent Perforin, Fas Ligand, or TNF-Mediated Cytolysis,” *The Journal of Immunology*, vol. 173, no. 3, pp. 1738–1743, Aug. 2004, doi: 10.4049/jimmunol.173.3.1738.

[45] A. Gallimore *et al.*, “Induction and Exhaustion of Lymphocytic Choriomeningitis Virus–specific Cytotoxic T Lymphocytes Visualized Using Soluble Tetrameric Major Histocompatibility Complex Class I–Peptide Complexes,” *Journal of Experimental Medicine*, vol. 187, no. 9, pp. 1383–1393, May 1998, doi: 10.1084/jem.187.9.1383.

[46] D. Zehn, R. Thimme, E. Lugli, G. P. de Almeida, and A. Oxenius, “‘Stem-like’ precursors are the fount to sustain persistent CD8+ T cell responses,” *Nature Immunology*, vol. 23, no. 6, pp. 836–847, Jun. 2022, doi: 10.1038/s41590-022-01219-w.

[47] L. Gattinoni *et al.*, “A human memory T cell subset with stem cell–like properties,” *Nature Medicine*, vol. 17, no. 10, pp. 1290–1297, Oct. 2011, doi: 10.1038/nm.2446.

[48] P. G. Coulie, B. J. van den Eynde, P. van der Bruggen, and T. Boon, “Tumor Ags recognized by T lymphocytes: at the core of cancer immunotherapy,” *Nature Reviews Cancer 2014 14:2*, vol. 14, no. 2, pp. 135–146, Jan. 2014, doi: 10.1038/nrc3670.

[49] S. L. Topalian, “Targeting Immune Checkpoints in Cancer Therapy,” *JAMA*, vol. 318, no. 17, p. 1647, Nov. 2017, doi: 10.1001/jama.2017.14155.

[50] W. B. COLEY, “The Treatment of Sarcoma with the Mixed Toxins of Erysipelas and Bacillus Prodigiosus,” *The Boston Medical and Surgical Journal*, vol. 158, no. 6, pp. 175–182, Feb. 1908, doi: 10.1056/NEJM190802061580601.

[51] FDA, “FDA Approves First Cell-Based Gene Therapy for Adult Patients with Multiple Myeloma,” 2021, Accessed: Jun. 13, 2022. [Online]. Available: https://www.fda.gov/news-events/press-announcements/fda-approves-first-cell-based-gene-therapy-adult-patients-multiple-myeloma.

[52] E. H. Byrne and D. E. Fisher, “Immune and molecular correlates in melanoma treated with immune checkpoint blockade,” *Cancer*, vol. 123, no. S11, pp. 2143–2153, Jun. 2017, doi: 10.1002/cncr.30444.

[53] C. Robert *et al.*, “Ipilimumab plus Dacarbazine for Previously Untreated Metastatic Melanoma,” *New England Journal of Medicine*, vol. 364, no. 26, pp. 2517–2526, Jun. 2011, doi: 10.1056/NEJMoa1104621.

[54] M. Reck *et al.*, “Pembrolizumab versus Chemotherapy for PD-L1–Positive Non–Small-Cell Lung Cancer,” *New England Journal of Medicine*, vol. 375, no. 19, pp. 1823–1833, Nov. 2016, doi: 10.1056/NEJMoa1606774.

[55] P.-W. Huang and J. W.-C. Chang, “Immune checkpoint inhibitors win the 2018 Nobel Prize,” *Biomedical Journal*, vol. 42, no. 5, pp. 299–306, Oct. 2019, doi: 10.1016/j.bj.2019.09.002.

[56] S.-C. Pao, M.-T. Chu, and S.-I. Hung, “Therapeutic Vaccines Targeting Neoantigens to Induce T-Cell Immunity against Cancers,” *Pharmaceutics*, vol. 14, no. 4, p. 867, Apr. 2022, doi: 10.3390/pharmaceutics14040867.

[57] F. Lang, B. Schrörs, M. Löwer, Ö. Türeci, and U. Sahin, “Identification of neoantigens for individualized therapeutic cancer vaccines,” *Nature Reviews Drug Discovery*, vol. 21, no. 4, pp. 261–282, Apr. 2022, doi: 10.1038/s41573-021-00387-y.

[58] J. S. Holm *et al.*, “Neoantigen-specific CD8 T cell responses in the peripheral blood following PD-L1 blockade might predict therapy outcome in metastatic urothelial carcinoma,” *Nature Communications*, vol. 13, no. 1, p. 1935, Dec. 2022, doi: 10.1038/s41467-022-29342-0.

[59] N. P. Kristensen *et al.*, “Neoantigen-reactive CD8+ T cells affect clinical outcome of adoptive cell therapy with tumor-infiltrating lymphocytes in melanoma,” *Journal of Clinical Investigation*, vol. 132, no. 2, Jan. 2022, doi: 10.1172/JCI150535.

[60] C. Lurquin *et al.*, “Structure of the gene of tum− transplantation Ag P91A: The mutated exon encodes a peptide recognized with Ld by cytolytic T cells,” *Cell*, vol. 58, no. 2, pp. 293–303, Jul. 1989, doi: 10.1016/0092-8674(89)90844-1.

[61] T. Jiang *et al.*, “Tumor neoantigens: from basic research to clinical applications,” *Journal of Hematology & Oncology*, vol. 12, no. 1, p. 93, Dec. 2019, doi: 10.1186/s13045-019-0787-5.

[62] A. Garcia-Garijo, C. A. Fajardo, and A. Gros, “Determinants for Neoantigen Identification,” *Frontiers in Immunology*, vol. 10, Jun. 2019, doi: 10.3389/fimmu.2019.01392.

[63] M. Bassani-Sternberg, “Mass Spectrometry Based Immunopeptidomics for the Discovery of Cancer Neoantigens,” 2018, pp. 209–221. doi: 10.1007/978-1-4939-7537-2_14.

[64] E. S. Borden, K. H. Buetow, M. A. Wilson, and K. T. Hastings, “Cancer Neoantigens: Challenges and Future Directions for Prediction, Prioritization, and Validation,” *Frontiers in Oncology*, vol. 12. Frontiers Media S.A., Mar. 03, 2022. doi: 10.3389/fonc.2022.836821.

[65] M. Yadav *et al.*, “Predicting immunogenic tumor mutations by combining mass spectrometry and exome sequencing,” *Nature*, vol. 515, no. 7528, pp. 572–576, 2014, doi: 10.1038/nature14001.

[66] U. K. Hansen *et al.*, “Tumor-Infiltrating T Cells From Clear Cell Renal Cell Carcinoma Patients Recognize Neoepitopes Derived From Point and Frameshift Mutations,” *Frontiers in Immunology*, vol. 11, Mar. 2020, doi: 10.3389/fimmu.2020.00373.

[67] E. S. Borden, S. Ghafoor, K. H. Buetow, B. J. LaFleur, M. A. Wilson, and K. T. Hastings, “NeoScore Integrates Characteristics of the Neoantigen:MHC Class I Interaction and Expression to Accurately Prioritize Immunogenic Neoantigens,” *The Journal of Immunology*, vol. 208, no. 7, pp. 1813–1827, Apr. 2022, doi: 10.4049/jimmunol.2100700.

[68] R. M. Samstein *et al.*, “Tumor mutational load predicts survival after immunotherapy across multiple cancer types,” *Nature Genetics*, vol. 51, no. 2, pp. 202–206, Feb. 2019, doi: 10.1038/s41588-018-0312-8.

[69] P. A. Ott *et al.*, “An immunogenic personal neoantigen vaccine for patients with melanoma,” *Nature*, vol. 547, no. 7662, pp. 217–221, Jul. 2017, doi: 10.1038/NATURE22991.

[70] N. Hilf *et al.*, “Actively personalized vaccination trial for newly diagnosed glioblastoma,” *Nature 2018 565:7738*, vol. 565, no. 7738, pp. 240–245, Dec. 2018, doi: 10.1038/s41586-018-0810-y.

[71] F. Duan *et al.*, “Genomic and bioinformatic profiling of mutational neoepitopes reveals new rules to predict anticancer immunogenicity,” *Journal of Experimental Medicine*, vol. 211, no. 11, pp. 2231–2248, Oct. 2014, doi: 10.1084/jem.20141308.

[72] A.-M. Bjerregaard *et al.*, “An Analysis of Natural T Cell Responses to Predicted Tumor Neoepitopes,” *Frontiers in Immunology*, vol. 8, Nov. 2017, doi: 10.3389/fimmu.2017.01566.

[73] V. Roudko *et al.*, “Shared Immunogenic Poly-Epitope Frameshift Mutations in Microsatellite Unstable Tumors,” *Cell*, vol. 183, no. 6, pp. 1634-1649.e17, Dec. 2020, doi: 10.1016/j.cell.2020.11.004.

[74] D. K. Wells *et al.*, “Key Parameters of Tumor Epitope Immunogenicity Revealed Through a Consortium Approach Improve Neoantigen Prediction,” *Cell*, vol. 183, no. 3, pp. 818-834.e13, Oct. 2020, doi: 10.1016/j.cell.2020.09.015.

[75] A. de Sousa Linhares, J. Leitner, K. Grabmeier-Pfistershammer, and P. Steinberger, “Not All Immune Checkpoints Are Created Equal,” *Frontiers in Immunology*, vol. 9, Aug. 2018, doi: 10.3389/fimmu.2018.01909.

[76] N. Riaz *et al.*, “Tumor and Microenvironment Evolution during Immunotherapy with Nivolumab,” *Cell*, vol. 171, no. 4, pp. 934-949.e16, Nov. 2017, doi: 10.1016/j.cell.2017.09.028.

[77] C. Thallinger *et al.*, “Review of cancer treatment with immune checkpoint inhibitors,” *Wien Klin Wochenschr*, vol. 130, no. 3–4, pp. 85–91, Feb. 2018, doi: 10.1007/s00508-017-1285-9.

[78] L. Robert *et al.*, “CTLA4 Blockade Broadens the Peripheral T-Cell Receptor Repertoire,” *Clinical Cancer Research*, vol. 20, no. 9, pp. 2424–2432, May 2014, doi: 10.1158/1078-0432.CCR-13-2648.

[79] B. T. Fife and J. A. Bluestone, “Control of peripheral T-cell tolerance and autoimmunity via the CTLA-4 and PD-1 pathways,” *Immunological Reviews*, vol. 224, no. 1, pp. 166–182, Aug. 2008, doi: 10.1111/j.1600-065X.2008.00662.x.

[80] R. S. Herbst *et al.*, “Predictive correlates of response to the anti-PD-L1 antibody MPDL3280A in cancer patients,” *Nature*, vol. 515, no. 7528, pp. 563–567, Nov. 2014, doi: 10.1038/nature14011.

[81] J. J. Havel, D. Chowell, and T. A. Chan, “The evolving landscape of biomarkers for checkpoint inhibitor immunotherapy,” *Nature Reviews Cancer*, vol. 19, no. 3, pp. 133–150, Mar. 2019, doi: 10.1038/s41568-019-0116-x.

[82] M. Fehlings *et al.*, “Checkpoint blockade immunotherapy reshapes the high-dimensional phenotypic heterogeneity of murine intratumoral neoantigen-specific CD8 + T cells,” *Nat Commun*, vol. 8, no. 1, Dec. 2017, doi: 10.1038/S41467-017-00627-Z.

[83] M. M. Gubin *et al.*, “Checkpoint blockade cancer immunotherapy targets tumor-specific mutant Ags,” *Nature*, vol. 515, no. 7528, pp. 577–581, Nov. 2014, doi: 10.1038/nature13988.

[84] S. Li *et al.*, “Characterization of neoantigen-specific T cells in cancer resistant to immune checkpoint therapies,” *Proceedings of the National Academy of Sciences*, vol. 118, no. 30, Jul. 2021, doi: 10.1073/pnas.2025570118.

[85] E. Blass and P. A. Ott, “Advances in the development of personalized neoantigen-based therapeutic cancer vaccines,” *Nature Reviews Clinical Oncology*, vol. 18, no. 4, pp. 215–229, Apr. 2021, doi: 10.1038/s41571-020-00460-2.

[86] J. Liu, M. Fu, M. Wang, D. Wan, Y. Wei, and X. Wei, “Cancer vaccines as promising immuno-therapeutics: platforms and current progress,” *Journal of Hematology & Oncology*, vol. 15, no. 1, p. 28, Dec. 2022, doi: 10.1186/s13045-022-01247-x.

[87] S. Kreiter *et al.*, “Mutant MHC class II epitopes drive therapeutic immune responses to cancer,” *Nature*, vol. 520, no. 7549, pp. 692–696, 2015, doi: 10.1038/nature14426.

[88] E. Alspach *et al.*, “MHC-II neoantigens shape tumor immunity and response to immunotherapy,” *Nature*, vol. 574, no. 7780, pp. 696–701, Oct. 2019, doi: 10.1038/s41586-019-1671-8.

[89] Z. Urban-Wojciuk *et al.*, “The Role of TLRs in Anti-cancer Immunity and Tumor Rejection,” *Frontiers in Immunology*, vol. 10, Oct. 2019, doi: 10.3389/fimmu.2019.02388.

[90] J. C. Castle *et al.*, “Exploiting the mutanome for tumor vaccination,” *Cancer Research*, vol. 72, no. 5, pp. 1081–1091, 2012, doi: 10.1158/0008-5472.CAN-11-3722.

[91] R. Hernandez and T. R. Malek, “Fueling Cancer Vaccines to Improve T Cell-Mediated Antitumor Immunity,” *Frontiers in Oncology*, vol. 12, May 2022, doi: 10.3389/fonc.2022.878377.

[92] K. S. Korsholm *et al.*, “Induction of CD8+ T-cell responses against subunit Ags by the novel cationic liposomal CAF09 adjuvant,” *Vaccine*, vol. 32, no. 31, pp. 3927–3935, Jun. 2014, doi: 10.1016/j.vaccine.2014.05.050.

[93] R. P. Gilley and P. H. Dube, “Checkpoint blockade inhibitors enhances the effectiveness of a *Listeria monocytogenes* -based melanoma vaccine,” *Oncotarget*, vol. 11, no. 7, pp. 740–754, Feb. 2020, doi: 10.18632/oncotarget.27490.

[94] M. Poorebrahim, N. Mohammadkhani, R. Mahmoudi, M. Gholizadeh, E. Fakhr, and A. Cid-Arregui, “TCR-like CARs and TCR-CARs targeting neoepitopes: an emerging potential,” *Cancer Gene Therapy*, vol. 28, no. 6, pp. 581–589, Jun. 2021, doi: 10.1038/s41417-021-00307-7.

[95] Ö. Met, K. M. Jensen, C. A. Chamberlain, M. Donia, and I. M. Svane, “Principles of adoptive T cell therapy in cancer,” *Seminars in Immunopathology*, vol. 41, no. 1, pp. 49–58, Jan. 2019, doi: 10.1007/s00281-018-0703-z.

[96] A. H. Kverneland *et al.*, “Adoptive cell therapy with tumor-infiltrating lymphocytes supported by checkpoint inhibition across multiple solid cancer types,” *Journal for ImmunoTherapy of Cancer*, vol. 9, no. 10, p. e003499, Oct. 2021, doi: 10.1136/jitc-2021-003499.

[97] H. Jespersen *et al.*, “Clinical responses to adoptive T-cell transfer can be modeled in an autologous immune-humanized mouse model,” *Nature Communications*, vol. 8, no. 1, p. 707, Dec. 2017, doi: 10.1038/s41467-017-00786-z.

[98] D. S. Chulpanova, K. v. Kitaeva, C. S. Rutland, A. A. Rizvanov, and V. v. Solovyeva, “Mouse Tumor Models for Advanced Cancer Immunotherapy,” *International Journal of Molecular Sciences*, vol. 21, no. 11, p. 4118, Jun. 2020, doi: 10.3390/ijms21114118.

[99] N. J. Rothenberger and L. P. Stabile, “Induction of Lung Tumors and Mutational Analysis in FVB/N Mice Treated with the Tobacco Carcinogen 4-(Methylnitrosamino)-1-(3-Pyridyl)-1-Butanone,” 2020, pp. 149–160. doi: 10.1007/978-1-0716-0223-2_7.

[100] M. F. Sanmamed, C. Chester, I. Melero, and H. Kohrt, “Defining the optimal murine models to investigate immune checkpoint blockers and their combination with other immunotherapies,” *Annals of Oncology*, vol. 27, no. 7, pp. 1190–1198, Jul. 2016, doi: 10.1093/annonc/mdw041.

[101] S. A. Quezada, “CTLA4 blockade and GM-CSF combination immunotherapy alters the intratumor balance of effector and regulatory T cells,” *Journal of Clinical Investigation*, vol. 116, no. 7, pp. 1935–1945, Jul. 2006, doi: 10.1172/JCI27745.

[102] J. F. Grosso and M. N. Jure-Kunkel, “CTLA-4 blockade in tumor models: an overview of preclinical and translational research.,” *Cancer Immun*, vol. 13, p. 5, 2013.

[103] T. R. Simpson *et al.*, “Fc-dependent depletion of tumor-infiltrating regulatory T cells co-defines the efficacy of anti-CTLA-4 therapy against melanoma,” *J Exp Med*, vol. 210, no. 9, pp. 1695–1710, 2013, doi: 10.1084/JEM.20130579.

[104] M. J. Selby *et al.*, “Anti-CTLA-4 Antibodies of IgG2a Isotype Enhance Antitumor Activity through Reduction of Intratumoral Regulatory T Cells,” *Cancer Immunol Research*, 2013, doi: 10.1158/2326-6066.CIR-13-0013.

[105] Y. Sato, Y. Fu, H. Liu, M. Y. Lee, and M. H. Shaw, “Tumor-immune profiling of CT-26 and Colon 26 syngeneic mouse models reveals mechanism of anti-PD-1 response,” *BMC Cancer*, vol. 21, no. 1, p. 1222, Dec. 2021, doi: 10.1186/s12885-021-08974-3.

[106] A.-H. Capietto *et al.*, “Mutation position is an important determinant for predicting cancer neoantigens,” *Journal of Experimental Medicine*, vol. 217, no. 4, Apr. 2020, doi: 10.1084/jem.20190179.

[107] M. Vormehr *et al.*, “A non-functional neoepitope specific CD8 + T-cell response induced by tumor derived Ag exposure in vivo,” *OncoImmunology*, vol. 8, no. 3, pp. 1–14, 2019, doi: 10.1080/2162402X.2018.1553478.

[108] S. Li *et al.*, “Characterization of neoantigen-specific T cells in cancer resistant to immune checkpoint therapies,” *Proceedings of the National Academy of Sciences*, vol. 118, no. 30, Jul. 2021, doi: 10.1073/pnas.2025570118.

[109] M.-H. Fortier *et al.*, “The MHC class I peptide repertoire is molded by the transcriptome,” *Journal of Experimental Medicine*, vol. 205, no. 3, pp. 595–610, Mar. 2008, doi: 10.1084/jem.20071985.

[110] V. Anagnostou *et al.*, “Evolution of Neoantigen Landscape during Immune Checkpoint Blockade in Non–Small Cell Lung Cancer,” *Cancer Discovery*, vol. 7, no. 3, pp. 264–276, Mar. 2017, doi: 10.1158/2159-8290.CD-16-0828.

[111] M. Vormehr *et al.*, “A non-functional neoepitope specific CD8 $^{+}$ T-cell response induced by tumor derived Ag exposure *in vivo*,” *OncoImmunology*, vol. 8, no. 3, p. 1553478, Mar. 2019, doi: 10.1080/2162402X.2018.1553478.

[112] A.-M. Bjerregaard, T. K. Pedersen, A. M. Marquard, and S. R. Hadrup, “Prediction of neoepitopes from murine sequencing data,” *Cancer Immunology, Immunotherapy*, vol. 68, no. 1, pp. 159–161, Jan. 2019, doi: 10.1007/s00262-018-2254-5.

[113] L. P. Richman, R. H. Vonderheide, and A. J. Rech, “Neoantigen Dissimilarity to the Self-Proteome Predicts Immunogenicity and Response to Immune Checkpoint Blockade,” *Cell Systems*, vol. 9, no. 4, pp. 375-382.e4, Oct. 2019, doi: 10.1016/j.cels.2019.08.009.

[114] A. Y. Huang *et al.*, “The immunodominant major histocompatibility complex class I-restricted Ag of a murine colon tumor derives from an endogenous retroviral gene product.,” *Proceedings of the National Academy of Sciences*, vol. 93, no. 18, pp. 9730–9735, Sep. 1996, doi: 10.1073/pnas.93.18.9730.

[115] M. D. Vesely, M. H. Kershaw, R. D. Schreiber, and M. J. Smyth, “Natural Innate and Adaptive Immunity to Cancer,” *Annual Review of Immunology*, vol. 29, no. 1, pp. 235–271, Apr. 2011, doi: 10.1146/annurev-immunol-031210-101324.

[116] J. D. Chan, J. Lai, C. Y. Slaney, A. Kallies, P. A. Beavis, and P. K. Darcy, “Cellular networks controlling T cell persistence in adoptive cell therapy,” *Nature Reviews Immunology*, vol. 21, no. 12, pp. 769–784, Dec. 2021, doi: 10.1038/s41577-021-00539-6.